Development of control methods for ultrasonic liquid crystal lens

Jessica Mieko Dias Onaka

Doshisha University

Graduate School of Science and Engineering

June 2022

ABSTRACT

New technologies for adaptive optics are becoming increasingly important for miniature devices such as cell-phone cameras. The human eye is an example of adaptive optical system, comprising of cornea, pupil and lens. The cornea is responsible for most of the optical power. The pupil acts as an aperture that controls the amount of light that forms images on the retina, and the eye lens can adjust its shape via the ciliary muscles, working as a variable focus lens.

Conventional optical systems are based on mechanically moving parts of glass or plastic lenses to adjust focus, magnification, and field of view. Miniature adaptive lens, however, is an alternative to change focal lengths while eliminating the need to mechanical moving parts. Many adaptive lenses that mimic eyes have been developed to replace the multiple solid elements in optical systems. Among these approaches, liquid crystal material is an attractive alternative to replace this conventional optical system based on solid elements, because of its easy controllability by using an external field. The light traveling through the liquid crystal medium bends at different angle depending on the orientation of the liquid crystal molecules in response to a control signal.

The combination of nematic liquid crystals and their technology to focus light, in combination with ultrasound actuation to improve the lens efficiency and flexibility, is addressed in this doctoral thesis. For ultrasound controlled liquid crystal lenses, the geometry of the lens and the design of the piezoelectric transducer are critical factors. The liquid crystal molecular reorientation and the transmitted light of the lens can be controlled by ultrasound, then acousto-optics effects can be observed. The lenses configuration presented in this thesis work were simulated by finite-element analysis using Ansys software.

This thesis will investigate control methods for liquid crystal lenses using a divided annular piezoelectric ceramic that uses ultrasound to drive a nematic liquid crystal layer sandwiched between two circular glass substrates. The aperture of the lens can be controlled using a combination of the resonant standing and traveling wave modes and three-

dimensional focus control could be realized according to the driving scheme. Additionally, a method to improve the performance of the ultrasound liquid crystal lens is also presented and discussed. A double-layer-based lens model tailored based on the liquid crystal's physical properties, e.g., its dielectric anisotropy and elastic constants, is presented as an alternative method to improve the lens's optical performance while forming weak anchoring surfaces for nematic liquid crystals, thus promoting easier reorientation of the liquid crystal molecules.

The optical, physical, and fabrication characteristics of ultrasound liquid crystal lens were analyzed in this thesis with the aim to develop control methods for the liquid crystal lenses based on acousto-optics effects using ultrasound vibration of a piezoelectric transducer.

DEDICATION

To my parents for their unconditional love and support, as well as for teaching me that there is no limit or borderline to achieve the dreams I have in life. All I want more than anything is to make them always proud of me.

To my beloved husband – without his love and constant enthusiasm and inspiration during my graduate studies I could not reach to this point. His support throughout this research was extraordinary.

ACKNOWLEDGEMENTS

Foremost, I would like to thank God, the Almighty, for all the blessings and for helping me through hard times, enabling me to carry out and complete these studies. I am forever indebted for his immeasurable blessings in my life.

Besides my efforts, this thesis would not be possible without the encouragement and guidance of many others. I would like to express my sincere gratitude to my supervisors Prof. Mami Matsukawa and Prof. Daisuke Koyama for their kindness, patience, encouragement and continuous help and advice in these 4 years from my master's to my PhD studies. Getting started on a project and finishing a PhD thesis in two years is not an easy feat. Their immense knowledge and plentiful experience have encouraged me in all the time of my academic research and daily life. I would not have reached here without their unwavering support. Prof. Mami Matsukawa has always been highly supportive and encouraged me in many endeavours, even in personal life. Prof. Daisuke Koyama has always supported me with any trouble I have faced, since the first e-mail I sent him back in Brazil asking if I could enroll the laboratory. He gave me all the assistance in getting a scholarship in Japan for both master's and doctoral studies. I feel extremely honored and appreciative to have the opportunity to learn about acousto-optics with him and for his precious time and invaluable insights. His knowledge and encouragement make him a true inspiration for me. With his help, not only I have improved my research skills but also my Japanese skills. He has always encouraged me to practice my Japanese – spoken and written language – making possible to level up quickly my communication abilities.

I would like to thank my examiners, Prof. Naoki Otani and Prof. Naoto Nagaoka, for their thoughtful comments/questions/discussions during the oral defense, as well as, for engaging with my thesis diligently and enthusiastically, providing insightful suggestions. Their discussions, ideas, and feedback have been absolutely invaluable. The review process turned out to be a precious chance for me to think about various aspects of my analysis from a range of perspectives.

I am also grateful to Prof. Akira Emoto for teaching me how to use the Birefringence Profiler and the theory behind the polarization gratings and birefringence distribution measurements. His great technique inspired me to find key results in my research.

The support of the Laboratory of Ultrasonic Electronics members – all the former and current members – have also been invaluable so far on this research effort. I am grateful for Ms. Kazumi Nishiyama to help me with the research material acquisition procedures.

I would also like to thank the Graduate School of Science and Engineering for their help from my arrival, to plans of my future, and everything in between.

In addition, I would like to express my gratitude for the Monbukagakusho Scholarship that I was granted during my master's and my PhD studies at Doshisha University.

A special thanks should be given to my father and to my mother. I highly appreciate their constant support and love throughout the years. Their belief in me has kept my motivation high during this process. I wish to extend my special thanks to my older brothers.

Finally, I thank my husband for the love and enthusiasm that give my life an extra dimension. It is not the first time I tell you, but I simply couldn't have done it without you. Mission accomplished! We made it!

Jessica Onaka

“Whatever you do, work at it with all your heart.” – Colossians 3:23

“Where God guides, he provides.” – Isaiah 58:11.

“If you want to find the secrets of the universe, think in terms of energy, frequency, and vibration!” – Nicola Tesla

“To raise new questions, new possibilities, to regard old problems from a new angle, requires creative imagination and marks real advance in science.” – Albert Einstein

"*A scientist in his laboratory is not a mere technician: he is also a child confronting natural phenomena that impress him as though they were fairy tales."* – Marie Curie

PUBLICATIONS

J. Onaka, D. Koyama, Y. Kuroda, A. Emoto, M. Matsukawa "Optical evaluation of a double-layered ultrasound liquid crystal lens". *Journal of Applied Physics*, vol. 131, no. 19, p.193103, 2022.

T. Iwase, Y. Kuroda, **J. Onaka**, A. Emoto, M. Matsukawa and D. Koyama, "Orientation angles of liquid crystals via ultrasound vibrations". *Japanese Journal of Applied Physics*, vol. 61, no. 6, p. 068002, 2022.

T. Iwase, **J. Onaka**, A. Emoto, D. Koyama and M. Matsukawa "Relationship between liquid crystal layer thickness and variable-focusing characteristics of an ultrasound liquid crystal lens". *Japanese Journal of Applied Physics*, vol. 61, no. SG, p. SG1013, 2022.

J. Onaka, T. Iwase, A. Emoto, D. Koyama and M. Matsukawa. "Ultrasound liquid crystal lens with a variable focus in the radial direction for image stabilization". *Applied Optics*, vol. 60, no. 33, pp.10365-10371, 2021.

J. Onaka, T. Iwase, D. Koyama and M. Matsukawa. "Evaluation of the Optical Characteristics of the Liquid Crystal Lens Using a Shack-Hartmann Wavefront Sensor". In *2021 IEEE International Ultrasonics Symposium (IUS)* (pp. 1-3). IEEE, Sep. 2021.

D. Sakata, T. Iwase, **J. Onaka**, D. Koyama, M. Matsukawa, "Varifocal optical lens using ultrasonic vibration and thixotropic gel". *Journal of the Acoustical Society of America*, vol. 149, no. 6, pp. 3954-3960, 2021.

J. Onaka, T. Iwase, M. Fukui, D. Koyama and M. Matsukawa "Ultrasound liquid crystal lens with enlarged aperture using traveling waves". *Optics Letters*, vol. 46, no. 5, pp.1169-1172, 2021.

PRESENTATIONS

黒田悠真, 岩瀬貴大, **J. Onaka**, 江本顕雄, 小山大介, 松川真美, 液晶層多層化が超音波式液晶レンズの光学特性に与える影響, 一般社団法人レーザー学会　学術講演会第42回年次大会 Jan. 2022 (Oral)

岩瀬貴大，**J. Onaka**, 小山大介，松川真美, 液晶層厚みが超音波式液晶レンズの光学特性に与える影響, 第42回超音波エレクトロニクスの基礎と応用に関するシンポジウム Oct. 2021 (Oral)

J. Onaka, T. Iwase, D. Koyama, M. Matsukawa, "Evaluation of the Optical Characteristics of the Liquid Crystal Lens Using a Shack-Hartmann Wavefront Sensor", *IEEE International Ultrasonics Symposium*, Sep. 2021 (Oral)

J. Onaka, T. Iwase, D. Koyama, M. Matsukawa, "Ultrasound Liquid Crystal Lens with Radial Focal Displacement", *IEEE International Ultrasonics Symposium*, Sep. 2021 (Poster)

T. Iwase, **J. Onaka**, D. Koyama, A. Emoto, M. Matsukawa, "Measurement of the Orientational Angle of Liquid Crystal Molecules Induced by Ultrasound Vibration", *IEEE International Ultrasonics Symposium*, Sep. 2021 (Poster)

岩瀬貴大，**J. Onaka**，江本顕雄, 小山大介，松川真美，超音波振動下における液晶レンズ内部の液晶配向の測定, 日本音響学会 2021 年秋季研究発表会 Sep. 2021 (Oral)

J. Onaka, T. Iwase, D. Koyama, M. Matsukawa, "Ultrasound liquid crystal lens based on multichannel transducer for image stabilization", 日本音響学会 2021 年秋季研究発表会 Sep. 2021 (Oral)

J. Onaka, T. Iwase, M. Fukui, D. Koyama, M. Matsukawa, “Expansion of ultrasonically controlled liquid crystal lens aperture using traveling wave”, 電子情報通信学会 超音波研究会 Jan. 2021 (Oral)

J. Onaka, T. Iwase, D. Koyama, “Variable-focus in radial direction in liquid crystal lens using ultrasound vibration”, *IEEE International Ultrasonics Symposium*, Sep. 2020 (Poster)

T. Iwase, **J. Onaka**, D. Koyama, A. Emoto, K. Nakamura, M. Matsukawa, “Concave liquid crystal lens with a large aperture using ultrasound traveling wave”, *IEEE International Ultrasonics Symposium*, Sep. 2020 (Poster)

J. Onaka, Y. Harada, M. Fukui, D. Koyama, M. Matsukawa, “Variable-focus in radial direction in liquid crystal lens using acoustic radiation force”, 第 40 回超音波エレクトロニクスの基礎と応用に関するシンポジウム Nov. 2019 (Poster)

PATENT

小山大介, **J. Onaka** 特願 2021-011098, 超音波式液晶レンズおよび超音波式液晶レンズの制御方法

TABLE OF CONTENTS

LIST OF SYMBOLS

Symbol	Meaning
$\vec{n}$	Vector which indicates the orientation of a nematic liquid crystal
Δn	optical anisotropy or birefringence
n_o	refractive index of ordinary light rays
n_e	refractive index of anomalous light rays
v	velocity of light in the medium
c	velocity of light in a vacuum
K_{11}	elastic constant of splay
K_{22}	elastic constant of twist
K_{33}	elastic constant of bend
F	free energy of distortions of nematic liquid crystal
V_{th}	threshold voltage
$\Delta\varepsilon$	dielectric anisotropy
k_{eff}	Average of the elastic constants
ε_0	dielectric constant of a vacuum
f	Focal length
d	liquid layer thickness
r	liquid layer radius
p	Acoustic wave pressure
c_m	speed of sound in the fluid media
CH1–CH4	piezoelectric ceramic quadrants from 1 to 4
E_x and E_y	electric field in the x and y directions respectively
E_x'and E_y'	electric field after passing the LC in the x and y directions respectively
J	Jones matrix
ϕ_x and ϕ_y	Shifted phase in the x and y directions respectively
k	wave number of the incident light
λ	wavelength of the incident light
$\Delta\phi$	phase difference
θ	liquid crystal molecular inclination
I(x,y)	intensity distributions
I_{max}	maximum diffraction intensity
ε	Tensor of anisotropic dielectric constants
ΔZ	optical path difference
n_{eff}	refractive index of LC

CHAPTER 1: GENERAL INTRODUCTION

1.1. MOTIVATION

The lens is one of the most commonly used optical devices. We even see the world through our own lenses. Lenses act as refracting devices that alter the light distribution, regardless of whether they are used for light waves, microwaves, radio waves, or even sound waves [1.1]. The configuration of any particular lens is determined by the wavefront reshaping required to accomplish its intended purpose. For example, through contraction of the surrounding muscles, the radius of curvature of the human eye (which has a crystalline lens) can be altered to perform focusing. This anatomy and image formation based on refracting lenses and mirrors have inspired the same mechanics for enhancing vision not possible with the naked eye [1.2]. Examples include microscopes and telescopes. Other adaptive optical elements mimic eyes, such as camera lenses, focus control in laser processing, and fast-focusing in machine vision, for scientific, commercial, and medical applications [1.3].

The miniaturization of electronics has made a significant impact in optical systems [1.4] through higher speeds, lower costs, and fewer mechanical parts. Traditional optical systems use actuators or gear systems to move glass and/or plastic lenses inside cameras to vary the focal length and adjust the focus. This type of optical system requires sufficient space to accommodate the components used to produce the physical movements that generate the focus control functions, magnification and field of view via a complex mechanical system composed of devices such as voice coil, piezoelectric, and stepping motors - which requires mechanical translation and may cause the systems to be bulky [1.5].

Although the first cameras appeared in around 1840, they were very bulky and not portable, mainly because of the poor sensitivity of the film used back [1.6]. The continuous improvement and advancement of the electronics of optical systems enabled significant reductions in the size of the camera making them more compact and portable. However, it remains true that the lens is generally the most expensive and least understood part of a

camera [1.7]. Furthermore, the optical lens design is not considered a simple task, because it involves many parameters, such as surface profile types, radius of curvature and image quality, in addition to cost and manufacturing limitations. The entire camera market has been experiencing exponential growth since the transition from analog to digital cameras around 2000, but the real breakthrough came with the smartphone photography market that started around 2005. Since then, a considerable number of people have had access to the camera phones. It is noticeable that the smartphone cameras have becoming the world's most popular way of capturing photographs in recent years.

Considering that around 40% of the world population (more than 7 billion people) has a smartphone, if we assume that each person that has a smartphone in the world takes one picture per day using their respective device, it is estimated that more than 1 trillion of pictures are taken per year by using only smartphone cameras around the world. Furthermore, the smartphone cameras provide even better images qualities every upgrade and optical zoom with additional cameras. However, compared to the digital single-lens reflex (DSLR) cameras, the cameras of smartphones still present lower performance and show disadvantages in some aspects, especially considering professional photography parameters. The main reason is that the DSLRs use a substantial space for a set of lenses that enable deeper optical zoom and to adjust the focal lengths, as already mentioned. Conversely, the smartphones are taking advantage of its multi-cameras combined with algorithms to produce high dynamic range (HDR) images, since the size is crucial for smartphones that are expected to be pocket-sized. Although the sensors built into these devices are getting better, improving image depth and performance in low-light conditions, it is noteworthy that there has been far more advancement in algorithms and hardware than in lenses technology in smartphones and other optical devices in general in the last years.

Smartphone cameras have changed the photography business and consequently the camera market [1.8]. According to the Camera & Imaging Products Association (CIPA) - a Japan-based industry group with members such as Olympus, Canon and Nikon, digital cameras went from their peak of 121 million units sold in 2010 to just 8 million in 2021 [1.9].

It represents an 11-year drop of 93%. On the other hand, global smartphone shipments reached 1.39 billion units in 2021 [1.10]. The portability, small size and multifunction of the smartphones make them the number-one way of taking pictures. However, a smartphone's camera system is usually its most expensive feature – 30% of those costs can be attributed to the optical elements, including image stabilization and autofocus actuator, 30% to the module and assembly and 40% to the image sensor [1.6, 1.11], meaning that the lenses and its mechanics represents a considerable cost in the smartphone's optical system. Furthermore, camera modules have also been developed and produced for automobile, medical and industrial applications, although smartphones represent over 80% of the market share [1.6].

One of the challenges faced by the smartphone camera manufactures is the fact that the cameras should be enclosed in a very flat device 7-10 mm thick, meaning that a miniaturized camera is required. Considering the dimensions of the device and the image sensor board, the depth of a smartphone optic elements must not exceed 6 mm [1.6]. In addition, for the image sensor to work effectively, the quality of the optical image as viewed through the lens must be adequate.

In the last few years, smartphone manufactures started to implement hybrid zooms through multi-camera systems using different lenses with different focal lengths (i.e., by increasing the number of individual cameras in the smartphone, it is possible to increase the zoom range). An optical resolution is strongly influenced by the lens's optical design, which is strongly influenced by its equivalent focal length. This multi-camera system become a trend due to size limitation of the smartphones. Digital zooms have been also implemented; however, it is not an ideal solution to optimize the zoom because of the image resolution limitations.

The majority of today's smartphones use plastic materials for camera lenses instead of glass. The main reason it that the aspherical plastic lens can improve the optical performance and it is suitable for volume production and flexible shapes, meaning the plastic lens is a key element with high accuracy to a miniaturized optical system [1.12 - 1.14]. Aspherical plastic lenses have been widely adopted due to the development of new optical

materials, designs, and simulation methods. Furthermore, lens module is one of the most crucial components for obtaining high-quality images [1.14]. However, a camera optical system is still a relatively large product, since many lenses are used, and a driving device for moving the lenses is also required. Therefore, it is expensive to manufacture such an optical system.

Another problem of the traditional camera system is that the mechanical moving parts decrease its robustness. In addition, miniaturization of these traditional mechanical element are desirable for many applications, thus increasing their cost and fragility, and making these elements impracticable for implementation in low-cost miniaturized devices. In terms of optical design complexity, the human eye structure is much simpler. Based on that consideration, single-element adaptive lenses have been in development as alternative elements with the aim of replacing traditional optical systems with multiple solid elements to produce more compact and robust optical systems with fewer mechanical elements. Liquid lenses [1.15, 1.16] and liquid crystal (LC) lenses [1.17, 1.18] are good examples of these adaptive elements. The former are based on changes in the shape of the liquid, while the latter are based on alteration of the refractive index of the liquid crystal material. These adaptive lenses with variable focal lengths have drawn considerable attention because of their wide range of applications in industry, including vision care, aberration correction, consumer electronics (e.g., smartphone, digital cameras), and biomedical imaging [1.19].

1.2. STATE OF ART OF LIQUID CRYSTAL LENSES

Over the last decades, researchers have developed effective techniques to reduce the size, weight, materials and assembly costs of optical systems. A better understanding of materials and manufacturing processes is fundamental for further advancements. Use of tunable variable-focus lenses that enable camera functionalities without mechanical moving parts is one way to meet the demands of miniaturized optical systems. Novel optical lenses with ultrathin structures and low weight have become very attractive and have played an important role in the miniaturization of traditional optical systems. For instance, in 2021,

Xiaomi, Chinese mobile company, released a brand-new smartphone with a variable-focus liquid lens [1.20]. The liquid lens works similarly to an eye's lens and may replace an existing, static optical glass/plastic lens. In liquid lenses, the focal length can be altered by varying the curvature of the isotropic liquid inside the lens [1.21-1.23]. In the case of Xiaomi's phone, the liquid lens covers the function of two lenses. In other words, the camera uses a voice coil motor system to manipulate the liquid, which allows the camera to perform a macro and telephoto camera module [1.20], indicating that the technology is still relying on mechanical moving parts. Although most of the liquid lens utilize electrowetting [1.24] to change the focal length, the response time for focusing depends mostly on the material properties of liquids, resulting in longer response time than that of the lens with conventional mechanical actuators (i.e., a few tens of milliseconds). A high-speed response can be achieved by using liquid lenses and high-speed piezoelectric actuators, although the system tends to be bulky [1.25].

The major limitation of these adaptive lenses technologies is related to the materials properties. For instance, the liquid lens can present bubbles and emulsion droplets depending on the temperature, which might reduce its operation life. In a traditional lens (made of glass or plastic), the lens shape and the optical path difference are determined by the molded shape of the glass/plastic surface, and the refractive index of the lens material is constant (it is not tunable). Conversely, liquid crystal materials can have their refractive indices altered and controlled via application of a voltage. The possibility of generation of the desired refractive index profile using an external field then becomes a promising alternative to optimize the lens performance. The anisotropic physical properties of nematic liquid crystals are similar to those of solids, but these crystals flow like liquids. Due to their physical properties, including their high liquidity and moderate dielectric anisotropy, nematic liquid crystals are widely used in optical devices, e.g., LC displays, and make downsizing of these devices possible.

LC variable-focus lenses without any mechanical movement were first proposed in the late 1970s [1.17, 1.18]. LC lenses contain liquid crystals that change orientation mostly

in response to an electric field, thus changing their refractive index. Strictly speaking, changes in the focal length can be obtained by applying an electric field with electrodes. As a voltage is applied over a LC layer, the average molecular orientation changes, aligning them along the direction of the electric field. Because of this reorientation, the light passing through the LC layer will experience a different refractive index. Having a suitable positional-dependent refractive index profile leads to curvature of the phase profile of the transmitted light, resulting in focused light beam - which is the operating principle of LC lenses. One of the first LC lens prototype was based on a glass spherical cavity filled with a liquid crystal. The LC directors were aligned by an applied electric field, and the effective refractive index of the LC layer was varied by a voltage applied using a discrete electrical circuit [1.18]. In the late 1980's, the use of indium tin oxide (ITO) electrodes in LC lenses to generate a nonuniform electric field and thus enable focusing effects was proposed [1.26]. Subsequently, several types of LC lenses with variable focusing functions have been reported [1.27-1.31].

Improvements and new LC device designs continue to be proposed, including use of an additional floating electrode to improve the optical quality of an LC lens [1.28, 1.32], and use of a weakly conductive layer to obtain the refractive index profile required for LC lens operation [1.33]. Most of the liquid crystal lenses that have been developed to date rely on use of indium-tin-oxide (ITO) electrodes to generate the required electric fields through their LC layers because of the relatively high conductivity and optical transparency of ITO and its compatibility with the LC alignment layers. Nevertheless, because they use the rare metal indium and the sputter deposition fabrication method, implying a combination of high costs and low flexibility, it is inconvenient to use these electrodes for more flexible LC devices.

Acoustic actuation offers an alternative method to replace the ITO electrodes and overcome the related drawbacks to enable development of tunable LC variable-focus lenses. Because the underlying theory applies to both mechanical and electromagnetic waves, acoustic lenses focus sound in a similar manner to the way in which optical lenses focus light [1.34]. For instance, a tunable acoustic gradient index of refraction lens (i.e., TAG lens) uses

acoustic waves to excite fluid inside a cylindrical cavity and continuously change its refractive index [1.35]. Induced refractive index change results in a lens capable of adjusting focal length at kHz rates, which can be used in imaging and beam shaping. In other words, TAG lens uses a piezoelectric transducer to create a standing acoustic wave in the refractive liquid, and thereby can achieve focal scanning rates that is widely used for optical inspection for high-speed three-dimensional (3D) imaging systems [1.35].

On the other hand, the acousto-optical properties of nematic liquid crystals have been studied since the 1960s [1.36-1.39]. Propagation of ultrasonic bulk waves in a nematic liquid crystal layer causes deformation of the orientational field of the liquid crystal molecules. However, there is a threshold ultrasonic wave intensity value, above which ultrasound can induce variations in the molecular orientation of the nematic liquid crystal layer because the layer becomes birefringent [1.37, 1.39]

The induced birefringence in liquid crystals by ultrasound is a function of acoustic energy. The phenomenon is analogous to birefringence caused by an electric field [1.40]. The following acousto-optical phenomena have been observed in nematic liquid crystals due to bulk acoustic waves: molecular reorientation, narrow domain formation, defect formation, light scattering. In this thesis, we focus our attention on molecular reorientation and light scattering, because they are fundamental for the optical devices.

This thesis manuscript presents a complete analysis on the liquid crystal lens controlled by ultrasonic waves, that use the interaction between nematic liquid crystals and bulk acoustic waves [1.41] based on the inverse piezoelectric effect, by which the piezoelectric ceramic uses acoustic waves to drive the liquid crystal molecules via the acoustic radiation force [1.42] to produce a variable-focus lens. The lens simulated design, experimental set-up and driving scheme were devised with the possibility of miniaturizing optical electronics devices kept in mind.

1.3. OBJECTIVE

The main objective of this thesis work is to study and to develop new control methods for an ultrasound liquid crystal lens. Fundamental principles, basic concepts, techniques, lens design, fabrication, and experimental and simulation results are provided in detail, as well as discussion of the results and conclusions.

Chapter 2 introduces the theory behind the liquid crystal lens, stating the liquid crystal material physical properties and the advantages of the use of this material compared to traditional lenses (i.e., made of plastic/glass). Additionally, the fundamental parameters considered for development of liquid crystal devices are provided.

Chapter 3 presents the fundamental of acousto-optics devices, including information about ultrasound waves and its main applications. The progress on acousto-optics devices, with general information about piezoelectric transducers and the acoustic actuation for ultrasound controlled liquid crystal lenses principles, were also presented.

Chapter 4 describes the experimental set-up and procedures used for the development of the ultrasound liquid crystal lens, including the simulations methods and the liquid crystal lens fabrication steps.

Chapter 5 describes the ultrasound liquid crystal lens geometry based on a multichannel transducer for the generation of traveling waves to expand the lens aperture.

Chapter 6 explore more the functionalities of the multichannel transducer and discuss the driving conditions to control the focal point in the radial direction for image stabilization.

Chapter 7 presents a double-layered ultrasound liquid crystal lens model, which illustrates combination of liquid crystal material properties in a structure with two liquid crystal layers to improve the lens performance overall.

Finally, Chapter 8 summarizes these studies and presents the conclusion and outlook of the control methods for the ultrasound liquid crystal lens considering its design and evaluation.

REFERENCES

[1.1] E. Hecht, “Optics”, 4th ed. *Addison-Wesley, San Francisco*, vol. 2, 2002.

[1.2] M. F. Land, “The optics of animal eyes”. *Contemporary Physics*, vol. 29, no. 5, pp.435-455, 1988.

[1.3] U. Wittrock, “Adaptive Optics for Industry and Medicine”, *Proceedings of the 4th International Workshop, Münster, Germany*, vol. 102, pp. 19-24, Springer Science & Business Media, 2005.

[1.4] W. A. Atherton, “From Compass to Computer: History of Electrical and Electronics Engineering,” *Macmillan International Higher Education*, 1984.

[1.5] L. Bergstein, “General theory of optically compensated varifocal systems,” *The Journal of the Optical Society of America*, vol. 48, pp. 154–171, 1958.

[1.6] V. Blahnik and O. Schindelbeck, "Smartphone imaging technology and its applications," *Advanced Optical Technologies*, vol. 10, no. 3, pp. 145-232, 2021.

[1.7] R. Kingslake, “A history of the photographic lens,” *Academic press*, 1989.

[1.8] DXO, “Smartphones versus Cameras: Closing the Gap on Image Quality”, 2020. Available at: https://www.dxomark.com/smartphones-vs-cameras-closing-the-gap-on-image-quality/.

[1.9]CIPA, Camera and Imaging Products Association. Available at: https://www.cipa.jp/e/stats/dc-2021.html.

[1.10] Counterpoint Research, 2021. Available at: https://www.counterpointresearch.com/global-smartphone-share/.

[1.11] R. Liu and P. Cambou, “CMOS camera module industry for consumer & automotive,” *Market & Technology Report*, Yole Développement, 2020.

[1.12] S. Yamaguchi, H. Sato, N. Mori and T. Kiriki, “Recent technology and usage of plastic lenses in image taking objectives,” *Advancements in Polymer Optics Design, Fabrication, and Materials*, vol. 5872, pp. 94-101 2005.

[1.13] M. P. Schaub, “The Design of Plastic Optical Systems,” Bellingham, *SPIE Press*, 2009.

[1.14] J.Y. Song, T. H. Ha , C.W. Lee , J.H. Lee and D.H. Kim, "Development of minimized-assembly system for camera phone lens module," *Proceedings of the 11th euspen International Conference*–Como., 2011.

[1.15] S. Xu, Y. J. Lin, and S. T. Wu, "Dielectric liquid microlens with well-shaped electrode," *Optics Express*, vol. 17, no. 13, pp. 10499-10505, 2009.

[1.16] A. Mermillod-Blondin, E. McLeod, and C. B. Arnold, "High-speed varifocal imaging with a tunable acoustic gradient index of refraction lens," *Optics Letters*, vol. 33, no. 18, pp. 2146-2148, 2008.

[1.17] C. Bricot, M. Hareng, and F. Spitz, “Optical projection device and an optical reader incorporating this device,” (U.S. Patent No. 4,037,929 1977).

[1.18] S. Sato, "Liquid-crystal lens-cells with variable focal length," *Japanese Journal of Applied Physics*, vol. 18, no. 9, pp. 1679 -1684, 1979.

[1.19] L. Guoqiang, “Chapter 4 - Adaptive Lens”, edited by E. Wolf, In *Progress in optics*, vol. 55, pp. 199–283. Elsevier, 2010.

[1.20] SystemPlus Consulting, "Liquid Lens Camera Module in the Xiaomi Mi MIX FOLD," 2021. Available at: https://www.systemplus.fr/reverse-costing-reports/liquid-lens-camera-module-in-the-xiaomi-mi-mix-fold/

[1.21] C. B. Gorman, H. A. Biebuyck, and G. M. Whitesides, "Control of the shape of liquid lenses on a modified gold," *Langmuir*, vol. 11, no. 6, pp. 2242–2246, 1995.

[1.22] S. Kuiper and B. Hendriks, "Variable-focus liquid lens for miniature cameras," *Applied Physics Letters*, vol. 85, no. 7, pp. 1128–1130, 2004.

[1.23] F. Krogmann, W. Mönch, and H. Zappe, "A MEMS-based variable micro-lens system," *Journal of Optics A: Pure and Applied Optics*, vol. 8, no. 7, pp. S330–S336, 2006.

[1.24] B. Berge and J. Peseux, "Variable focal lens controlled by an external voltage: An application of electrowetting," *The European Physical Journal E*, vol. 3, no.2, pp.159–163, 2000.

[1.25] H. Oku and M. Ishikawa, "High-speed liquid lens with 2 ms response and 80.3 nm root-mean-square wavefront error," *Applied Physics Letters*, vol. 94, no. 22, p. 221108, 2009.

[1.26] T. Nose and S. Sato, "A liquid crystal microlens obtained with a non-uniform electric field." *Liquid Crystals*, vol. 5, no. 5, pp. 1425-1433, 1989.

[1.27] L. Li, D. Bryant, T. V. Heugten, and P. J. Bos, "Near-diffraction-limited and low-haze electro-optical tunable liquid crystal lens with floating electrodes," *Optics Express*, vol. 21, no. 7, pp. 8371-8381, 2013.

[1.28] J. Beeckman, T. H. Yang, I. Nys, J. P. George, T. H. Lin, and K. Neyts, "Multi-electrode tunable liquid crystal lenses with one lithography step," *Optics Letters*, vol. 43, no. 2, pp. 271-274, 2018.

[1.29] M. Ye and S. Sato, "Optical properties of liquid crystal lens of any size," *Japanese Journal of Applied Physics*, vol. 41, no. 5B, pp. L571-L573, 2002.

[1.30] M. Ye, S. Hayasaka and S. Sato, “Liquid crystal lens array with hexagonal-hole-patterned electrodes,” *Japanese Journal of Applied Physics*, vol. 43, no. 9R, pp. 6108-6111, 2004.

[1.31] M. Kawamura, K. Nakamura, and S. Sato, "Liquid-crystal micro-lens array with two-divided and tetragonally hole-patterned electrodes," *Optics Express*, vol. 21, no. 22, pp. 26520-26526, 2013.

[1.32] T. Galstian, K. Asatryan, V. Presniakov, A. Zohrabyan, A. Tork, A. Bagramyan, S. Careau, M. Thiboutot, and M. Cotovanu, “High optical quality electrically variable liquid crystal lens using an additional floating electrode,” *Optics Letters*, vol. 41, no. 14, pp. 3265-3268, 2016.

[1.33] T. Vanackere, T. Vandekerckhove, E. Claeys, J. P. George, K. Neyts, and J. Beeckman, "Improvement of liquid crystal tunable lenses with weakly conductive layers using multifrequency driving," *Optics Letters*, vol. 45, no. 4, pp. 1001-1004, 2020.

[1.34] D. Tarrazó-Serrano, S. Pérez-López, P. Candelas, A. Uris, and C. Rubio, “Acoustic focusing enhancement in fresnel zone plate lenses," *Scientific Reports*, vol. 9, no.1, p. 7067, 2019.

[1.35] S. Kang, E. Dotsenko, D. Amrhein, C. Theriault, and C. B. Arnold, "Ultra-high-speed variable focus optics for novel applications in advanced imaging," *Photonic Instrumentation Engineering V*, vol. 10539, International Society for Optics and Photonics, 2018.

[1.36] H. Heilmeier, L. A. Zanoni, and L. A. Barton, “Dynamic scattering in nematic liquid crystals,” *Applied Physics Letters*, vol. 13, no. 1, pp. 46-47, 1968.

[1.37] W. Helfrich, “Orienting action of sound on nematic liquid crystals,” *Physical Review Letters*, vol. 29, no. 24, pp. 1583-1586, 1972.

[1.38] E. Lord and M. M. Labes, “Anisotropic ultrasonic properties of a nematic liquid crystal,” *Physical Review Letters*, vol. 25, no. 9, pp. 570-572, 1970.

[1.39] M. Witkowska-Borysewicz and A. Śliwiński, "Optically detected variations of nematic liquid crystal orientation induced by ultrasound," *Journal de Physique*, vol. 44, no. 3, pp. 411-420, 1983.

[1.40] M. Bertolotti, S. Martellucci, F. Scudieri and D. Sette, “Acoustic modulation of light by nematic liquid crystals,” *Applied Physics Letters*, vol. 21, no. 2, pp. 74-75, 1972.

[1.41] W. G. Laidlaw, “Response of a Nematic Liquid Crystal to an Acoustic Field,” *Molecular Crystals and Liquid Crystals*, vol. *59*, no. 1-2, pp. 13-26, 1980.

[1.42] B. T. Chu and R. E. Apfel, “Acoustic radiation pressure produced by a beam of sound.” *The Journal of the Acoustical Society of America*, vol. 72, no. 6, pp. 1673-1687, 1982.

CHAPTER 2: THEORY BEHIND LIQUID CRYSTAL LENSES

2.1. TRADITIONAL LENSES

The optical studies started with the philosophers of antiquity that speculated about the nature of light, being familiar with burning glasses, with rectilinear propagation of the light, and with refraction and reflection [2.1]. Lens can be defined as a refracting device that reconfigures the transmitted energy distribution to focus light [2.2]. In other words, the light wave passing through the lens surface will be converged (convex lens) or diverged (concave lens), for instance.

Optical lenses are one of the crucial components to imaging systems. They are made in a wide range of shape and materials. Traditionally, lenses are made from glass, resin, or plastic after injection molding or cutting process. Increasing numerical aperture (or resolution) of the lens necessitates thicker and heavier optics [2.3]. If optical systems are designed with economic constraints in mind, it is not generally possible to achieve diffraction-limited performance through extremely precise shaping and polishing processes. Most often, systems are made with undesired optical distortions and aberrations. For the purpose of correcting those aberrations, more than one lens group is usually used, usually with spherical elements. The system may be simplified by replacing two or three spherical lenses with one aspheric lens with a parabolic profile. However, this method generally results in higher costs for the system [2.4].

The focal length of a conventional lens is also fixed. In imaging systems with variable focal lengths, variable power is achieved by mechanically moving components that adjust the distance between lenses. Consequently, this approach makes the system bulky, inefficient, and unusable for some applications. In a typical lens design (e.g., for plastic/glass-based lenses), the lens shape and the optical path difference are determined by the polished shape of the material surface, and the refractive index of the lens material is homogeneously constant. Liquid crystal materials, in contrast, can have their refractive indexes tuned via application of a voltage. The possibility of generation of the desired refractive index profile

using an external stimulus then becomes key to the lens performance [2.4]. For this reason, liquid crystal materials are highly appealing for use in optical devices.

2.2. LIQUID CRYSTAL FUNDAMENTALS

Liquid crystal is a material that presents an intermediate state between liquid and crystal. Despite having similar anisotropic physical properties to solids, liquid crystals flow like liquids. In addition, liquid crystals are classified according to the type and shape of constituent molecules, or the generation method. They are considered thermotropic if the order of its components is determined or changed by temperature and lyotropic if experiences its phase transitions by adding or removing a solvent [2.5]. However, many systems share characteristics of both thermotropic and lyotropic liquid crystal. Thermotropic liquid crystals can be classified into the phases smectic, cholesteric and nematic depending on the spatial regularity of the alignment structure and the transitions from one phase to another phase are driven by varying temperature (Fig. 2.1). Typically, these phases are fluidic, with individual molecules able to freely move and rotate, but they can also possess orientational and positional order.

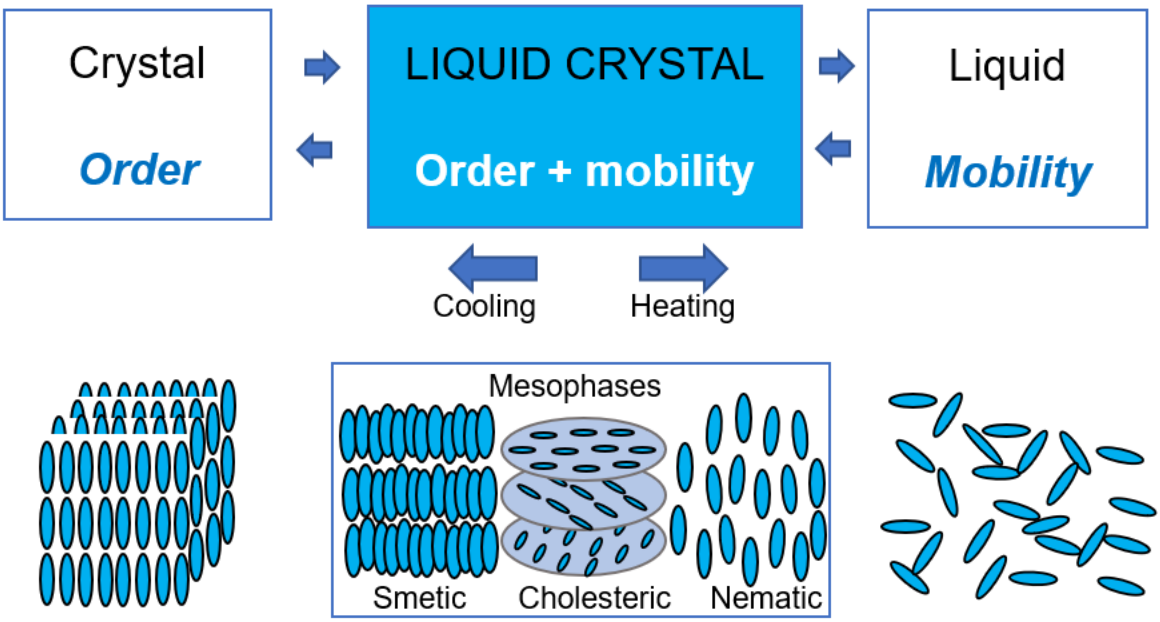

Figure 2.1 Schematic representation of liquid crystal material according to temperature variation.

The materials used in this thesis work form nematic liquid crystal phases only. As a result of their directional ordering, nematic liquid crystals exhibit many anisotropic properties, and can be manipulated with relatively small fields thanks to their large response functions [2.6]. Their physicochemical properties, such as their dielectric properties and their birefringence, are remarkable features that make nematic liquid crystals uniquely suitable for many industrial electro-optical and photonics applications, including liquid crystal displays and lenses, phase modulators, and optical interconnections, especially because their molecular orientations can be controlled easily using an external field [2.7].

2.3. NEMATIC LIQUID CRYSTAL PHYSICS

2.3.1. OPTICAL ANISOTROPY OR BIREFRINGENCE

The nematic liquid crystal consists of a group of rod-shaped molecules and forms a regular molecular arrangement. The orientation of a nematic liquid crystal is normally

determined by a vector $\vec{n}$, also called the director *n* (Figure 2.2 (a)). Because of this molecular alignment, the physical properties of the material, such as refractive index, electrical conductivity, permeability, differ depending on the direction of the long axis.

In the liquid crystalline phase, anisotropy appears in various physical quantities, reflecting the intermediate state between liquid and solid. For example, in the isotropic phase, the material is spherical in three dimensions and has a uniform refractive index no matter how light is incident. In contrast, the nematic phase has uniaxial anisotropy, which means that the perceived refractive index of light traveling through the liquid crystal changes depending on the relationship between the optic axis of the nematic phase and the direction of polarization of the incident light (Figure 2.2 (b)).

Therefore, light whose polarization plane does not coincide with the optic axis of the nematic phase changes its polarization state due to a phenomenon called birefringence. In nematic phases with uniaxial anisotropy, the anisotropy of the refractive index is often expressed as the difference Δn (i.e., optical anisotropy or birefringence) between the refractive index n_o of ordinary light rays (polarization direction perpendicular to the anisotropic axis) and the refractive index n_e of anomalous light rays (polarization direction parallel to the anisotropic axis) as:

$$\Delta n = n_0 - n_e \tag{2.1}$$

For nematic liquid crystal with rod-like shape molecules $n_e > n_o$, where Δn is positive and between 0.02 and 0.4 [2.8]. For discotic and chiral shape nematic liquid crystal molecules $n_e < n_o$ and then the negative birefringence is associated with the discotic or columnar phase [2.8]. The nematic liquid crystal used in this work is the rod-like shape type.

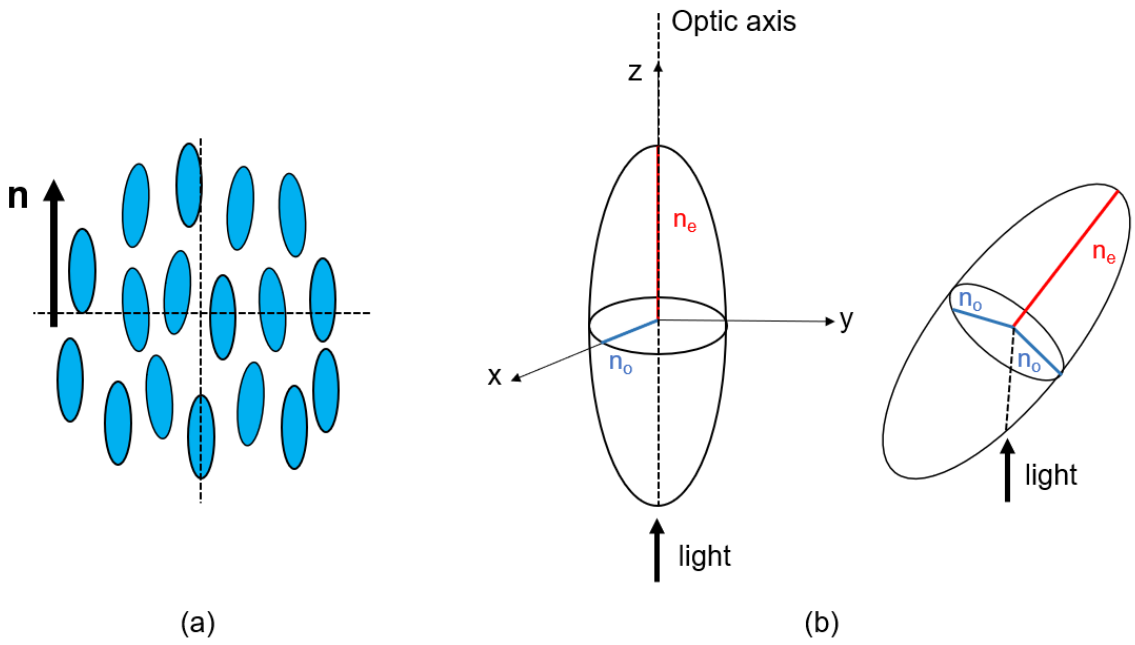

Figure 2.2 (a) Director *n* of nematic liquid crystal, (b) uniaxial liquid crystal molecule schematic

2.3.2. DIELECTRIC ANISOTROPY AND ALIGNMENT MECHANISM

When an electric field is applied to liquid crystal molecules, they exhibit dielectric anisotropy ($\Delta\varepsilon$). The permittivity of a material determines how an electric field is acted upon a dielectric medium and it is determined by a material's ability to polarize upon application of an electric field, which in turn partially cancels the field induced within it [2.9]. Strictly speaking, the intermolecular forces are rather weak and can be perturbed by an applied electric field. The liquid crystal molecules would align themselves with their dipoles parallel to the field, reversing their previous orientation (Fig. 2.3). Large permittivity values lead to large refractive indices, which result in relatively slow wave propagation. The refractive index *n* is related to the velocity of light in the medium (*v*) and the velocity in a vacuum (*c*) by $n = c/v$.

In most liquid crystal devices, the liquid crystals are sandwiched between two substrates coated with alignment layers. In the absence of externally applied fields, the

orientation of the liquid crystal in the cell is determined by the anchoring condition of the alignment layer.

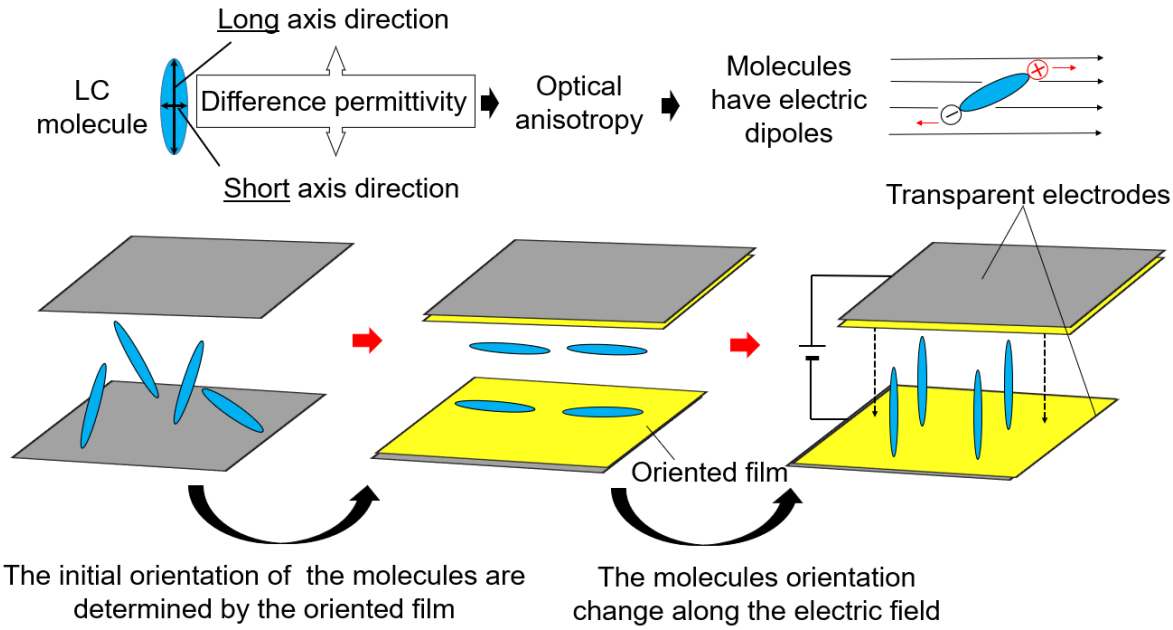

Figure 2.3 Principle of nematic liquid crystal devices

In electro-optical devices, it is usually required that the liquid crystal director is unidirectional. Due to the physical properties of the oriented film, the alignment of liquid crystal molecules is aligned in a certain direction. As a result, the initial orientation of the liquid crystal molecules is determined, and it is possible to change the orientation by applying an electric field, as shown in Fig. 2.3.

Therefore, the initial state of nematic liquid crystal must be well-controlled in order to use it in optical devices. In the absence of external stimuli, this alignment determines the homogeneity of the director field. The surfaces surrounding the nematic liquid crystal can be manipulated to achieve precise alignments (Fig. 2.4), eg., horizontal (planar) and vertical (homeotropic) alignment types.

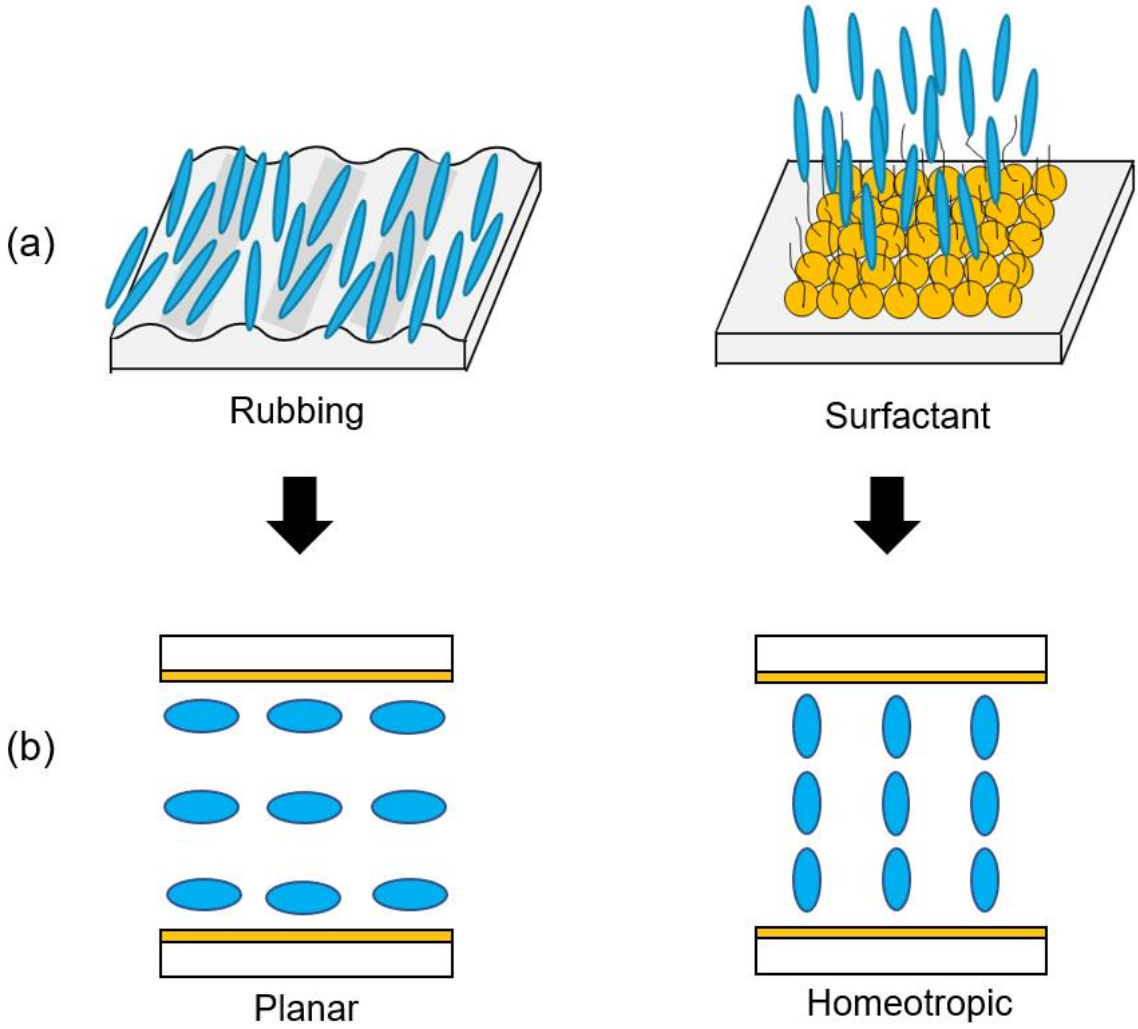

Figure 2.4 (a) Initial orientation mechanism, (b) Planar and homeotropic alignment

A variety of alignment techniques have been developed, including mechanically rubbed thin films (Fig. 2.4 (a)) that promotes planar alignment [2.10] and the homeotropic alignment (Fig. 2.4 (b)) that can be achieved by treating the surface with a surfactant (e.g., lecithin and polymers [2.11]). In this thesis work, the alignment film used was vertical alignment type (SE-5811, 248 Nissan Chemical, Japan) to define the initial orientation (homeotropic alignment) without rubbing.

2.4. ELASTIC PROPERTIES

The resistance of a nematic liquid crystal phase to orientational deformation is defined using quadratic order terms and their respective coefficients, which are called elastic constants (splay K_{11}, twist K_{22}, bend K_{33}) [2.12]. The elasticity is the result of an energetic cost associated with deformation of the nematic field due to *n* changes in orientation in space. The deformations can be understood by Fig. 2.5 and their associated elastic constants K_{11}, K_{22} and K_{33} as well as the free energy of distortions of nematic liquid crystal are given by *F* [2.5]:

$$F = \frac{1}{2}\left[K_{11}\left(\nabla .\, \vec{n}\right)^2 + K_{22}\left(\vec{n}.\nabla \times \vec{n}\right)^2 + K_{33}\left(\vec{n}\times\nabla\times\vec{n}\right)^2 \right] \tag{2.2}$$

There is a tendency for the elastic constants to obey $K_{33} > K_{11} > K_{22}$ [2.5]. When weak fields are applied at right angles to the director *n*, they cannot overcome the internal forces. A Fréedericksz transition [2.13] occurs when the applied field is strong enough to overcome these forces and provides the threshold voltage (V_{th}) for perturbation. In addition to the elastic constants presented in this section, the birefringence (Δn) and the dielectric anisotropy ($\Delta\varepsilon$) presented in Section 2.3.1 and in Section 2.3.2, respectively, are crucial parameter for nematic liquid crystal devices, since Δn allows switchable optical properties depending on the polarization plane of the light relative to *n*, while $\Delta\varepsilon$ allows a mechanism to control *n* [2.14]. According to the Fréedericksz transition, the reorientation of the nematic liquid crystal molecules starts to occur with voltage (V) applied above V_{th}. Since the anchoring at the surfaces is strong (due to the alignment film effects), the reorientation will not occur uniformly throughout the liquid crystal material and it will depend on the cell thickness (*d*) – Fig. 2.6.

The value of V_{th} may be predicted from the following equation [2.15]:

$$V_{th} = \pi\sqrt{\frac{k_{eff}}{\varepsilon_0 \Delta\varepsilon}} \tag{2.3}$$

Where k_{eff} denotes the average elastic constants (splay, twist and bend) and ε_0 the dielectric constant of a vacuum.

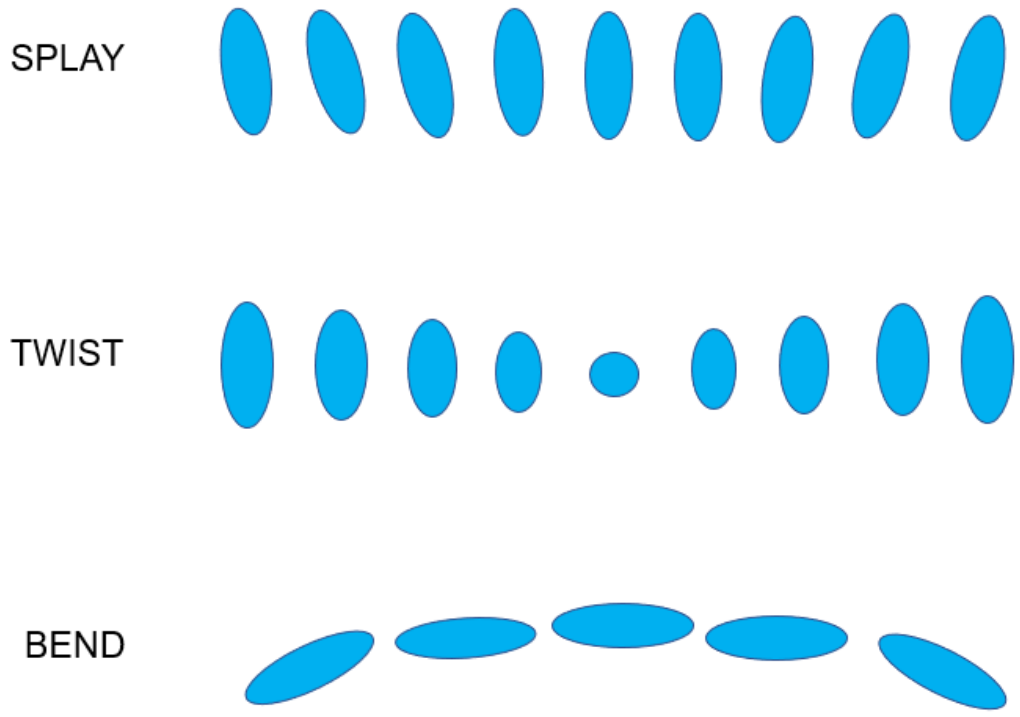

Figure 2.5 Schematic of splay, twist and bend deformation of a nematic field

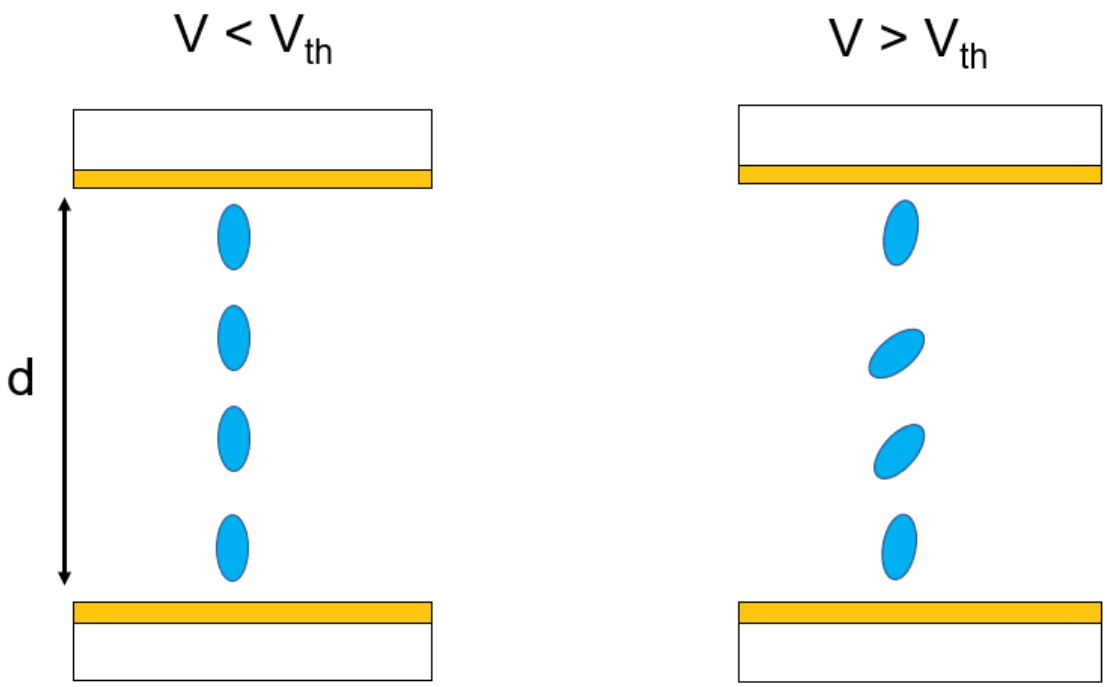

Figure 2.6 Fréedericksz transition and its effects in the reorientation of the LC molecules

2.5. LIQUID CRYSTAL DEVICES

Liquid crystals devices have developed over the years presenting broad applications in display technology such as calculators, smartphones, TVs; and opto-electronic devices, such as laser beam steering. There are a large number of photonic devices which demonstrate the unique advantages of liquid crystals, such as aberration compensators [2.16], polarization controllers [2.17], phase shifters [2.18] and beam modulators [2.19].

2.5.1. LIQUID CRYSTAL LENSES

Liquid crystals are birefringent complex fluids that can be manipulated thermally, electrically, magnetically, or optically, for flexible or reconfigurable lenses. Usually, liquid

crystal lenses consist to a liquid crystal material confined to a thin cell with transparent electrodes (e.g. ITO electrodes in the majority of the cases), as described in Chapter 1. The confined liquid crystal molecules tend to align according to the alignment film that they are in contact with – the elastic forces spread this alignment preference throughout the liquid crystal medium. Finally, by applying an external stimulation (eg., electric field), the molecular reorientation occurs, which can be understood by considering the Fréedericksz transition [2.14]. Because of this reorientation, the light passing through the liquid crystal layer will experience a different refractive index. In contrast, the traditional lenses (i.e. glass and plastic) have a homogeneous index distribution, determined by the material curvature and properties.

Although the first liquid crystal lens prototype was developed in 1979 [2.20], the liquid crystal material was adapted into curved lenses without changing the curvature of the lens structures – Fig. 2.7 – so this lens presented some issues such as low response time, due to the increased liquid crystal layer thickness, and the molecular orientation inhomogeneity in the employed thick and curved layers. In the late 1980's, the LC lens based on liquid crystal sandwiched between two planar ITO coated glass substrates [2.21] inspired many liquid crystal lens prototypes that have been developed to date [2.22]. The sandwiched-type structure is the mostly used for liquid crystal lens configuration. ITO electrodes and ITO-glass substrate have attracted attention due to their relatively high conductivity and high optical transmittance in visible area, and compatibility with liquid crystal alignment layers. Although, ITO present some disadvantages, such as high costs from its sputtering deposition fabrication and use of the rare metal indium, no substance better than ITO, which exhibits transparency, has been found. Furthermore, although the most of the liquid crystal lenses are ITO based lens, they presented different operating principles, including thermal control [2.23, 2.24], voltage control [2.25, 2.26] and different lens design, such as using multi-ring ITO electrode [2.27], hole-pattern ITO electrode [2.28], having similar approaches but using different ITO pattern and characteristics. The alternative lenses prototypes using ultrasound actuation instead of ITO electrodes will be discussed in this thesis.

Liquid crystal lenses with sandwich-based structures then change the curvature of the light wavefront in response to a control signal. Based on wave optics, specifically on Huygen's principle [2.29], the wavefront passing through the lens material then varies (Fig. 2.8), leading to convergence or divergence of the light wave and characterizing positive or negative focal lengths, respectively – liquid crystals are usually stimuli-responsive and thus have tunability of focal length (*f*). A liquid crystal lens modulates waves in this manner by using a gradient-index (GRIN) profile – Fig. 2.8 (b). The focal length of this GRIN-liquid crystal lens depends on the liquid layer thickness (*d*), radius (*r*), and refractive index difference from the center to the edge of the gradient layer. Strictly speaking, there is a gradual variation of the refractive index without the using any curved interfaces. As the wavefront's speed decreases in optically dense regions and accelerates in areas of lower density, a parabolic refractive index is created (with the shape similar to the conventional lenses). The spatial gradient of the refractive index and the lens focal length is then electrically controlled and tunable.

In traditional lenses, conversely, the focal length is not adjustable, but fixed by the shape and characteristics of the material – Fig. 2.8 (a). Furthermore, traditional lenses rely on difference between the refractive index of the lens material and the surrounding environment (e.g. air) and the curvature of their interfaces in order to modify the wavefront.

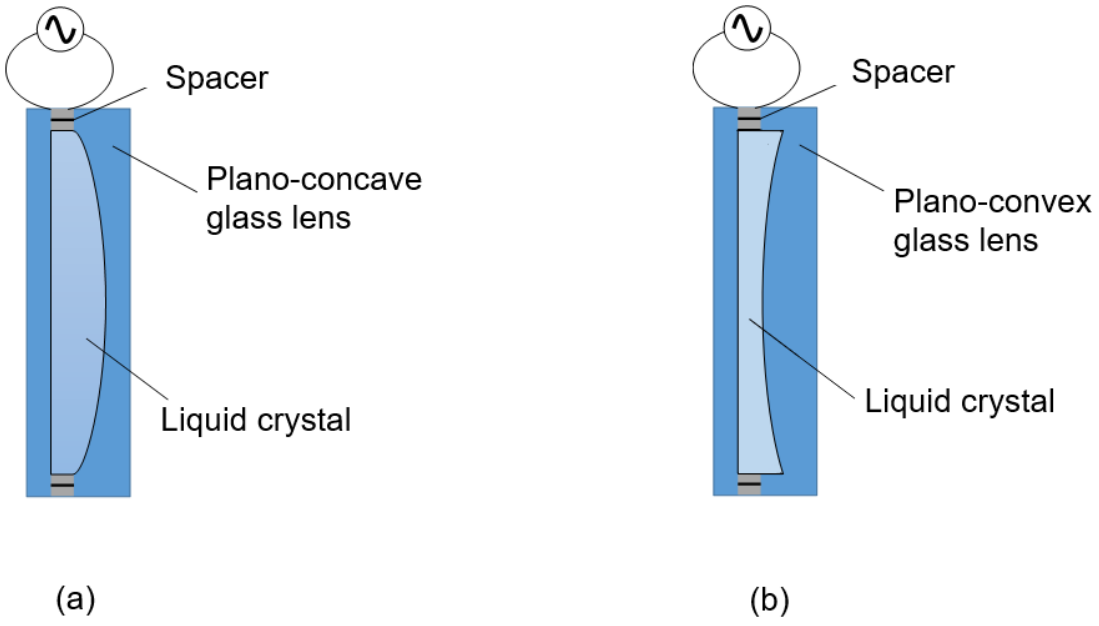

Figure 2.7 First prototypes of liquid crystal lenses: (a) Plano-concave lens (b) Plano-convex lens. Adapted from [2.20]

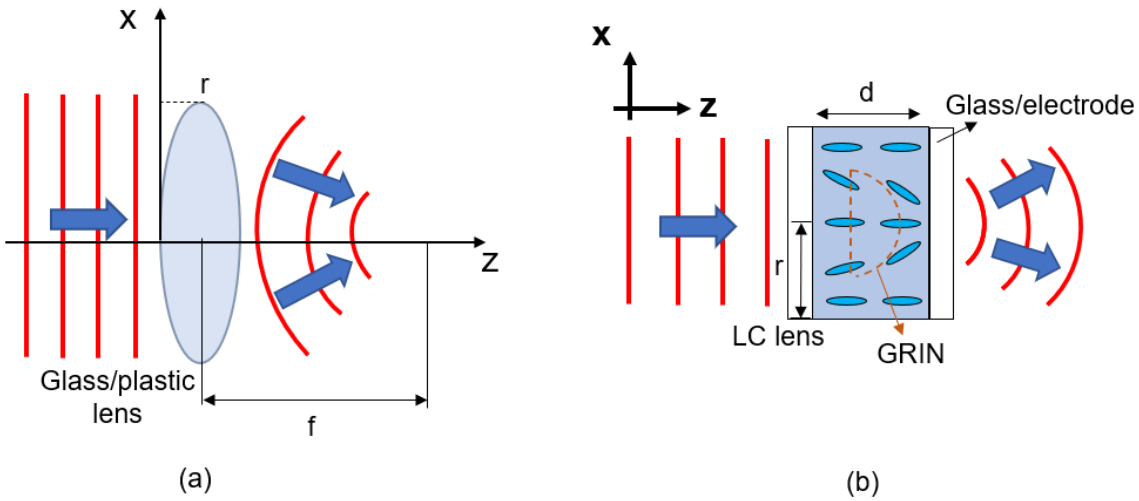

Figure 2.8 (a) Traditional lens (b) LC crystal lens (GRIN type)

REFERENCES

[2.1] M. Born and E. Wolf, “Principles of optics: electromagnetic theory of propagation, interference and diffraction of light,” *Elsevier*, 2013.

[2.2] E. Hecht, “Optics”, 4th ed. *Addison-Wesley, San Francisco*, vol. 2, 2002.

[2.3] S. Banerji, M. Meem, A. Majumder, F. G. Vasquez, B. Sensale-Rodriguez, and R. Menon, "Imaging with flat optics: metalenses or diffractive lenses?" *Optica*, vol. 6, no. 6, pp. 805-810, 2019.

[2.4] L. Shi, L. Li, D. Bryant, D. Duston, and P. J. Bos, "Modeling and design of a tunable refractive lens based on liquid crystals," *Frontiers in Optics 2010/Laser Science XXVI*, p. FThU2, Optical Society of America, 2010.

[2.5] D. K. Yang and S. T. Wu, “Fundamentals of liquid crystal devices.” *John Wiley & Sons*, 2014.

[2.6] P. G. De Gennes, Pierre-Gilles and J. Prost, “The physics of liquid crystals,” *Oxford University Press*, UK, 1993.

[2.7] M. F. Schiekel and K. Fahrenschon, “Deformation of nematic liquid crystals with vertical orientation in electrical fields,” *Applied Physics Letters*, vol. 19, no. 10, pp. 391-393, 1971.

[2.8] P. H. J. Kouwer and G. H. Mehl, "Nematic phases of disc-and rod-shaped molecules," *Molecular Crystals and Liquid Crystals*, vol. 397, no. 1, pp. 1-16, 2003.

[2.9] M. Schadt and W. Helfrich, "Voltage-dependent optical activity of a twisted nematic liquid crystal," *Applied Physics Letters*, vol. 18, no. 4, pp. 127-128, 1971.

[2.10] B.R. Acharya, J. H. Kim and S. Kumar, "Material independent determination of anchoring properties on rubbed polyimide surfaces," *Physical Review E*., vol. 60, no. 6, pp. 6841-6846, 1999.

[2.11]A. A. Sonin, "The surface physics of liquid crystals," *Gordon and Breach: Luxembourg*, 1995.

[2.12] C. W. Oseen, "The theory of liquid crystals," *Transactions of the Faraday Society*, vol. 29, no. 140, pp. 883-899, 1933.

[2.13] C. V. Brown and N. J. Mottram, "Influence of flexoelectricity above the nematic Fréedericksz transition," *Physical Review E*, vol. 68, no. 3, p. 031702, 2003.

[2.14] R. Morris, "Hydrodynamics of nematic liquid crystals for diffractive optical elements," *Ph.D. thesis: University of Leeds*, 2021.

[2.15] V.Fréedericksz and V. Zolina, "Forces causing the orientation of an anisotropic liquid," *Transactions of the Faraday Society*, vol. 29, no. 140, pp. 919-930, 1933.

[2.16] J. F. Algorri, V. Urruchi, N. Bennis, J. M. Sánchez-Pena, and J. M. Otón. "Tunable liquid crystal cylindrical micro-optical array for aberration compensation." *Optics express*, vol. 23, no. 11, pp. 13899-13915, 2015.

[2.17] Y. H. Oh, M. S. Kwon, S. Y. Shin, S. Choi, and K. Oh, "In-line polarization controller that uses a hollow optical fiber filled with a liquid crystal." *Optics letters*, vol. 29, no. 22, pp. 2605-2607, 2004.

[2.18] S. Li, J. Wang, H. Tian, L. Li, J. Liu, G. C. Wang, J. Gao, C. Hu, and Z. Zhou, "Super terahertz phase shifter achieving high transmission and large modulation depth." *Optics Letters*, vol. 45, no. 10, pp. 2834-2837, 2020.

[2.19] N. V. Tabiryan and S. R. Nersisyan, "Large-angle beam steering using all-optical liquid crystal spatial light modulators." *Applied physics letters*, vol. 84, no. 25, pp. 5145-5147, 2004.

[2.20] S. Sato, "Liquid-crystal lens-cells with variable focal length", *Japanese Journal of Applied Physics*, vol. 18, no. 9, pp. 1679-1684, 1979.

[2.21] T. Nose and S. Sato, "A liquid crystal microlens obtained with a non-uniform electric field." *Liquid Crystals*, vol. 5, no. 5, pp. 1425-1433, 1989.

[2.22] Y. H. Lin, Y. J. Wang and V. Reshetnyak, “Liquid crystal lenses with tunable focal length”, *Liquid Crystals Reviews*, vol. 5, no. 2, pp. 111-143, 2017.

[2.23] J. Knittel, H. Richter, M. Hain, S. Somalingam, and T. Tschudi, “A temperature controlled liquid crystal lens for spherical aberration compensation.” *Microsystem Technologies*, vol. 13, no. 2, pp. 161–164, 2006.

[2.24] K.C, Heo, S. H. Yu, J. H. Kwon, J.S. Gwag, “Thermally tunable focus lenticular lens using liquid crystal”. *Applied Optics*, vol. 52, no. 35, pp. 8460–8464, 2013.

[2.25] Y.J. Lee, C.J. Yu, J.H. Lee, J.H. Baek, Y. Kim, and J.H. Kim, “Optically isotropic switchable microlens arrays based on liquid crystal”. *Applied Optics*, vol. 53, no. 17, pp. 3633–3636, 2014.

[2.26] Y.Y. Kao, C.P. Chao Paul and C.W. Hsueh, “A new low voltage-driven GRIN liquid crystal lens with multiple ring electrodes in unequal widths”. *Optics Express*, vol. 18, no. 18, pp. 18506–18518, 2010.

[2.27] P.P. Chao, Y. Y. Kao and C. J. Hsu, “A new negative liquid crystal lens with multiple ring electrodes in unequal widths”. *IEEE Photonics Journal*, vol. 4, no. 1, pp.250-266, 2012.

[2.28] M. Kawamura and Y. Ito, “Liquid crystal lens with double circularly hole-patterned electrodes”. *Molecular Crystals and Liquid Crystals*, vol. 542, no. 1, pp.176-698, 2011.

.

[2.29] M. Avendaño-Alejo, L. Castañeda, A. Maldonado, and N. Qureshi, "Huygens’ Principle: Exact wavefronts produced by aspheric lenses," *Optics Express*, vol. 21, no. 24, pp. 29874-29884, 2013.

CHAPTER 3: FUNDAMENTAL OF ACOUSTO-OPTICS

Acousto-optics is a subfield of optical science and engineering that studies the interaction between sound waves (acoustic) and light waves (optics). Acoustic effects result from the change in the refractive index of a medium caused by the presence of sound waves. In fact, the development of optics and acoustics paralleled in the sense that most phenomena observed in optics also occur in acoustics [3.1]. The interaction of sound and light can be observed in many applications. In optical communications systems, for instance, Bragg cells are important components for acousto-optic modulators. Laser ultrasonics is another notable example of acousto-optic usage.

3.1. ULTRASOUND WAVES AND APPLICATIONS

Ultrasound is defined as a sound wave propagating at frequency band above 20 kHz (higher than the upper audible limit of human hearing). Ultrasonics is a valuable tool to further understand the properties of solids and liquids since the wave propagation will depend mainly on the medium properties. Ultrasonics has many applications, such as medical diagnosis and control, oceanography, food industry. The remarkable event that emerged the ultrasonics is related to the discovery of the piezoelectricity in 1880 [3.2]. In 1889, Rayleigh published about the principle of acoustics [3.3], making many contributions in the acoustic field, including acoustic surface (Rayleigh) waves and acoustic pressure.

The idea of using ultrasound as a therapeutic tool was reportedly first inspired by radar and sonar in the military in the early 1950s. Thereafter, most of the developments for industry, such as ultrasonic cleaning, and ultrasonic soldering, started. Subsequently, in the following years, it was then possible to carry out quantitative experiments on velocity and attenuation in function of magnetic field, temperature, frequency, following developments in transducer technology, electronic instruments, and high-quality crystals [3.2]. The advent of increasingly capable software has led to drastic improvements in image reconstruction

through electronic beamforming - significantly improving focus and speed of image acquisition in recent years, leading to new applications for ultrasonic devices.

3.1.1. PIEZOELECTRIC MATERIALS AND PIEZOELECTRIC EFFECT

New high-performance materials and better electronics have been responsible for much of the remarkable progress made in ultrasonics. For instance, in Langevin's work, he applied quartz to transduction, developed composite transduction, and developed composite transducers [3.2]. One of the significant developments in piezoelectric materials is the development of the poled ceramic transducer of the lead zirconate (PZT) family, which is relatively inexpensive, robust, and has high performance characteristics. Some materials for ultrasonic technology such as quartz, lithium sulphate or barium titanate are almost never used today. Instead, lead zirconate titanate (PZT) is most commonly used piezoelectric ceramics in industry. The piezoelectric ceramic vibrates due to the piezoelectric effect, and ultrasonic waves are excited when the frequency of the applied AC voltage is 20 kHz or higher - they are used for up to a maximum of 30 MHz. Large amplitude can be obtained by vibrating at the resonance frequency.

In a piezoelectric effect, mechanical energy is converted into electrical energy when a crystal is compressed. This is how ultrasound transducers receive sound waves. The opposite effect can be used – inverse piezoelectric effect – whereby the application of an electric field to a crystal causes realignment of the internal dipole structure. This realignment results in crystal lengthening or contraction, converting electrical energy into kinetic or mechanical energy. Substances that exhibit these phenomena are then called piezoelectric materials. In this thesis, ultrasonic waves are generated using the inverse piezoelectric effect.

Piezoelectric ceramics can be easily fired and processed into any size and shape, and various properties can be obtained by modifying the composition or controlling additives. Therefore, it is suitable for a wider range of applications than crystalline materials, but many ceramics require polarization treatment in order to be used as piezoelectric materials. Table 3.1 shows the important physical characteristics of lead zirconate titanate (PZT).

Table 3.1 Physical properties of a PZT [3.4]

Acoustic Impedance Z [10^6 kg/m^{2}s]	33.7
Resonance Frequency f [MHz]	< 25
Coupling Coefficient (thickness mode) k_t	0.45
Coupling Coefficient (thickness mode) k_p	0.58
Relative Dielectricity e_r	1700
Maximum Temperature [^{o}C]	365

In this work, lead zirconate titanate (PZT) is used. The composition formula of PZT used is represented by $PbZrO_3$— $PbTiO_3$, which is a mixed crystal of ternary metal oxide lead titanate and lead zirconate. Due to the high Curie point (300^{o}C) and high electromechanical coupling coefficient of PZT-based ceramics, they have been put to practical use as cooperative ultrasonic wave generators and oscillators. However, if ultrasound shall be radiated into liquids or plastics, most part of the acoustic energy generated by the piezoceramic element is reflected at the boundary between the piezoelectric material and the medium of propagation.

3.1.2. ACOUSTIC RADIATION FORCE

As with electromagnetic waves, acoustic waves can exert force on objects. The force produce by acoustic waves is known as acoustic radiation force or acoustic radiation pressure. Acoustic radiation force is a static force that is generated by a difference in the acoustic energy densities of different media [3.5]. There are several applications that use the phenomenon of the acoustic radiation force. These applications include the measurement of mechanical properties, acoustic levitation, acoustic separation, the manipulation of cells and bioeffects. In addition, these applications depend on static patterns of ultrasonic pressure and are commonly referred to as ultrasonic standing wave devices.

The resulting motion from the application of acoustic radiation force can be tracked using different modalities, including ultrasound, magnetic resonance imaging (MRI) and optical techniques. Vibrations of a plate in a fluid media act as a source of acoustic waves. According to the fundamental wave equation, acoustic waves of pressure *p* propagate three-dimensionally [3.6]:

$$\frac{\partial^2 p}{\partial t^2} = c_m^2 \nabla^2 p \tag{3.1}$$

Where c_m is the speed of sound in the fluid media, the Laplacian ∇^2 is for a three-dimensional coordinate system. Acoustic pressure over an infinitesimal area balanced by acceleration over an infinitesimal area is the basis of the three-dimensional wave equation. It is possible to solve the second order partial differential wave equation given certain boundary conditions [3.6]. Larger maximum vibration velocity leads to stronger acoustic pressure in fluids [3.7], so the development of ultrasonics electronics require ultrasonic transducers larger maximum vibration, velocity and energy-efficient.

3.2. ACOUSTO-OPTICS DEVICES

3.2.1. ULTRASOUND LIQUID LENS

Ultrasonic liquid lens based on acoustic radiation force was developed [3.5] using a cylindrical acrylic cell filled with degassed water/silicone oil and a concave ultrasound PZT transducer. The annular PZT transducer is attached to one end of a cylindrical cell with an outer diameter of 6 mm to form a water droplet hemisphere in the center of the transducer, and then the periphery is filled with water and silicone oil with a different refractive index. The oil– water interface served as a lens (i.e., 4-mm-high and 6-mm-diameter liquid lens) – Fig. 3.1, and the lens profile was altered by changing the acoustic radiation force generated from the PZT transducer.

Light is transmitted in the optical axis direction by sealing the other end of the cell and the center of the oscillator with a glass plate. Once the lens is sealed, the shape of the

water droplet hemisphere that corresponds to the lens, hardly changes even if the lens is tilted or inverted due to the Van der Waals force acting between the water droplet hemisphere and the glass plate. In addition, by using supersonic waves in the MHz band, it is possible to prevent the generation of cavitation in the liquid and the emulsification of water and oil [3.5].

When an electric signal is input to the transducer, an acoustic standing wave is generated in the lens, and acoustic radiation is applied to the two-component interface. Since the acoustic radiation force is the static pressure caused by the difference in acoustic energy density between different media, the direction in which the force works depends on the speed of sound and density of each medium [3.8]. The dynamic response of such lens deformation depends on the surface tension, viscosity and density between the fluids, and it can be approximated by a simple one -dimensional spring / mass / damper model [3.5].

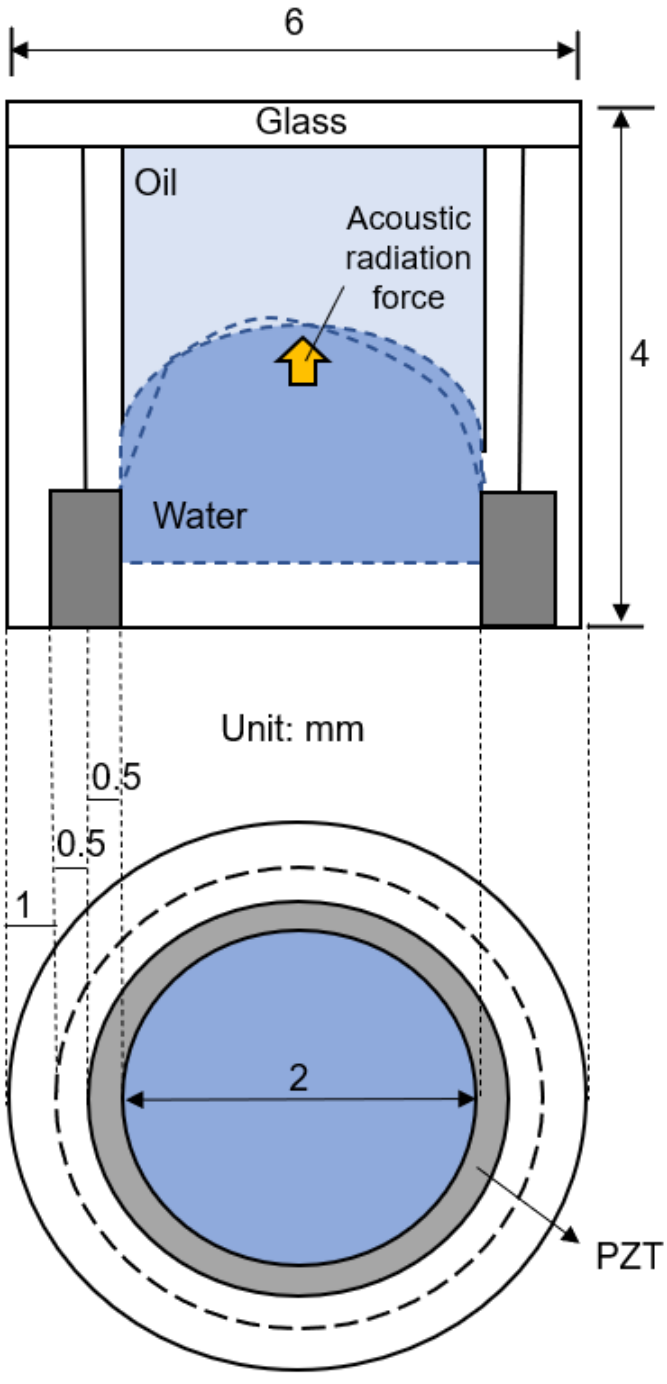

Figure 3.1 Ultrasonic liquid lens structure

3.2.2. ULTRASOUND GEL LENS

In the liquid lenses, including the ultrasonic liquid lens described in the Section 3.2.1, the temperature characteristics may be unstable due to changes in the physical properties of the liquid, so bubbles can be generated in the liquid due to long-term use. Also, since the two liquids are mixed, there is a risk in industrial use that the lens becomes cloudy. Ultrasonic gel lenses (Fig. 3.2) presented in [3.9], which use a transparent gel with temperature stability as the lens material, overcome these problems, resulting in a varifocal lens with a simpler structure.

The variable-focus gel lens consisted of an annular ultrasonic transducer, silicone gel, and a polyethylene terephthalate (PET) film [3.9]. The PET film was attached to one side of the transducer, and a silicone-gel circular plate was constructed inside the annular transducer as the lens material. The lens profile was altered by conducting the acoustic radiation force of the transducer. In other words, when a voltage is applied to an ultrasonic transducer, ultrasonic vibrations propagate through the gel, creating a difference in acoustic energy density at the boundary between the gel surface and air. The acoustic radiation force of the ultrasonic waves acts on the gel surface, changing the shape of the gel and causing it to act as a lens. By changing the input voltage to the ultrasonic transducer, the shape of the lens changes and the curvature of the convex lens changes, making it possible to control the focal length by the input voltage [3.9]. The deformed shape of the lens is determined by the relationship between the acoustic radiation force, the surface tension of the gel, and the elastic restoring force. Along with this, the lens acts as a convex lens and the transmitted light is focused. Micro-optical devices such as microlens arrays and optical scanners have been developed by applying this technology.

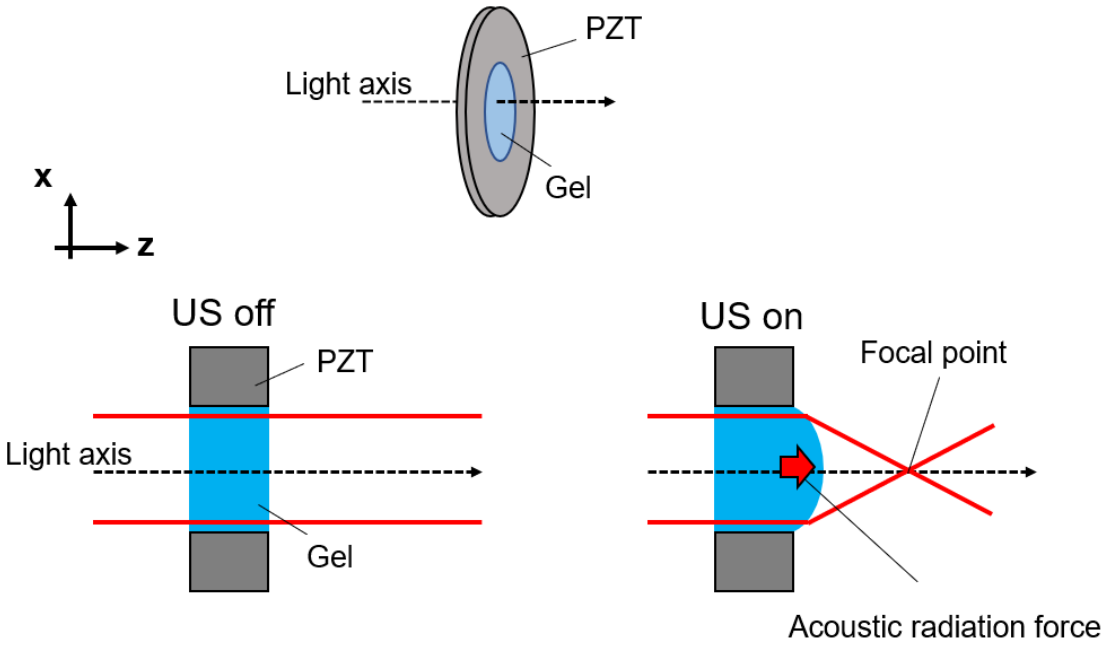

Figure 3.2 Ultrasonic gel lens scheme

3.2.3. ULTRASONIC LENS ARRAY

Lenses with a variable focus function as the gel lens [3.9] presented in the Section 3.2.2 can be applied to lens arrays [3.10]. An ultrasonic varifocal lens array that can change not only the focal length but also the lens pitch by using the deflection vibration mode of the plate was developed by Koyama *et al* [3.11]. By inputting in-phase continuous sinusoidal signals to the four PZT transducers (Fig. 3.3 (a), the grid-like deflection vibration mode is excited (Fig. 3.3(b)). This vibration changes the gel shape and forms a lens array. The focal length can be controlled by the voltage input to the PZT transducers and the lens spacing (pitch) can be controlled by the drive frequency (Fig. 3.3 (c)).

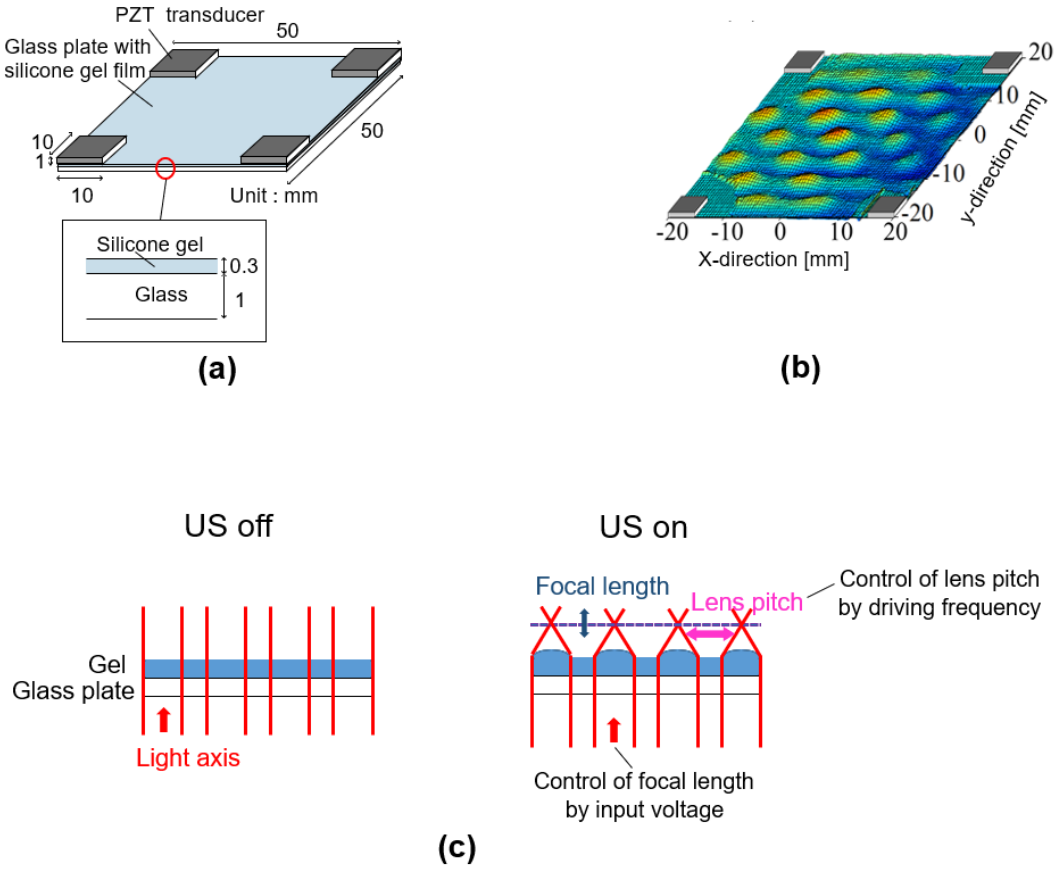

Figure 3.3 Ultrasound liquid lens array: (a) Configuration (b) Surface profile of a lens array simulated by Finite Element Analysis (FEA) in Ansys Software (c) Control of the focal length by input voltage and control of the lens pitch by driving frequency.

3.2.4. CONTROL OF THE LIQUID CRYSTAL MOLECULAR ORIENTATION BY ACOUSTIC WAVES TO THE DEVELOPMENT OF OPTICAL LENSES

An acoustic field can rotate the optical axis of liquid crystal molecules in nematic liquid crystals [3.12]. This rotation of the molecules results in a change in the optical birefringence of the liquid crystal and the acousto-optic effect is analogous to the electro-optic effect that is the basis of liquid crystal displays.

Figure 3.4 shows an ultrasonic liquid cell [3.13] for evaluating liquid crystal molecular orientation. A polyimide alignment film that orients the liquid crystal vertically is applied on two glass substrates, and ultrasonic transducers are attached to both ends of one of the base plates. A spacer is sandwiched between two glass substrates, both glass substrates are bonded together, and then a nematic liquid crystal is injected in the middle to form a liquid crystal layer confined in the cell. When an electric signal with a resonance frequency is input to the transducers, a flexural vibration is generated in the longitudinal direction of the substrate, then the acoustic radiation force acts in the liquid crystal layer due to the difference in acoustic energy density between the air, the liquid crystal layer, and the glass substrate, and the orientation of the molecule changes.

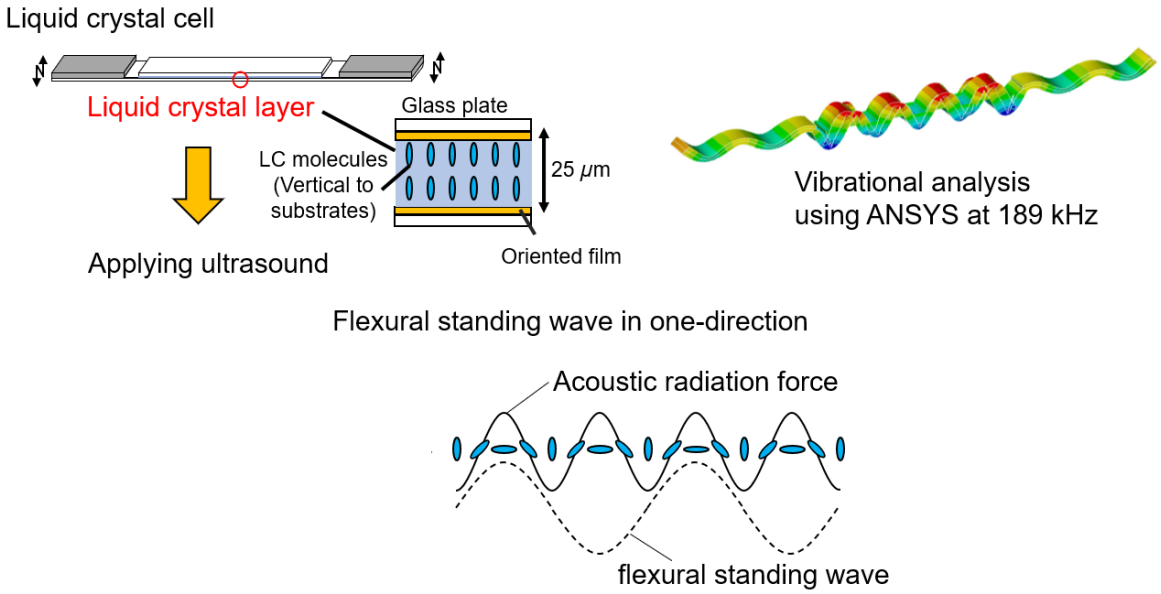

Figure 3.4 Ultrasound liquid crystal cell

3.2.5. ULTRASOUND LIQUID CRYSTAL LENS

Based on the operating principles discussed in the Section 3.2.4, an ultrasonically controlled liquid crystal lens that uses acoustic waves generated by a piezoelectric material to radially excite the liquid crystal confined between two glasses substrates was developed [3.14] (Fig. 3.5). The flexural vibration promoted by the piezoelectric transducer generate the sound waves that will achieve the steady state. These flexural standing waves promote the molecular reorientation that will continuously vary the gradient of the refractive index (GRIN) of the refraction under ultrasound vibration, creating the same parabolic pattern of refractive index mentioned in the Section 2.5.1. However, in the case of the ultrasonic liquid crystal lens, it is possible to change the refractive index of the liquid crystal to perform a lens without use of ITO electrodes, by using acoustic actuation, showing not only an alternative to overcome the drawbacks of ITO, but also an alternative for creating tunable lenses with simpler structures. Most of the liquid crystal lens structures currently utilized in production are of GRIN LC lens type, including the ultrasonically controlled liquid crystal lens.

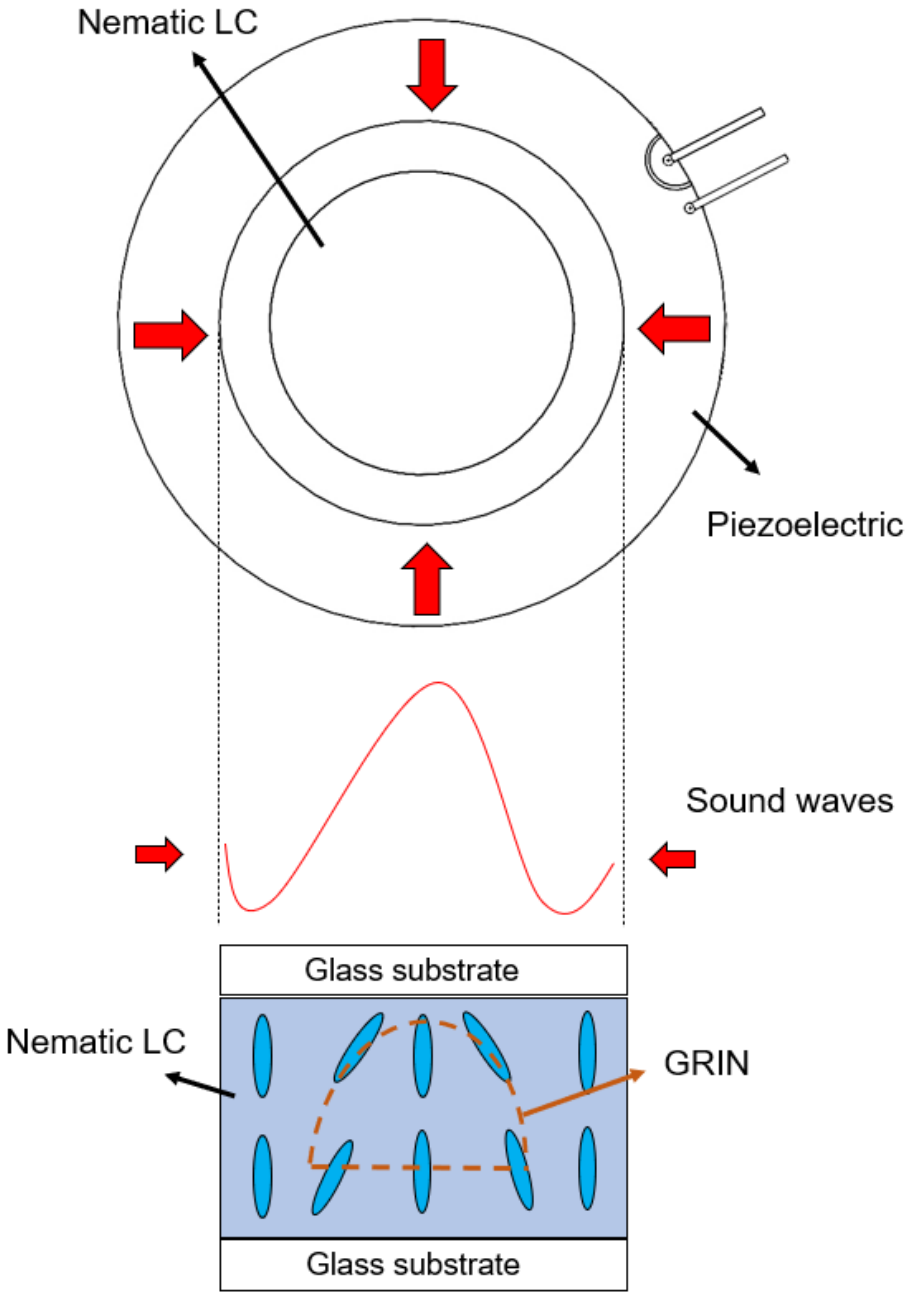

Figure 3.5 Ultrasonically controlled liquid crystal lens principle

The ultrasound liquid crystal lens tunability and focal length (Fig. 3.6) under ultrasound excitation will depend on many parameters, such as liquid crystal material (e.g., refractive index, elastic constants, dielectric anisotropy), liquid crystal layer thickness (*d*), driving conditions and lens design. The influence and contribution of these parameters in the ultrasound liquid crystal lens optical performance will be further discussed in this thesis work.

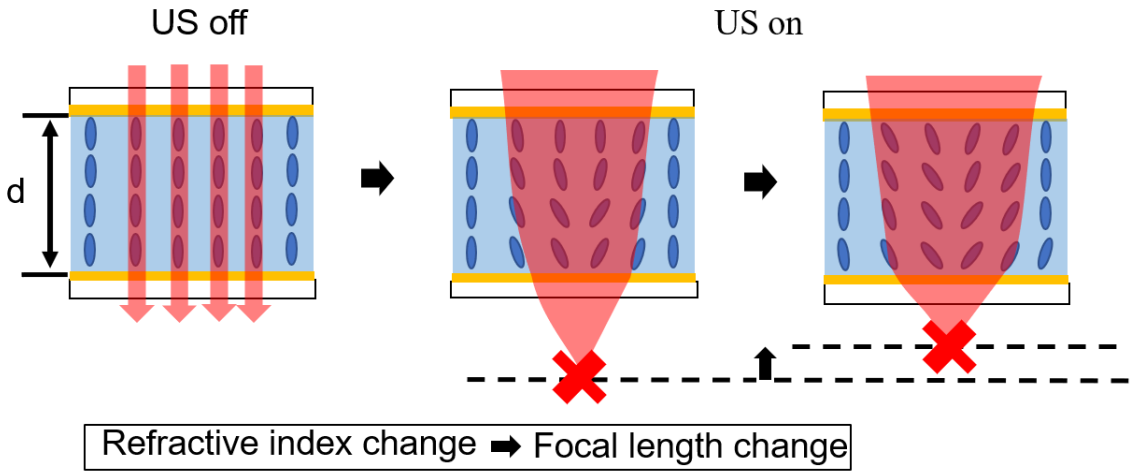

Figure 3.6 Focal length change according to the refractive index variation under ultrasound (US) excitation

REFERENCES

[3.1] A. Korpel, "Acousto-optics—a review of fundamentals," *Proceedings of the IEEE*, vol. 69, no. 1, pp.48-53, 1981.

[3.2] J. David and N. Cheeke "Fundamentals and applications of ultrasonic waves," *CRC press*, vol. 1, 2010.

[3.3] J. W. S. Rayleigh, "The theory of sound", vol. 1 and 2, *Dover Publications*, New York, 1945.

[3.4] M. Lach, M. Platte, and A. Ries, "Piezoelectric materials for ultrasonic probes", *Transducer Workshop*, vol. 1, no. 9, 1996.

[3.5] D. Koyama, R. Isago, and K. Nakamura, "Compact, high-speed variable-focus liquid lens using acoustic radiation force," *Optics Express*, vol. 18, no. 24, 2010.

[3.6] K. M. Smyth, "Design and modeling of a PZT thin film based piezoelectric micromachined ultrasonic transducer," *Master thesis: Massachusetts Institute of Technology*, 2012.

[3.7] X. Lu, J. Hu, H. Peng and Y. Wang, "A new topological structure for the Langevin-type ultrasonic transducer," *Ultrasonics*, vol. 75, pp. 1–8, 2017.

[3.8] B. Chu and E. Apfel, "Acoustic radiation pressure produced by a beam of sound," *Journal of the Acoustical Society of America*, vol. 72, no. 6, pp. 1673-1687, 1982.

[3.9] D. Koyama, R. Isago, and K. Nakamura, "Ultrasonic variable focus optical lens using viscoelastic material," *Applied Physics Letters*, vol. 100, no. 9, p. 091102, 2012.

[3.10] L. Dong, A.K. Agarwal, D.J. Beebe and H. Jiang, "Adaptive liquid microlenses activated by stimuli-responsive hydrogels," *Nature*, vol. 442, no. 7102, pp.551-554, 2006.

[3.11] D. Koyama, Y. Kashihara, M. Hatanaka, K. Nakamura and M. Matsukawa, "Movable optical lens array using ultrasonic vibration," *Sensors and Actuators A: Physical*, vol. 237, pp.35-40, 2016.

[3.12] V. A. Greanya, M.S. Spector, J. V. Selinger, B.T. Weslowski and R. Shashidhar "Acousto-optic response of nematic liquid crystals," *Journal of Applied Physics*, vol. *94*, no. 12, pp.7571-7575, 2003.

[3.13] S. Taniguchi, D. Koyama, Y. Shimizu, A. Emoto, K. Nakamura and M. Matsukawa, "Control of liquid crystal molecular orientation using ultrasound vibration," *Applied Physics Letters*, vol. 108, p. 101103, 2016.

[3.14] Y. Shimizu, D. Koyama, M. Fukui, A. Emoto, K. Nakamura and M. Matsukawa, "Ultrasound liquid crystal lens," *Applied Physics Letters*, vol. 112, no. 16, p. 161104, 2018.

CHAPTER 4: EXPERIMENTAL METHODS AND PROCEDURES

Based on the lens model presented in the Chapter 3, Section 3.2.5, new design and geometry for an ultrasonically liquid crystal lens were simulated and tested in order to evaluate and to improve its optical performance.

4.1. SIMULATION METHODS

The configurations of the ultrasound liquid crystal lens, its material properties, geometrical deformations, and boundary conditions were defined with finite-element analysis (FEA) via ANSYS 11.0 software (ANSYS. Inc., PA), whereas all the mechanical properties of the components for the simulation can be found in Table 4.1. It determined the resonant flexural vibrational modes on the glass substrates in the tens of kilohertz range. The modeling revealed that a combination of lens geometry, electrode scheme, and appropriate driving voltages enabled the focal point control. By driving the transducer with a continuous sinusoidal electric signal, several flexural vibration modes were generated in the liquid crystal layer through the two glass substrates at the resonance frequencies of the liquid crystal lens above 20 kHz. The minimum mesh size of the FEA model was approximately 0.5 mm, and the mechanical vibration on the device at the steady state was calculated by applying the input voltage to the PZT electrodes as the boundary conditions.

Table 4.1 Material properties for ANSYS simulation

Material	Young's modulus / GPa	Density / $Kg \cdot m^{-3}$	Poisson's ratio
Glass	71.3	2400	0.22
PZT (C-213)	6640 / 5380 $\varepsilon_{11}^{T} / \varepsilon_0$ / $\varepsilon_{33}^{T} / \varepsilon_0$ Relative permittivity	7700	0.3
Piezoelectric constant ($\times 10^{-12}$m/V)		**Elastic constants (GPa)**	
d_{31}	-135	Y_{11}^{E}	82
d_{33}	310	Y_{33}^{E}	66
d_{15}	510	Y_{55}^{E}	26

4.2. ULTRASONIC LIQUID CRYSTAL LENS CONFIGURATION

4.2.1. LIQUID CRYSTAL LENS STRUCTURE

The typical geometry of the ultrasound liquid crystal lenses developed in this thesis is that of a common sandwich-type device (Fig. 4.1) in which the liquid crystal material is sealed to ensure that it cannot flow out, along with an alignment layer that allows the initial molecule orientation to be set without ultrasound excitation. The spacer thickness defines the liquid crystal layer thickness. This lens geometry is transparent to the majority of light, while allowing ultrasound waves changing the molecular orientation of the liquid crystal, making it ideal for studying optical properties.

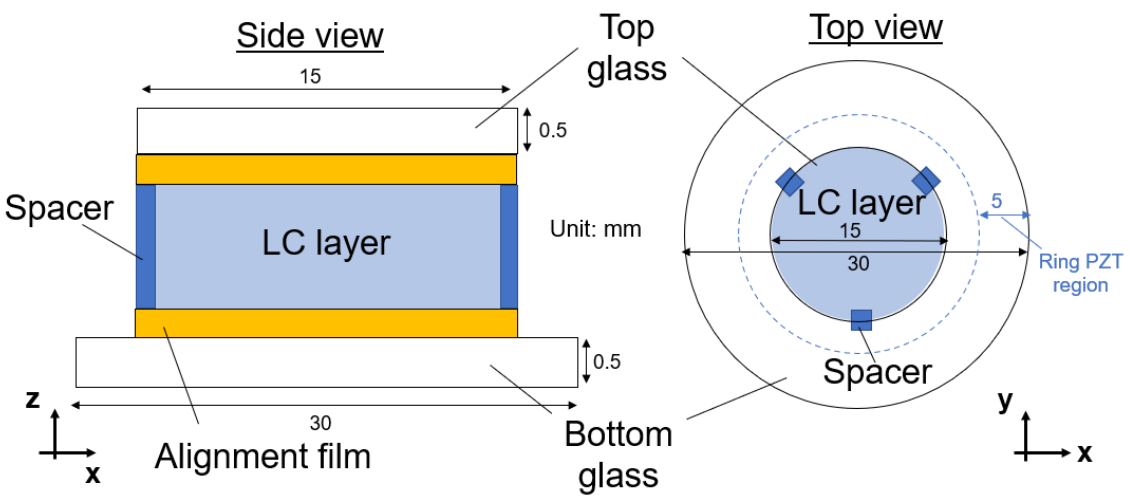

Figure 4.1 Ultrasound liquid crystal lens sandwich-type model

4.2.2. ULTRASONIC TRANSDUCERS CONFIGURATION

The configurations of the piezoelectric transducer and the glass substrates used in this thesis were determined via FEA using ANSYS to determine the resonance flexural vibration modes on the glass substrates as detailed in Table 4.1. Previously [4.1 – 4.3], it was observed experimentally that the excitation of the annular PZT transducer using a continuous sinusoidal electric signal allowed several flexural vibration modes to be generated on the liquid crystal layer through the two glass substrates at the resonance frequencies of the entire liquid crystal lens at more than 20 kHz. Considering the influence of the ultrasound vibration on the liquid crystal molecular reorientation, a single-channel PZT transducer and a four-channel PZT transducer were used to evaluate the lens performance (Fig. 4.2).

In Fig. 4.2 (a) the piezoelectric ceramic is a ring shape and consists in a single channel. In Fig. 4.2 (b), the piezoelectric ceramic is divided into four quadrants that are independently driven with sinusoidal voltages at the resonant frequency of the lens. The PZT electrode has four parts (numbered CH1–CH4) to enable four-phase drive. For both cases, the annular piezoelectric PZT ultrasound transducer (C-213, Fuji Ceramics; thickness: 1 mm; inner

diameter: 20 mm; outer diameter: 30 mm) was used and it was bonded to a glass plate with a larger diameter (30 mm, as shown in Fig. 4.1).

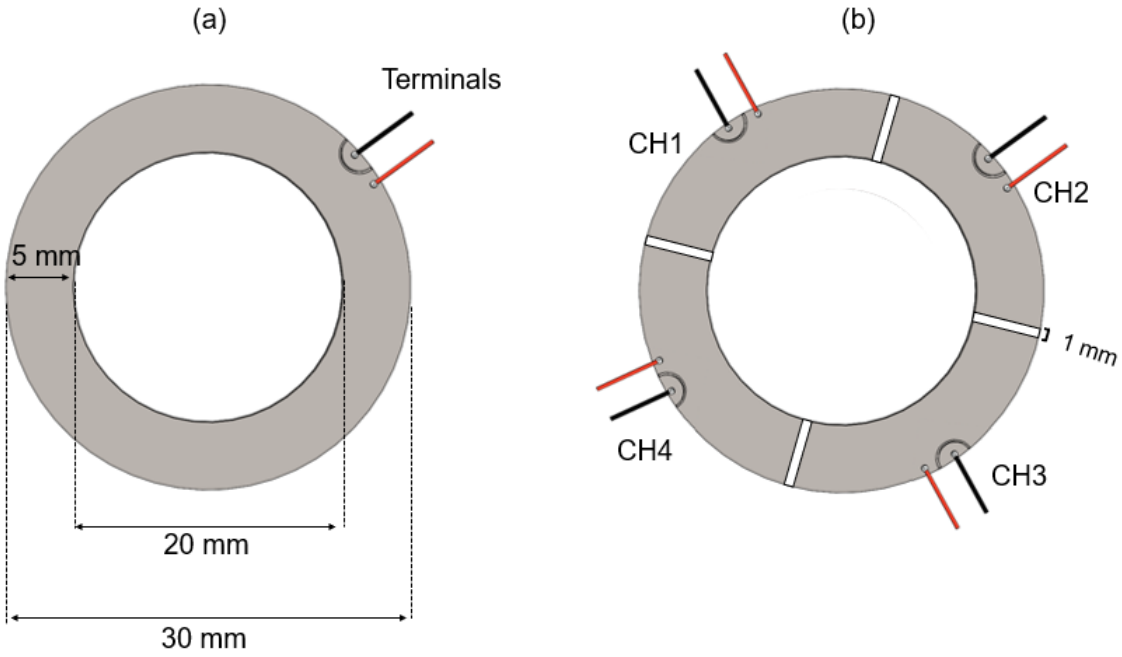

Figure 4.2 PZT configuration: (a) Single-channel, (b) Four channel ultrasound transducer

4.3. ULTRASOUND LIQUID CRYSTAL LENS FABRICATION

4.3.1. GLASS PREPARATION

The first step of the lens fabrication is the glass substrate cleaning process. Cleanliness is of great importance throughout the lens fabrication. Therefore, in order to clean the substrates, it was used the subsequent sonication (T420, Elma, Transsonic Ultrasonic bath) steps with acetone, ethanol and pure water, respectively. This process took 15 minutes per step to eliminate possible contaminants.

4.3.2. ALIGNMENT FILM PROCESS

After cleaning the glass substrates (diameter: 30 mm and 15 mm, thickness: 1 mm), the alignment material (Polyimide, vertical alignment type, SE-5811, Nissan Chemical, Japan) was applied using a syringe. Then, by using a spin coater machine from Active Inc. (ACT-220D II), the substrates were spun to a high-speed (1500 rpm for 40 seg) to achieve uniform thin Polyimide films – Fig. 4.3. Material viscosity, solids concentration and spin speed determine the final alignment film thickness [4.4].

During the spin-coating process, most of the solvent evaporates, leaving a relatively solid layer of Polyimide. After the spin coating process, glass substrates were placed on a hotplate for 15 minutes at 75^{o}C, followed by 25 minutes at 225^{o}C. Liquid crystals can be aligned by these Polyimide materials thanks to the Van der Waals and steric forces created between the polymer chains and the stiff core of the liquid crystal [4.5]. In other words, the polyimide film covered the inside surfaces of the glass substrates and defined the initial liquid crystal molecular orientation, which was vertical to the glass (homeotropic alignment) because of chemical interactions between the liquid crystal molecules and the oriented film.

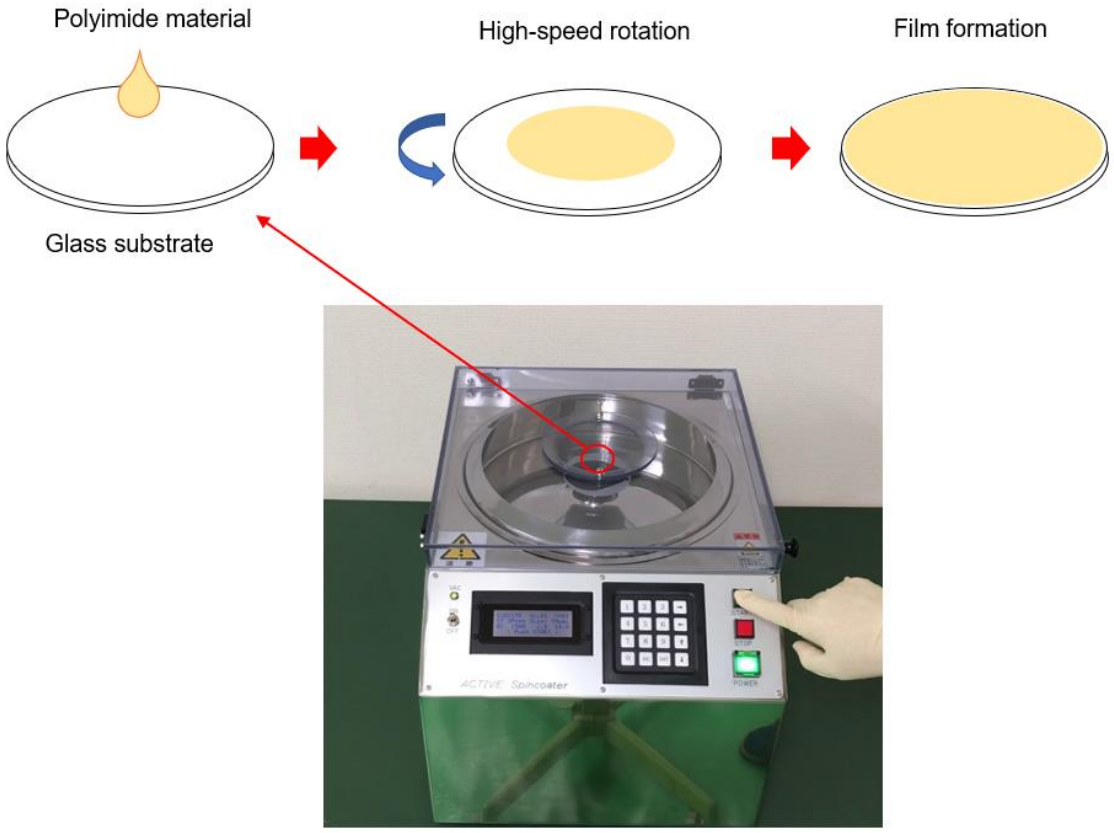

Figure 4.3 The spin coating process to apply the Polyimide alignment film to the glass substrates

4.3.3. LIQUID CRYSTAL, SPACING AND GLUING.

After the alignment film process, polyethylene terephthalate (PET) film spacers were used to make the sandwich structure for the lens, and they will define the distance between the two glasses (*vide* Fig. 4.1 and Fig. 4.4). Therefore, the spacers were used to create the gap (d) before inserting the liquid crystal material. Two different nematic liquid crystal materials were used in this thesis: RDP-85475 [DIC, Japan; refractive index n_o = 1.525; n_e = 1.823 at 589 nm; transition temperature of smectic-to-nematic (SN) transition point: 10^{o}C; nematic-to-isotropic (NI) transition point: 123.7^{o}C; rotational viscosity γ: 93.7 mPa·s] and *4*-

cyano-40-heptylbiphenyl (5CB; TCI, Japan; refractive index n_o = 1.533; n_e = 1.716 at 589 nm and 24°C; rotational viscosity γ at 25°C: 28 mPa·s). After a nematic liquid crystal was injected into the gap via the capillary effect, the liquid crystal layer was sealed completely using epoxy (Araldite RT30). Finally, the ultrasonic PZT transducer (inner diameter of 20 mm, outer diameter of 30 mm, thickness of 1 mm; C-213, Fuji Ceramics, Fujinomiya, Japan) was glued to the circular glass substrate with larger diameter (30 mm) using epoxy (Strong Glue Araldite, To – GL–03) and clips were used during 12h as a method to apply pressure and to attach the transducer to the glass substrate effectively (Fig. 4.4). As already mentioned in Section 4.2.2 and in Fig. 4.2, two types of transducers were used: single-channel and four-channel transducer. The latter has the annular transducer divided into four symmetrical pieces and each part was physic and electrically independent with a gap of 1 mm, so that each transducer can be excited by an independent electrical signal. Figure 4.5 shows two fabricated ultrasound liquid crystal lenses with their respective PZT transducer.

The liquid crystal molecules are assumed to reorient in the x–z plane under application of an input voltage that is higher than the threshold voltage, as explained in Section 2.4. The refractive indices and the liquid crystal thickness determine the phase shifts, whereas the dielectric constants and the elastic constants (K_{11}, K_{22}, K_{33}) determine the threshold voltage jointly [4.6]. These constants are molecular parameters that are used to describe the restoring forces acting on a molecule in response to application of an external force that modifies the medium from its lowest energy configuration. Furthermore, smaller elastic constant values will result in a lower threshold voltage. According to their respective liquid crystal manufacturers, the liquid crystals used in this work have the physical properties listed in Table 4.2.

Table 4.2 Physical properties of the liquid crystal materials

	Elastic constants [pN] (at 25°C)			Dielectric anisotropy
	K_{11}	K_{22}	K_{33}	$\Delta\varepsilon$
5CB	6.1	4.1	9.7	+13.0 (1.5 kHz)
RDP-85475	14.4	10.6	23.5	+19.1 (1 kHz)

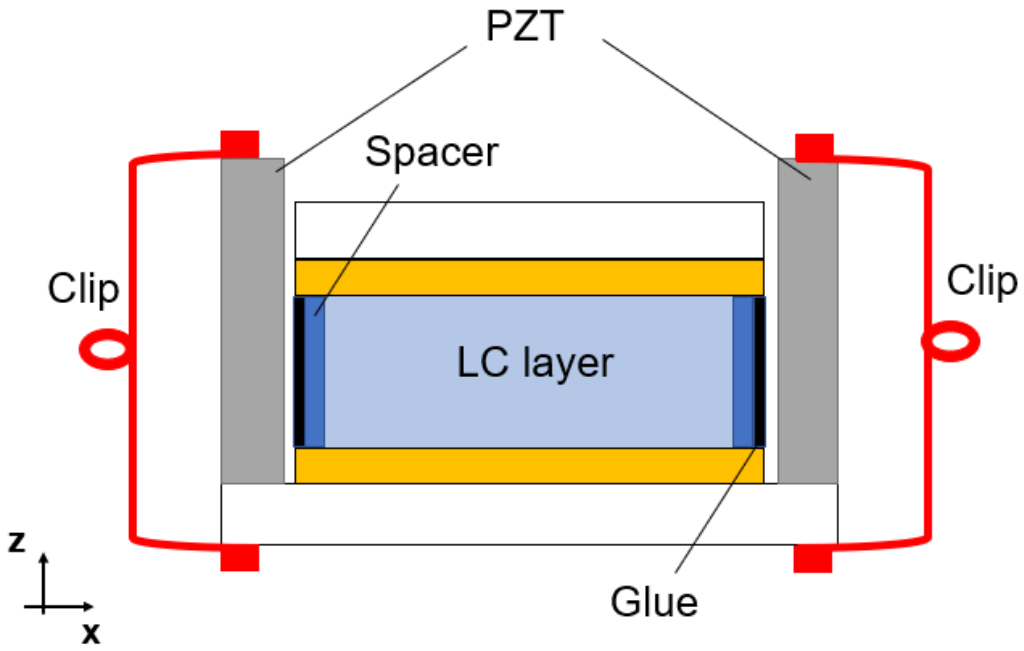

Figure 4.4 Spacing, liquid crystal and gluing process

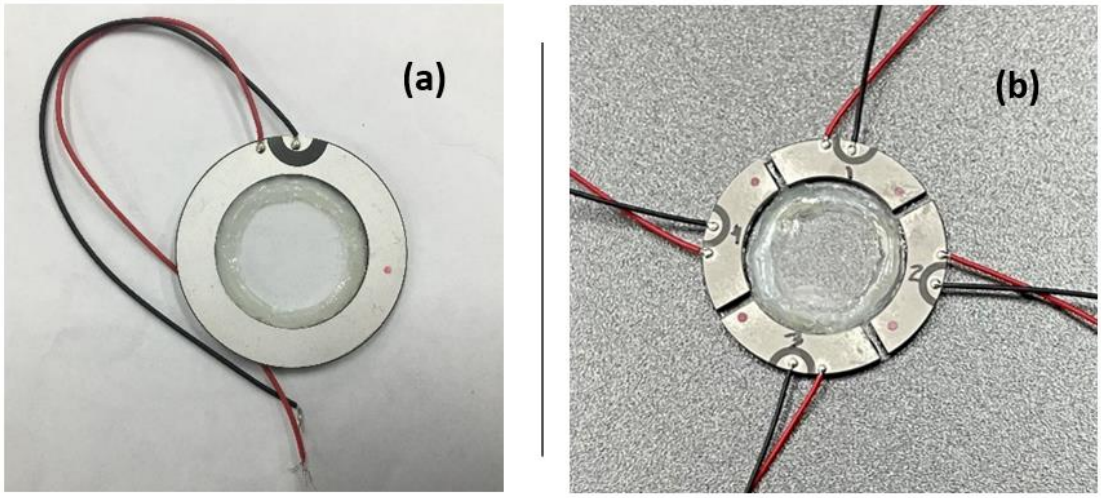

Figure 4.5 Photograph of fabricated ultrasound liquid crystal lenses: (a) single-channel, (b) 4-channels lens

4.4. EXPERIMENTAL SET-UP

4.4.1. RESONANCE FREQUENCY MEASUREMENT

The configurations of the PZT transducer and the glass substrates were previously determined via FEA using the software Ansys to determine the resonance flexural vibration modes on the glass substrates before the lens's fabrication. The fabricated lenses were measured by using the Impedance Analyzer (E4990A, Keysight, 20 Hz – 120 MHz), Fig. 4.6, to verify and to confirm if the resonance frequencies were in accordance with the Ansys simulated values. Impedance (Z) is generally defined as the total opposition a device or circuit offers to the flow of an alternating current at a given frequency [4.7]. The impedance analyzer measures the frequency response to capacitors (C), inductors (L) and resistors (R), according to the device characteristics. A Van Dyke model (Figure 4.7) is the most basic

model for characterizing a piezoelectric ceramic near its resonant frequency [4.8]. This model is commonly used to determine the electromechanical resonance characteristics of crystal oscillators, including a PZT ring [4.8]. The parallel connection of a series RLC representing mechanical damping, mass, and elastic compliance, and a capacitor [4.9].

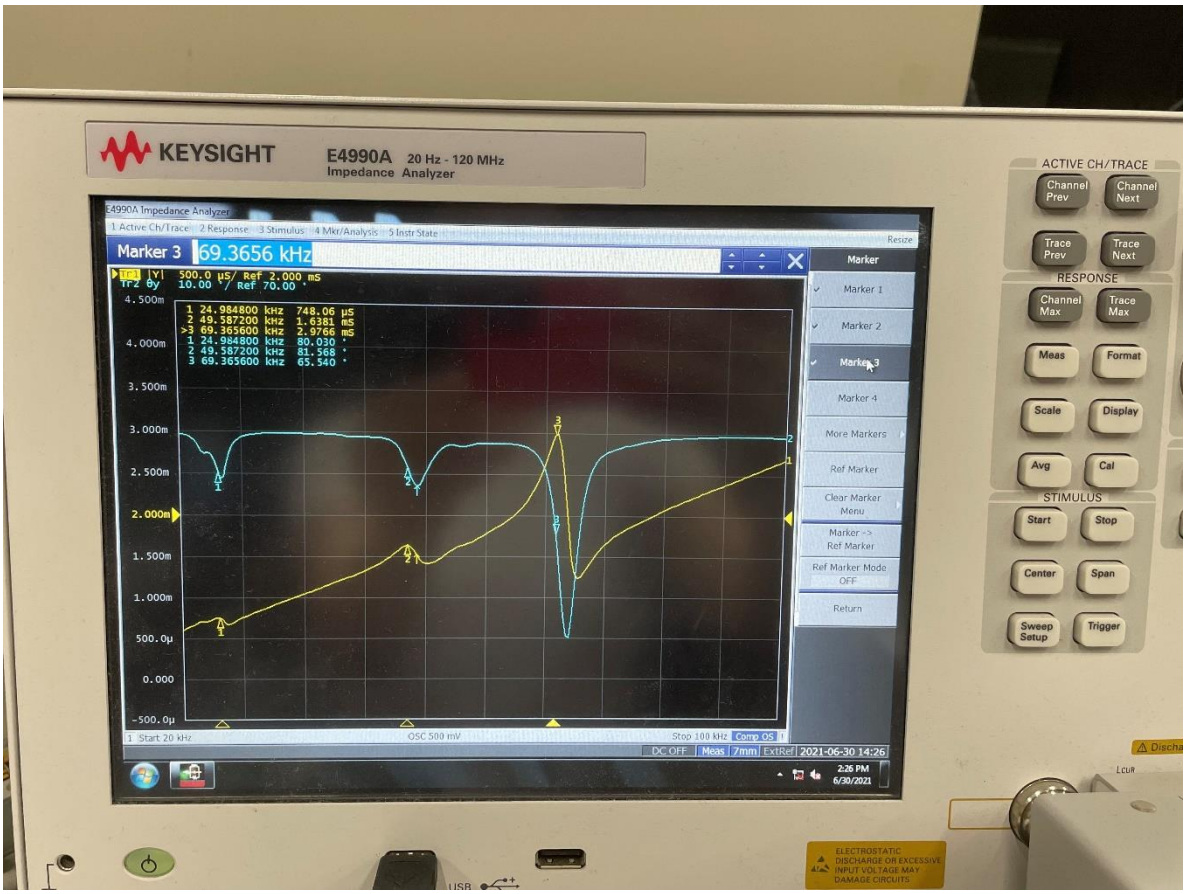

Figure 4.6 Impedance Analyzer (E4990A) during measurement of the resonance frequencies of an ultrasound liquid crystal lens

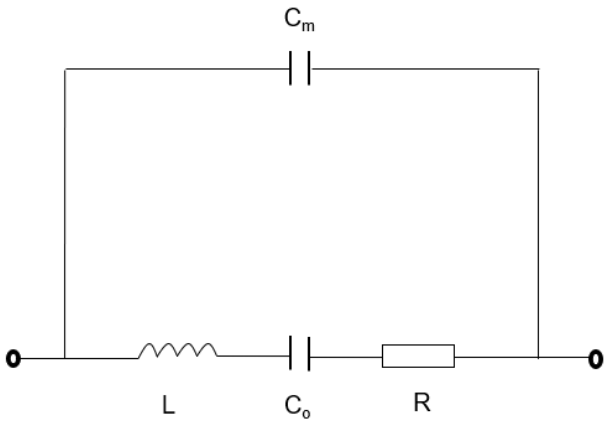

Figure 4.7 Electrical equivalent circuit of a PZT ring (Van Dyke model)

4.4.2. VIBRATION MODE MEASUREMENTS

Figure 4.8 shows a schematic of the experimental set-up for the vibration mode measurement. The vibrational displacement amplitude on the surface of the glass plate at the center (10x10 mm^2) at the resonance frequency of the lenses was measured by using a laser Doppler vibrometer (LDV, NLV-2500, Polytec) as a non-contact measurement to compare with the vibration modes simulated in the Ansys software.

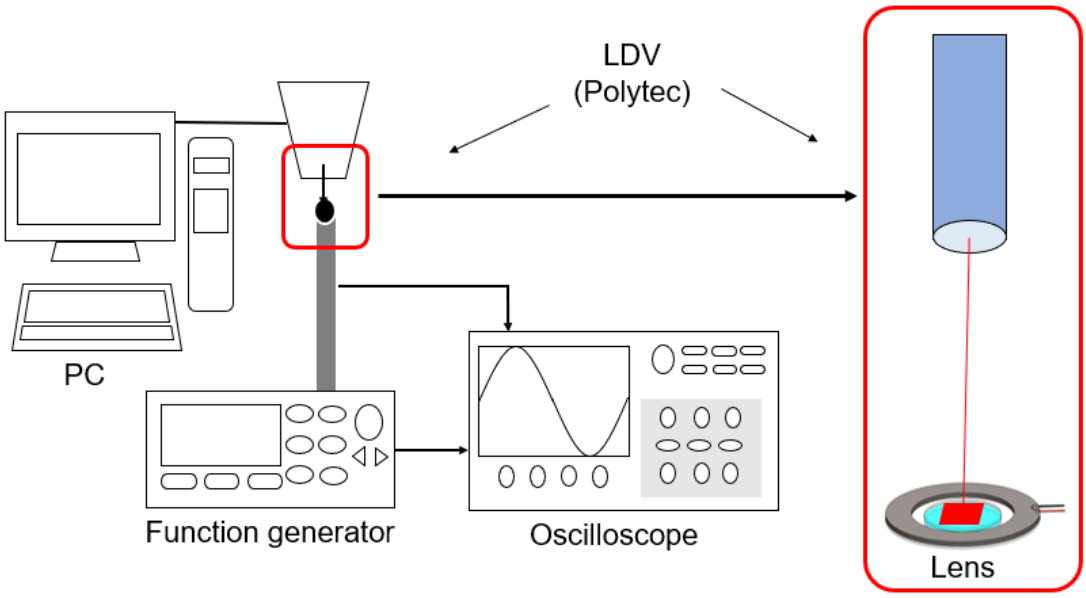

Figure 4.8 Glass surface vibration measurement using LDV

4.4.3. OPTICAL EVALUATION

In order to observe the transmitted light through the ultrasound controlled liquid lenses, two equipment's based in on the polarization of light were utilized: photodetector (2051-FS, Newport) – Fig. 4.9 (a) and an inverted polarization microscope (IX83, Olympus) – Fig. 4.9 (b). Both equipment's use two polarizers placed orthogonally to each other (i.e. crossed-Nicol configuration). In other words, if the polarizing direction of the first polarizer is oriented vertically to the incident beam, so only the waves with vertical direction can pass through it. The passed wave is subsequently blocked by the second polarizer (analyzer), since this polarizer is oriented horizontally to the incident wave. When the liquid crystal molecules have their orientation changed, it is possible to change the light polarization state and then the light can pass through the analyzer, and it can be detected. Figure 4.9 (c) illustrate the case without ultrasound excitation, in which a dark optical image can be observed – since the

molecules are vertically oriented as an initial condition (as described in Section 4.3.2). When the voltage is applied to the lens under ultrasound excitation, the flexural vibration generated in the lens allows the change in molecular orientation and consequently the polarized light can pass through the lens, increasing the brightness of the optical image Fig. 4.9 (d), enabling the measurement of the transmitted light through the lenses.

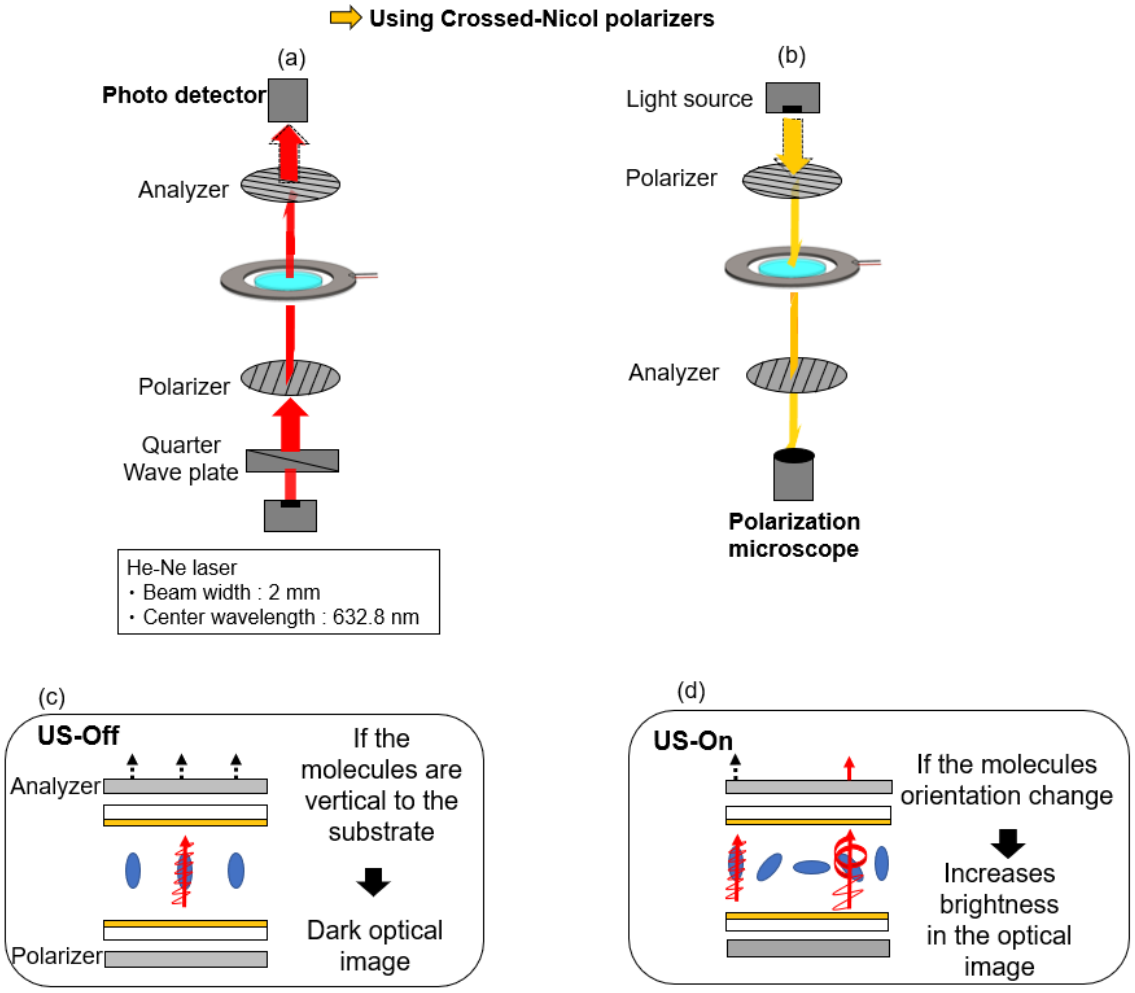

Figure 4.9 (a) Photodetector (2051-FS, Newport), (b) Polarization microscope (IX83, Olympus), observation system by the crossed-Nicol condition and relationship between the brightness and the molecular orientation :(c) without ultrasound; (d) with ultrasound.

A transmitted optical microscope (VW-9000, Keyence) with an objective lens (200×) and a single Nicol element was used to measure the focal length of the ultrasonically controlled liquid crystal lenses. A test target (1951 USAF) placed between the light source and the polarizer was moved vertically to evaluate the optical characteristics of the lenses without and under ultrasound (US) excitation – Fig. 4.10.

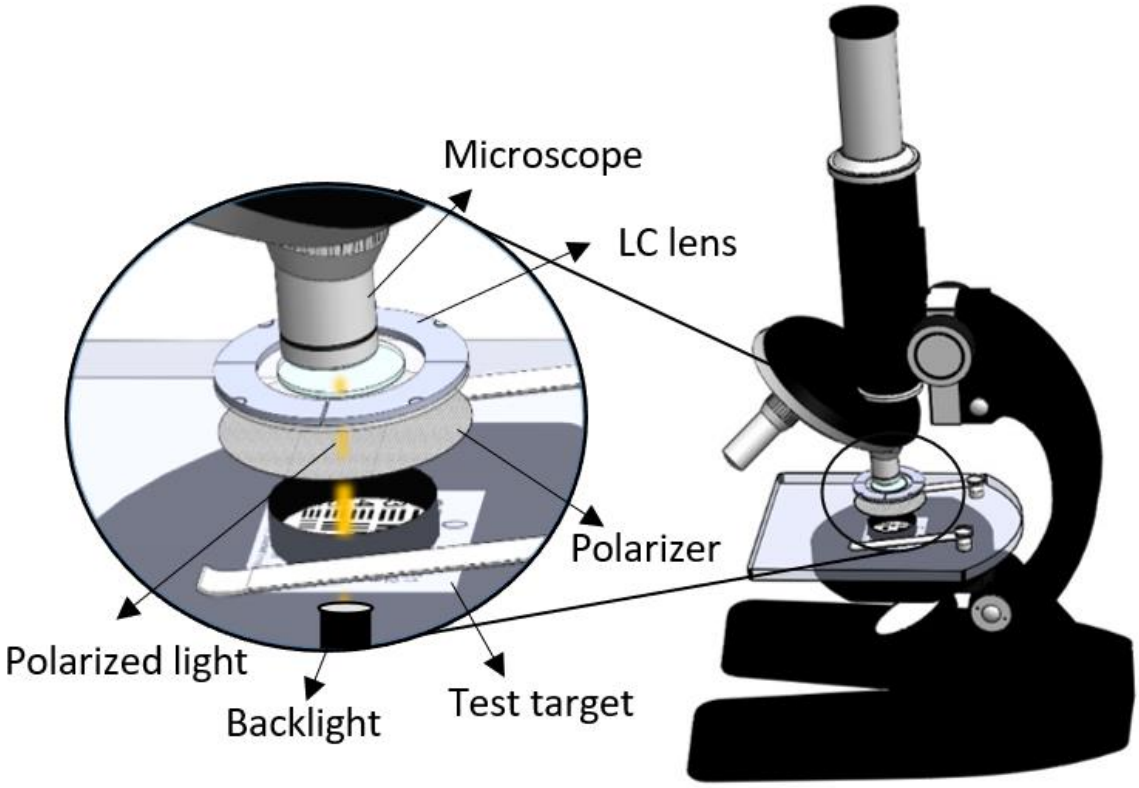

Figure 4.10 Observation set-up using a transmitted optical microscope

4.4.4. BIREFRINGENCE MEASUREMENTS

The rotation of the molecules results in a change in the optical birefringence of the liquid crystal, which is observable with polarized light [4.10]. One possible way to measure the effective birefringence of the liquid crystal material is through crossed-Nicol polarizers. However, this method relies on simultaneous rotation of both the polarizer and the analyzer

for the birefringence measurements. In this thesis, as an alternative, we used a birefringence profiler system [4.11], to measure the two-dimensional effective birefringence distribution for the fabricated liquid crystal lenses without the use of crossed polarizers as described below.

First, elliptically polarized light was obtained through use of an elliptical polarizer (i.e., a combination of a linear polarizer and a quarter-wave plate). The elliptically polarized beam that emerged from the quarter-wave plate is composed of two linearly polarized components with different amplitudes; their electric field (E-field) vectors (represented by E_x and E_y) in Fig. 4.11(a) were derived from Maxwell's equations. When the light beam travels through the liquid crystal along a principal axis, its phase is shifted because the light travels more slowly in the liquid crystal medium; the liquid crystal thus acts as a wave retarder. The light that is output after passing through the liquid crystal lens is represented by the output *E*-field vectors [E_x' E_y'] shown in Fig. 4.11(a). It is possible to describe the polarized light and its interaction with the optical elements using Jones calculus, whereas the polarization is described as a vector (Jones vector), and the linear optical elements are represented by the matrix *J* (Jones matrix). In other words, because it is possible to write the polarization state as a Jones vector [E_x E_y], the matrix *J* is used to transform from the input polarization [E_x E_y] into the output polarization [E_x' E_y']. *J* then operates as a transfer function to model the effect of the liquid crystal medium on the light's polarization state. Because the optical properties of an anisotropic crystal are dependent on the (*x, y*) directions, as shown in Fig. 4.11(a), we use the Jones matrix method, in which *J* represents the general form of a matrix to represent a wave retarder, to obtain:

$$J = \begin{bmatrix} \exp(i\phi_x) & 0 \\ 0 & \exp(i\phi_y) \end{bmatrix} \tag{4.1}$$

where, by considering the crystal properties, the phase ϕ is shifted by $\phi_x = k\ d\ n_x$ (in the *x*-direction) and $\phi_y = k\ d\ n_y$ (in the *y*-direction), with $k = 2\pi/\lambda$, where *k* is the wave number, and λ is the wavelength of the incident light; *d* is the liquid crystal layer thickness, and n_x and n_y

can be defined as the differences in the refractive index caused by the ultrasound ($\Delta n' = n_y - n_x$) because the polarized light that propagates into the liquid crystal is refracted as a result of the ultrasound excitation. However, from Fig. 4.11 (a), we can consider the following:

$$\begin{bmatrix} E_x' \\ E_y' \end{bmatrix} = \begin{bmatrix} \exp(i\phi_x) & 0 \\ 0 & exp(i\phi_y) \end{bmatrix} \begin{bmatrix} E_x \\ E_y \end{bmatrix} \tag{4.2}$$

Finally, the differences in the refractive index or the measured birefringence (Δn') upon ultrasound excitation can then be detected as a phase difference ($\Delta\phi$) between E_x' and E_y', related to the *x* and *y* polarization directions, as indicated in Fig. 4.11 (a). In contrast, the phase difference $\Delta\phi$ between the two components (E_x' and E_y') and the ratio of the ellipse are dependent upon the thickness (*d*) and the optical properties of the birefringent material target (i.e., the liquid crystal) used, and also upon the angle that the plane of vibration of the incident light makes with the principal plane of the lens. Strictly speaking, if light related to each orthogonal E-vibration travels with different speeds through the retardation element (the liquid crystal medium), there will then be a cumulative phase difference when the incident light emerges that is defined as the phase difference $\Delta\phi$, which appears in the polarization state. When the amplitudes of E_x' and E_y' are identical, the polarization changes are only reflected in the ellipticity of the polarization. Mathematically, the relationship between the phase difference ($\Delta\phi$), the liquid crystal molecular inclination (θ) and the birefringence in the *x*-*y* planes ($\Delta n'$), i.e., the change in the refractive index induced by the ultrasound, can be represented by:

$$\Delta\phi = \frac{2\pi}{\lambda}\{\Delta n'(\theta)d\} \ [rad] \tag{4.3}$$

where λ and *d* are the incident light wavelength and the liquid crystal lens thickness, respectively.

To acquire the distribution of this phase difference through the liquid crystal lens, it was used the birefringence profiler [4.11] as an appropriate measurement system. In this system, a two-dimensional effective birefringence distribution can be obtained via use of the

birefringence-light intensity conversion principle developed using a diffraction grating that shows a specific polarization dependence [4.12, 4.13]. Diffraction gratings formed by periodic modulation of their birefringence direction are known as polarization holograms and are recorded using two orthogonal circular polarizations in polarization-sensitive materials (Fig. 4.12(a)). In such gratings, the first-order diffraction intensities show symmetrical sinusoidal changes that depend on the phase difference of the incident light, as shown in Fig. 4.12(b) and 4.12(c). Note here that the sinusoidal changes are independent of the direction of the optical axis. In other words, the diffraction intensity is determined by the polarization ellipticity of the incident light. First, the observation light was adjusted to have left-handed circular polarization (polarization I in Fig. 4.12 (d)), where the +1- order diffraction intensity is almost zero. When a birefringent sample (i.e., the LC lens) is placed in the optical path, the polarization distribution is modulated (polarization II), and the diffraction intensity increases in a manner corresponding to the birefringence phase difference, based on the birefringence distribution. These phase differences can be detected as an optical intensity distribution using a digital camera based on the characteristics of the polarized light separation elements (i.e., the polarization gratings) shown in Fig. 4.12 (c). In this study, a closed-circuit television lens and the polarization gratings are combined to construct a birefringence profiler with a relatively broad observation field region that covers the entire liquid crystal lens.

Because the target effective birefringence distribution corresponds to the phase modulation distribution, the inverse transformation is performed by data processing using the following equation:

$$\Delta\phi(x, y) = 2\sin^{-1}\sqrt{\frac{I(x, y)}{\mathrm{I}_{\max.}}}\ [\mathrm{rad}] \tag{4.4}$$

where $\Delta\phi(x,y)$ and $I(x,y)$ represent the phase modulation and intensity distributions, respectively, in the x and y plane of the polarization directions, and I_{max} is the maximum diffraction intensity obtained as a result of the phase modulation given by a half-wave plate. With this optical system, variations in the phase shift between the ordinary and extraordinary

beams of the polarized light were produced by differences in the liquid crystal molecule orientation induced by ultrasound, where the magnitude of the birefringence can be detected and quantified as a phase difference ($\Delta\phi$). For the liquid crystal lens characterizations using the birefringence profiler, the detected phase difference distribution can also reveal the deviation angle ($\Delta\phi$) distribution analytically, as shown in Fig. 4.11 (b). In the off state, the liquid crystal molecules are vertically aligned ($\Delta n'$=0), which means that the polarization state of the incident light does not change while propagating through the liquid crystal lens. After incident light propagating along the z-axis emerges from the liquid crystal lens, the optical electric field is then used to evaluate the birefringence. In the birefringent medium (the liquid crystal layer) the anisotropic dielectric constants are characterized using the tensor ε in Eq. (4.5) [4.14], where ε_0 is the dielectric constant of a vacuum.

$$\varepsilon = \varepsilon_0 \begin{bmatrix} \varepsilon_{xx} & \varepsilon_{xy} & \varepsilon_{xz} \\ \varepsilon_{yx} & \varepsilon_{yy} & \varepsilon_{yz} \\ \varepsilon_{zx} & \varepsilon_{zy} & \varepsilon_{zz} \end{bmatrix} \tag{4.5}$$

It is assumed that the molecular reorientation caused by ultrasound excitation arises in the x-z plane (Fig. 4.11 (b)); then, by considering the uniaxial optical anisotropy of the liquid crystal medium, the element ε_{xx}, relative to the x-axis, can be written as $\varepsilon_{xx} = n_o^2 + (n_e^2 - n_o^2)\cos^2\theta$. We can also define n_x as:

$$\mathrm{n_x} = \sqrt{\varepsilon_{xx}} = \sqrt{n_o^2 + (n_e^2 - n_o^2)\cos^2\theta} \tag{4.6}$$

Given that $n_x \equiv n_x(\theta)$ and $n_y = n_o$, we obtain:

$$\Delta n(\theta) = n_x(\theta) - n_y \tag{4.7}$$

Equation (4.7) is substituted into Eq. (4.3) and is modified with regard to n_x as follows:

$$n_x = \frac{\Delta\phi\lambda}{2\pi d} + n_y \tag{4.8}$$

Finally, Eq. (4.8) is substituted into Eq. (4.6), and θ can then be expressed as:

$$\theta = \cos^{-1}\sqrt{\frac{n_x^2 - n_o^2}{n_e^2 - n_o^2}} \tag{4.9}$$

Therefore, the deviation angle ($\Delta\theta$) in Fig. 4.11(b) that represents the angular variation of the liquid crystal's molecular orientation under ultrasound excitation can be calculated from $\Delta\theta = \pi/2 - \theta$.

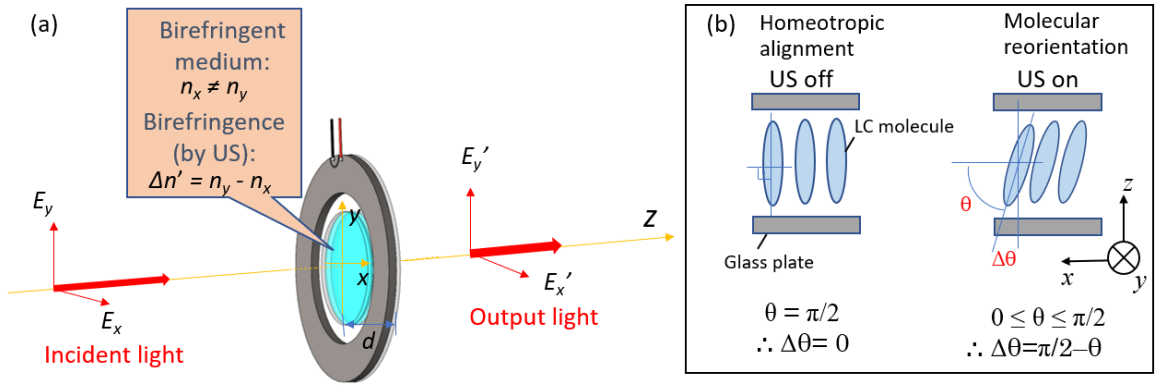

Figure 4.11 (a) Birefringence and phase difference—polarization direction. (b) Molecular reorientation under ultrasound (US) excitation.

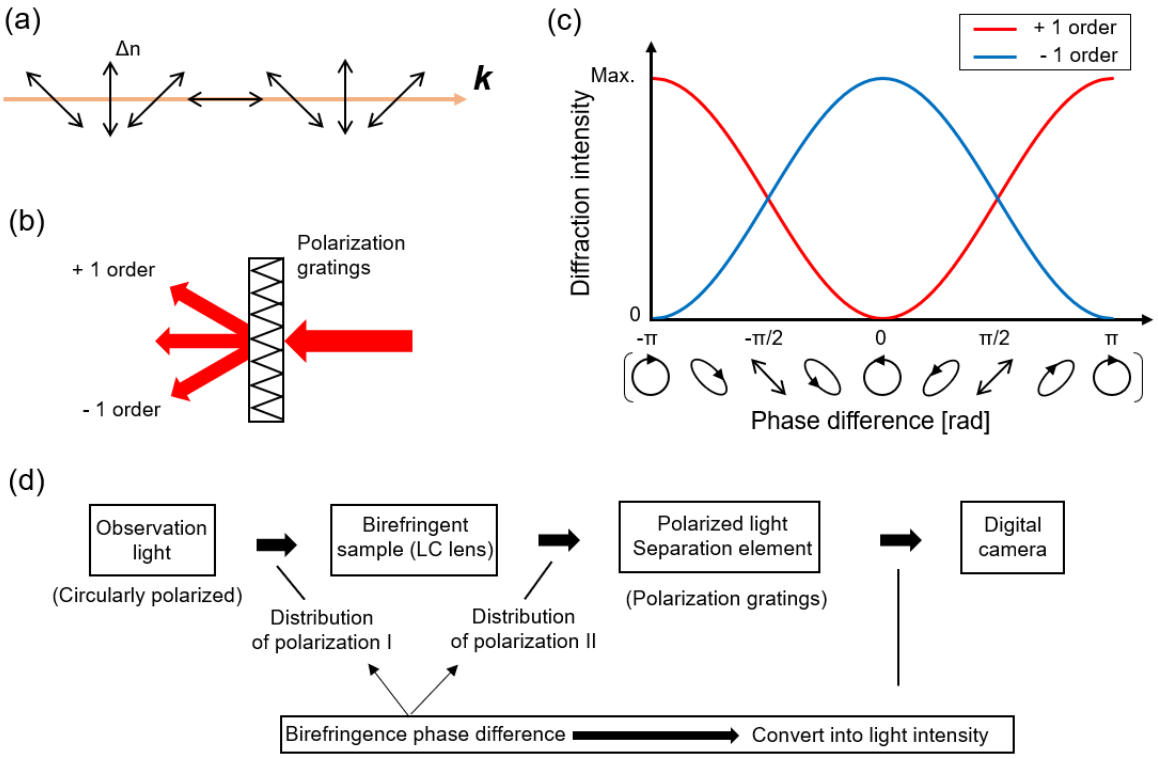

Figure 4.12 Birefringence profiler operating principle: (a) periodic modulation of the birefringence, (b) first-order diffractions, (c) diffraction intensity dependence on the ellipticity of the incident light, and (d) phase modulation detection diagram.

REFERENCES

[4.1] S. Taniguchi, D. Koyama, Y. Shimizu, A. Emoto, K. Nakamura and M. Matsukawa, "Control of liquid crystal molecular orientation using ultrasound vibration," *Applied Physics Letters*, vol. 108, no. 10, p. 101103, 2016.

[4.2] Y. Shimizu, D. Koyama, S. Taniguchi, A. Emoto, K. Nakamura and M. Matsukawa, "Periodic pattern of liquid crystal molecular orientation induced by ultrasound vibrations," *Applied Physics Letters*, vol. 111, no. 23, p. 231101, 2017.

[4.3] Y. Shimizu, D. Koyama, M. Fukui, A. Emoto, K. Nakamura and M. Matsukawa, "Ultrasound liquid crystal lens," *Applied Physics Letters*, vol. 112, no. 16, p. 161104, 2018.

[4.4] D. Meyerhofer, "Characteristics of resist films produced by spinning,*"Journal of Applied Physics,* vol. 49, no. 7, p. 3993–3997, 1978.

[4.5] S. Kobayashi, K. Kuroda, M. Matsuo, M. Nishikawa, "Alignment Films for Liquid Crystal Devices," In The Liquid Crystal Display Story, *Springer Japan: Tokyo*; pp. 59–80, 2014.

[4.6] S. T. Wu and D. K. Yang, "Fundamentals of Liquid Crystal Devices," *John Wiley & Sons*, Hoboken, NJ, 2006.

[4.7] Keysight Technologies, "Impedance Measurement Handbook: A Guide to Measurement Technology and Techniques.", 2016.

[4.8] S. Butterworth, "On electrically-maintained vibrations," *Proceedings of the Physical Society*, London, vol. 27, no. 1, pp. 420–424, 1915.

[4.9] P.V. Kasambe, V.V. Asgaonkar, A.D. Bangera, A.S. Lokre, S.S. Rathod and D.V. Bhoir, "Piezoelectric lead zirconate titanate (PZT) ring shaped contour-mode MEMS resonators," In *IOP Conference Series: Materials Science and Engineering*, vol. 310, no. 1, p. 012069. IOP Publishing, 2018.

[4.10] V. A. Greanya, M. S. Spector, J. V. Selinger, B. T. Weslowski and R. Shashidhar, "Acousto-optic response of nematic liquid crystals," *Journal of Applied Physics*, vol. 94, no. 12, pp.7571-7575, 2003.

[4.11] A. Emoto, N. Otani, and T. Fukuda, "Birefringence measurement device and birefringence measurement method," (U.S. patent 10,119,904 2018).

[4.12] T. Sasaki, A. Hatayama, A. Emoto, H. Ono, and N. Kawatsuki, "Simple detection of light polarization by using crossed polarization gratings". *Journal of Applied Physics*, vol. 100, no. 6, p.063502, 2006.

[4.13] H. Ono, A. Emoto, F. Takahashi, N. Kawatsuki and T. Hasegawa "Highly stable polarization gratings in photocrosslinkable polymer liquid crystals". *Journal of Applied Physics*, vol. 94, no. 3, pp.1298-1303, 2003.

[4.14] A. Emoto, M. Nishi, M. Okada, S. Manabe, S. Matsui, N. Kawatsuki, and H. Ono, "Form birefringence in intrinsic birefringent media possessing a subwavelength structure," *Applied Optics*, vol. 49, no. 23, pp.4355-4361, 2010.

CHAPTER 5:LENS APERTURE EXPANSION

5.1. INFLUENCE OF THE LENS GEOMETRY IN THE OPTICAL PROPERTIES

5.1.1. MODEL CREATION AND TRAVELING WAVE GENERATION

The first ultrasound liquid crystal lens with 50 μm of layer thickness [5.1] developed was based in a single-channel transducer, as described in Section 3.2.5 of Chapter 3. Using the single channel' lens, the liquid crystal molecular orientation was controlled using a standing wave (SW), and the center point corresponded to the antinodal position of the lens when operating as a convex lens, although the lens aperture was not considered. It was also observed experimentally that the optical characteristics of the liquid crystal lens were related directly to the vibrational mode and the sound pressure distribution within the liquid crystal layer. When an axisymmetric standing wave mode is applied, the lens aperture tends to have a fixed small area because the molecular orientation is correlated with the lens' vibrational distribution and the acoustic radiation force is stronger exclusively at the lens center, where the vibrational amplitude has a higher value.

In addition, there is a strong relationship between the liquid crystal lens aperture and the liquid crystal layer thickness. By controlling the spatial orientation of the liquid crystal molecules under application of an electric field, each point on the wavefront of a plane wave passing through the liquid crystal layer presents a different light speed. Consequently, the incident plane wave is converted into a paraboloidal wave, where the parabola's concavity then determines the effective aperture of the liquid crystal lens. The focal length will depend on the molecular orientation within the liquid crystal layer. Furthermore, a larger focal length range requires a thicker liquid crystal layer. However, the nematic liquid crystal lens shows strong light scattering at higher thicknesses [5.2]. There is thus a trade-off between the liquid crystal layer thickness and the liquid crystal lens aperture size.

To overcome the dilemma between the lens thickness and aperture size, an ultrasonically controlled liquid crystal lens based on a multichannel piezoelectric transducer with the aim of expanding the liquid crystal lens aperture was developed. The novel ultrasound liquid crystal was fabricated as shown in Fig. 5.1. A nematic liquid crystal (5CB) layer with the thickness of 0.2 mm was sandwiched between two circular glass plates with thickness of 0.5 mm (diameters: 15 mm and 30 mm). Initially, liquid crystal molecular orientation is perpendicular to the glass plates due to chemical interaction between liquid crystal molecules and the oriented film formed on the surface of the glass plates. An annular piezoelectric lead zirconate titanate (PZT) ultrasound transducer (C-213, Fuji Ceramics, thickness: 1 mm; inner diameter: 20 mm, outer diameter: 30 mm) was bonded to a glass plate with larger diameter. The PZT electrode was separated electrically in four quadrants (CH1 to CH4) for four-phase drive. A traveling wave (TW) carries energy across a distance in the medium [a lead zirconate titanate (PZT) element] and this energy can be used as a propulsion mechanism to enable concave lens functionality with larger aperture sizes. In the standing wave case, because the standing wave consists of nodes and antinodes, the energy remains associated with a specific location, thus limiting the lens aperture – Fig. 5.2.

Traveling waves propagate along the circumference of the piezoelectric ring to produce the characteristics of the concave lens. The theory that applies to ultrasonic motors [5.3] and piezoelectric transformers [5.4] was taken into consideration for development of the LC lens application. To apply traveling wave theory within the liquid crystal lens geometry, two SWs must be generated in the PZT structure (Fig. 5.2). For this purpose, the standing wave generation will mostly depend on the electrode scheme at the PZT element surface. Sinusoidal electric signals with phase shifts of 90^o were applied to the four electrodes ($\theta = 0^o$, 90^o, 180^o, 270^o for CH1–CH4, respectively). The model of the liquid crystal lens using a traveling must also consider the material properties, the geometrical deformation, and the boundary conditions. In this way, a concave lens model was simulated using the finite element analysis (FEA) software ANSYS to characterize the behavior and attributes of the traveling before fabrication [Fig. 5.3]. The modelling results showed that a combination of the lens geometry, the electrode scheme with the four input electrodes, and selection of

appropriate excitation voltages for the piezoelectric transducers allow generation of a traveling wave at 47 kHz.

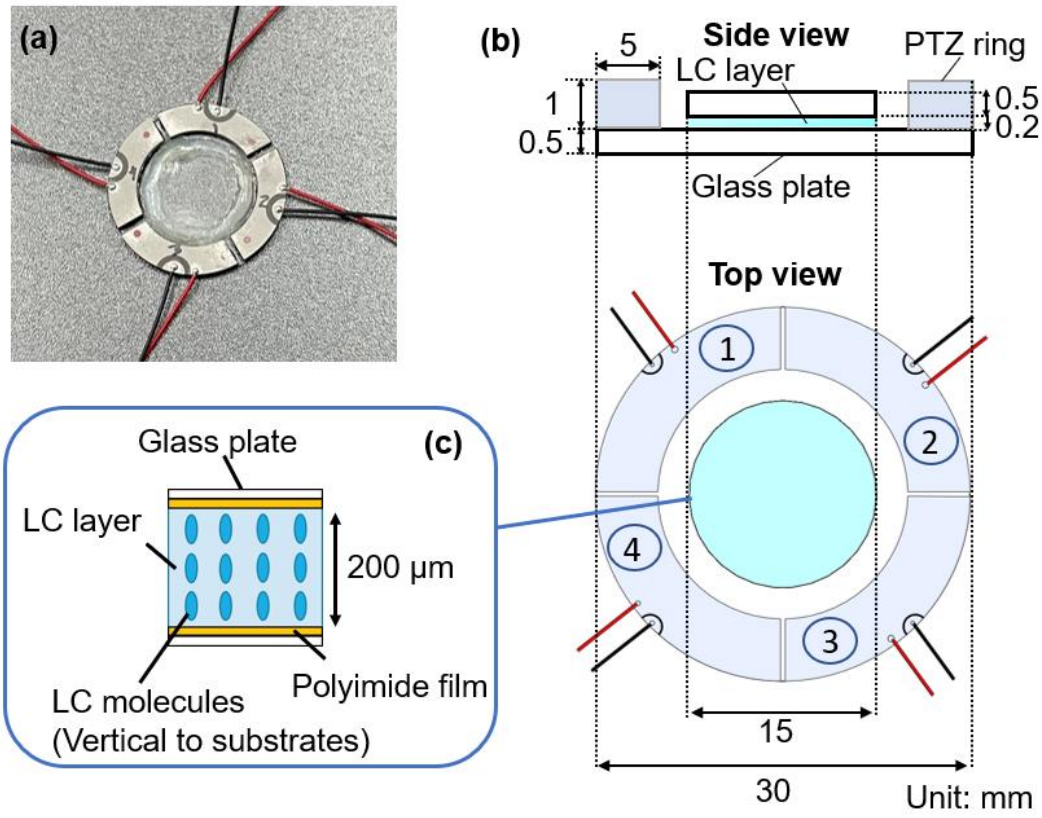

Figure 5.1 Ultrasound liquid crystal lens. (a) Photograph; (b) cross sectional and top view; and (c) initial orientation (vertical) of the nematic liquid crystal molecules.

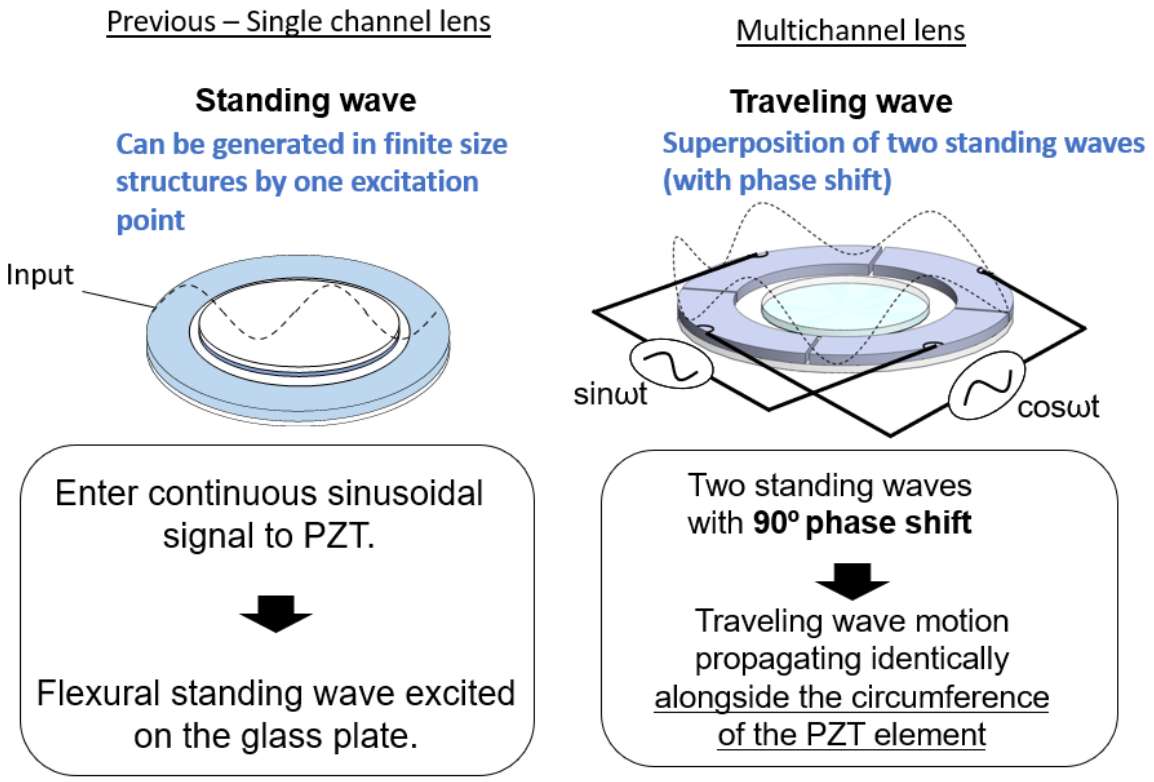

Figure 5.2 Standing wave and traveling wave principles

The operational characteristics of the proposed lens were investigated experimentally to validate both the concept and the analytical model. The same flexural vibration mode calculated using FEA [Fig. 5.3] was generated at 32.2 kHz. The difference between the resonance frequency values in the experimental and simulated results was attributed to a difference between the values of the elastic moduli of the glass plates used in the two cases. Figure 5.4 provides an illustrated comparison of the flexural vibration mode results from the simulations and those obtained under the experimental conditions. The measurement area of 10x10 mm^2 was located at the center of the upper glass plate. The plots at the bottom of Fig. 5.4 show the profiles along the line A-A' when the input voltages were applied. The curves represent the vibrational displacement amplitude distributions of the glass substrates at the ultrasound frequencies when measured using a laser Doppler vibrometer (LDV; NLV2500, PI Polytec, Germany) and from the simulations using Ansys. Although the driving

frequencies used in the experiments and simulations were distinct, the curves have similar shapes, indicating goodness-of-fit (r-squared value 0.98), and thus validating the simulated model.

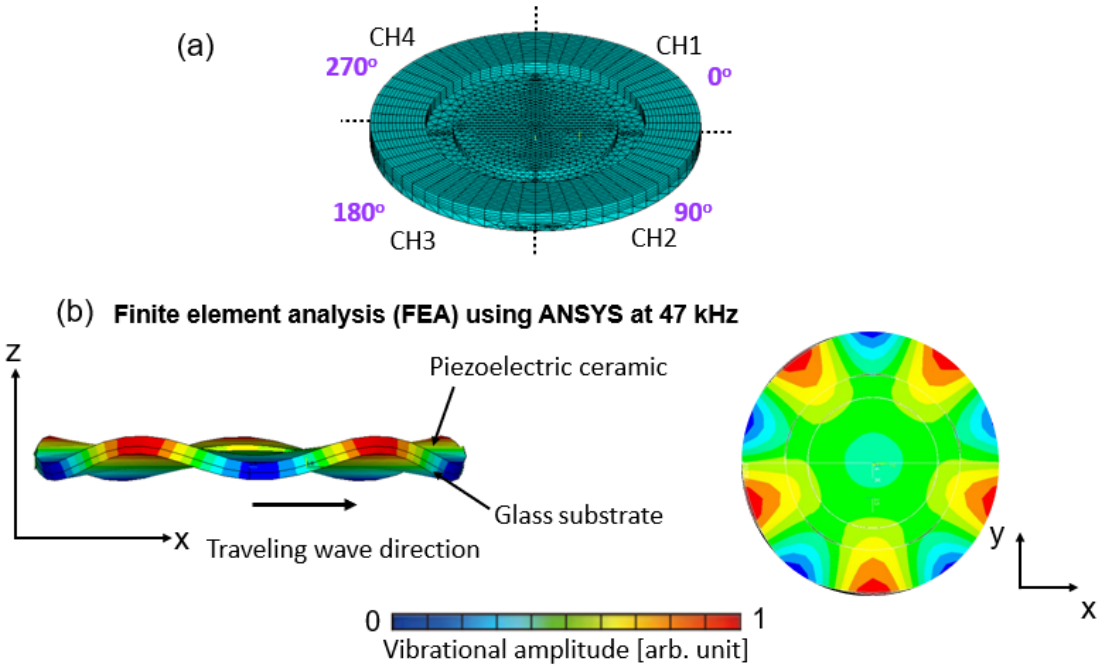

Figure 5.3 Ansys simulation for the generation of the traveling wave: (a) meshed model, (b) Traveling wave generated at 47 kHz

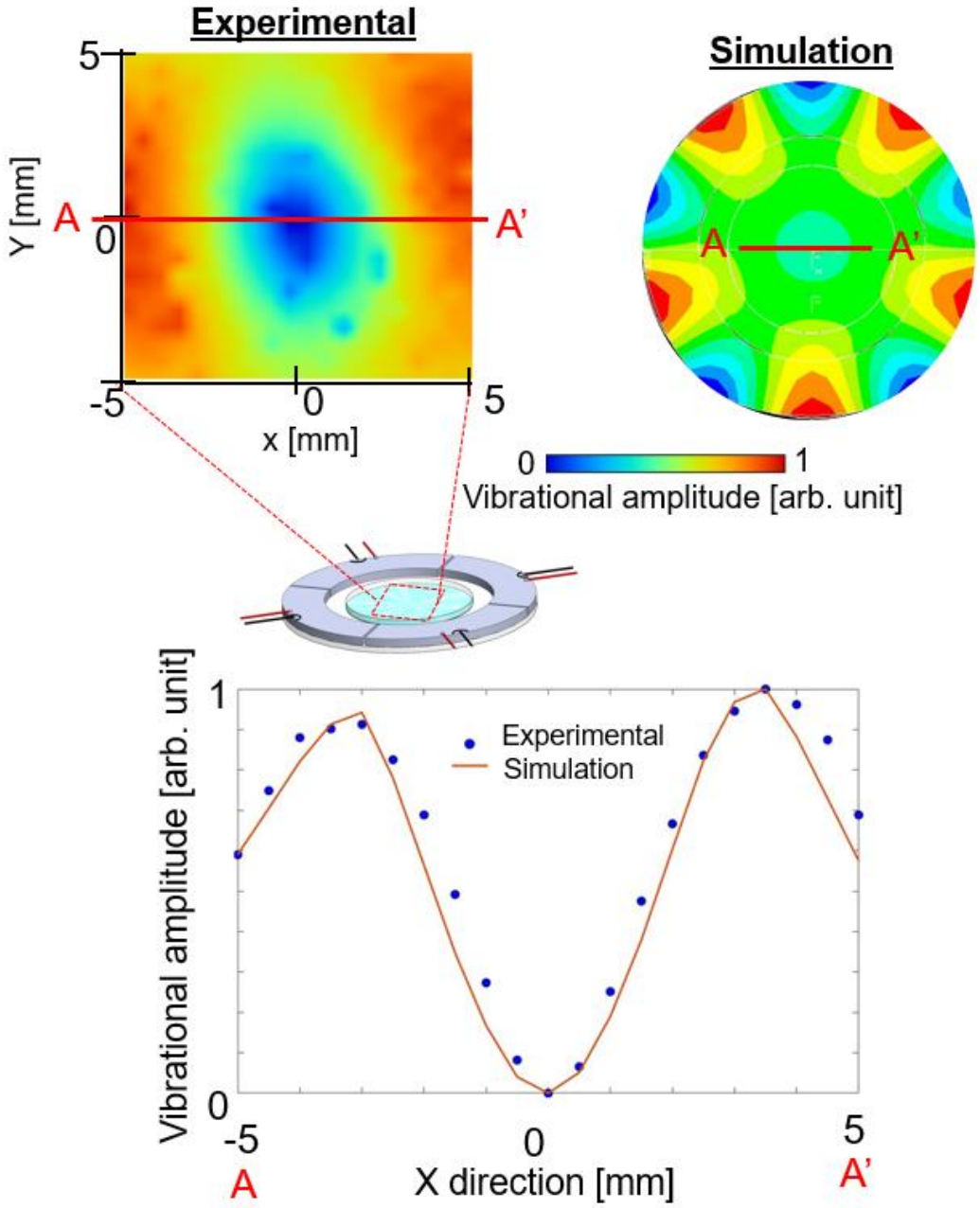

Figure 5.4 Ansys vibrational amplitude distributions of the glass substrates (experimental and simulated) of the lens using the traveling wave.

The vibration distribution on the upper glass plate was varied by controlling the driving channel conditions. When all channels were excited in phase using the same voltage amplitude and the same resonance frequency (32.2 kHz) by a flexural standing wave, an axisymmetric flexural vibration mode was generated in the lens, as reported in the previous study [5.1], and the liquid crystal layer was statically deformed by the acoustic radiation forces acting on the boundaries among the liquid crystal layer, the glass plates, and the surrounding air. Strictly speaking, the ultrasound wave that propagated from the SW flexural vibration was partially reflected at the boundaries, thus enabling the acoustic radiation force to change the liquid crystal molecular orientation and producing the variable-focus lens. However, when the input voltage was applied using two standing waves excited at 90^{o} in both space and phase relative to each other, a flexural traveling wave could be generated on the lens [Fig. 5.3 (b)] at 32.2 kHz. The acoustic radiation force was generated by flexural vibration of the glass substrates, thus changing the liquid crystal molecular orientation. The lens center corresponded to the nodal position with minimum displacement for this vibration [5.5].

5.1.2. WAVE FRONT ANALYSIS

A precise determination of the optical properties of a lens is commonly critical for building an accurate optical system model. Wavefront analysis [5.6] is a method to measure and better understand the lens properties, such as focal length, lens aperture, refractive index and optical aberrations. It allows, for instance, the creation and improvement of lenses fabrication, providing the highest quality vision. To better understand the ultrasonically controlled liquid crystal lens properties, a Shack–Hartmann wavefront sensor was used to generate the lens profile. Moreover, it was possible to perform optical characterization of the liquid crystal lens by this wavefront analysis.

The Shack-Hartmann wavefront sensor (Thorlabs Inc., Newton, NJ), in Fig. 5.5 (a), was used to generate a profile of the ultrasound liquid crystal lens and perform the wavefront analysis, by tracking the position of the focal spots on the detector [Fig. 5.5 (b)]. In the case

of an incoming wavefront is plane, all focal spot images are located in a regular grid defined by the lens array geometry. As soon as the wavefront contains aberration, the images of the focal spots become displaced from their initial positions [Fig. 5.5 (c)]. Then, by comparing the shift in position of the rays with an ideal lens, the aberrations and other optical parameters can be determined.

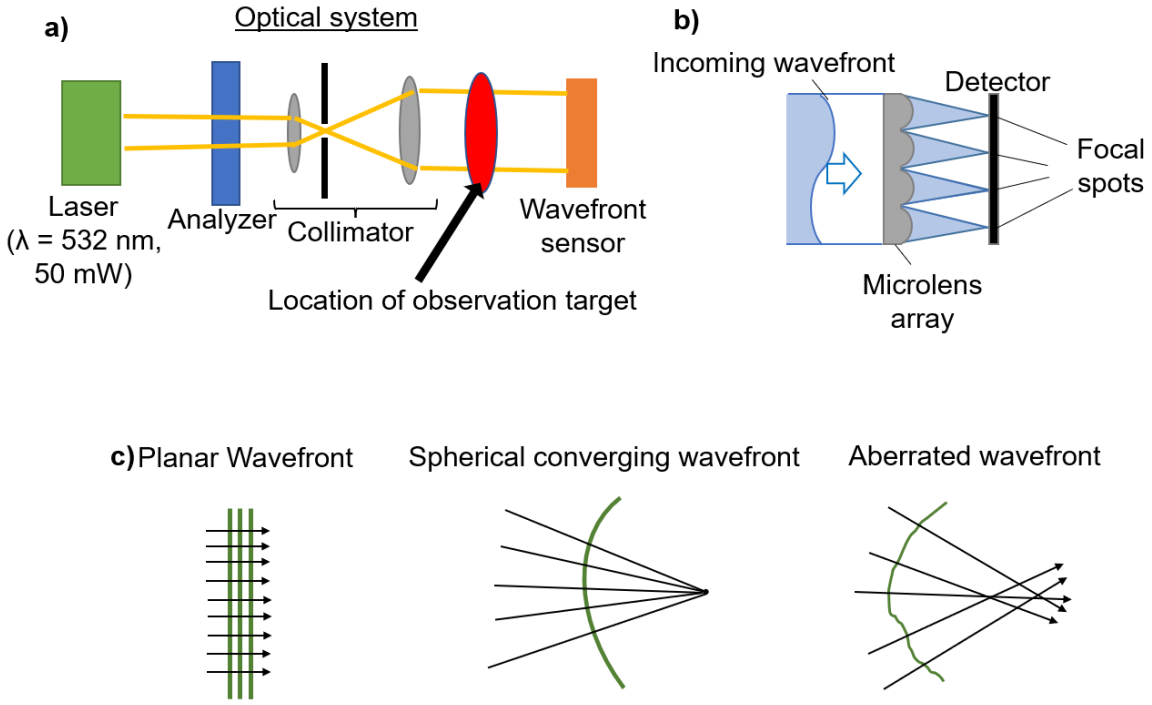

Figure 5.5 Wavefront sensor working principle: a) Set-up; b), c) incoming wavefronts examples

The wavefront analysis and optical characterization were determined by considering the physical principals presented in Fig. 5.6, where ΔZ is optical path difference, $2\Delta Z$ corresponds to the effective area of the wavefront sensor. D represents the distance between the sensor and liquid crystal lens during the measurements and f is the estimated focal length. A commercial plastic lens was first tested to verify the reliability of the physical model and the set-up. The relative error of focal length (f) calculated was 1.02%, compared to the manufacturer-reported f. The liquid crystal lens was clamped in vertical orientation in close

proximity to the wavefront sensor (D = 55 mm). The lens focal length, $f = R$ (radius of curvature of incoming light) - D (distance between test lens and sensor). The calculated focal length value was 3.8×10^3 mm. The effective aperture of the LC lens ($2C$) is determined by the parabolic wavefront at the LC lens. According to Fig. 5.6 (c), using similarity of triangles, we have the following relation:

$$\frac{C}{\Delta x} = \frac{f}{R/\cos\theta} \tag{5.1}$$

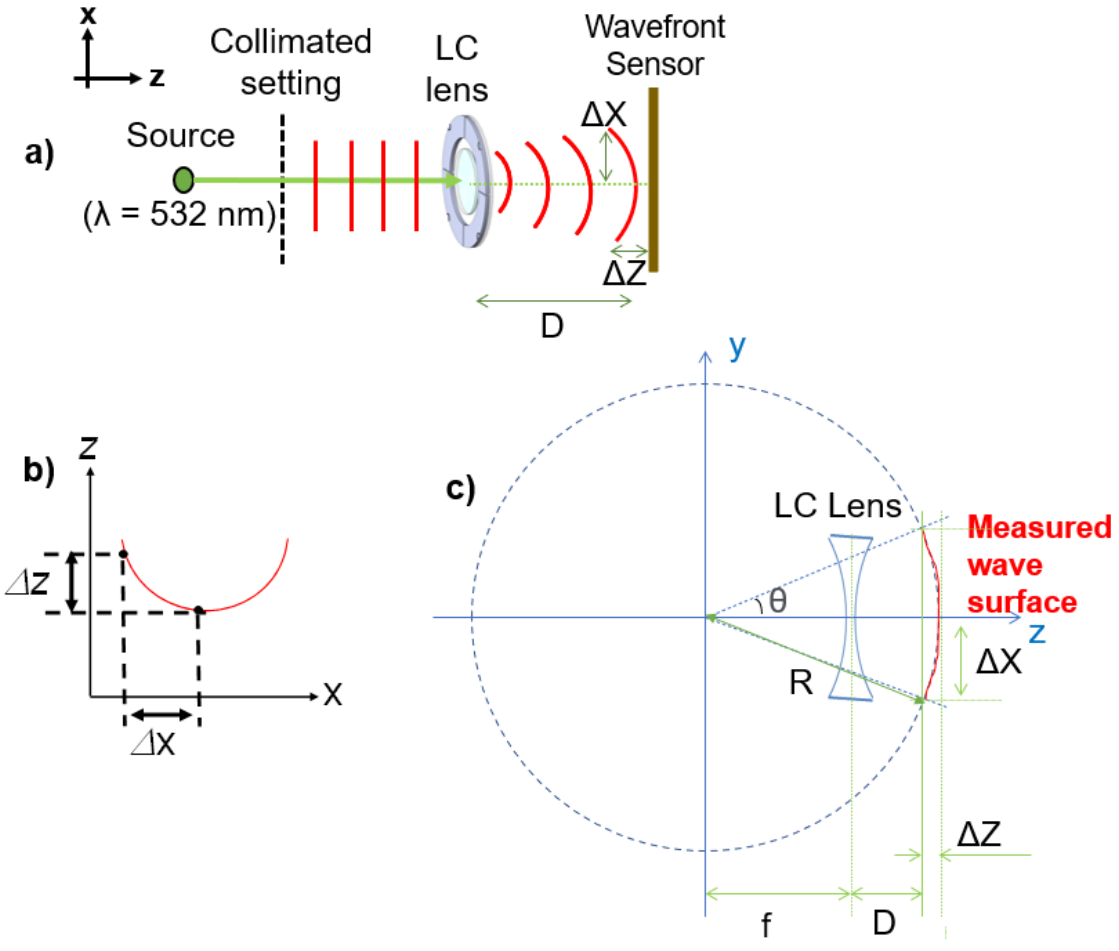

Figure 5.6 (a) Set-up and (b),(c) physical principles of the wavefront sensor.

The calculated lens effective aperture was equivalent to 4.4 mm and 2.5 mm for traveling wave and standing wave, respectively. By using a Shack–Hartmann wavefront sensor to generate a three-dimensional (3D) profile of the LC lens, it becomes possible to perform optical characterization of the lens. A laser beam (λ=532 nm) with a beam width slightly smaller than 4 mm was collimated and passed through the LC lens. The transmitted light was received by the wavefront sensor at the position located 55 mm from the LC lens. The outgoing wavefront was determined via the optical path difference, which was dependent on the refractive index distribution in the LC lens. The measurement area of the wavefront sensor was 4x4 mm^2 at the center of the LC lens. Figure 5.7 shows the surface profile of the LC lens measured using the wavefront sensor (top figure) and the two-dimensional profile plots (bottom figure) for (a) the SW mode (CH1–CH4: 19 V_{pp}, in phase) and (b) the TW mode (CH1 and CH3: 12.8 V_{pp}; CH2 and CH4: 12.4 V_{pp}; phase-shift 90^o). The vertical axis indicates the optical path difference. The z-scale and the corresponding color bar units are given in wavelengths (which correspond to 532 nm).

Because the effective optical refractive index distribution in the LC layer varies according to the molecular orientation distribution, it is possible to estimate the refractive index distribution in the LC lens using both SW and TW modes. Besides, the wavefront measured is derived from a summation of orthonormal Zernike functions weighted by Zernike coefficients (C_n). Each C_n corresponds to one optical aberration. The goal was to make sure that C_n would be as close to 0 as possible. This sensor follows the ANSI Standard Z80.28-210.

To quantify and verify the optical quality of LC lens, the high-order Zernike coefficients (Spherical aberration, Coma and Astigmatism) were compared between standing wave and traveling wave. Overall, the Zernick coefficients presented small aberrations for the TW, indicating a higher image quality for the TW mode, as shown Table 5.1. Wavefront aberrations are the deviations in optical lens between the actual and ideal wavefronts. Rayleigh defined that one quarter-wave aberration diminishes the irradiance of the images disk by about 20% [5.7]

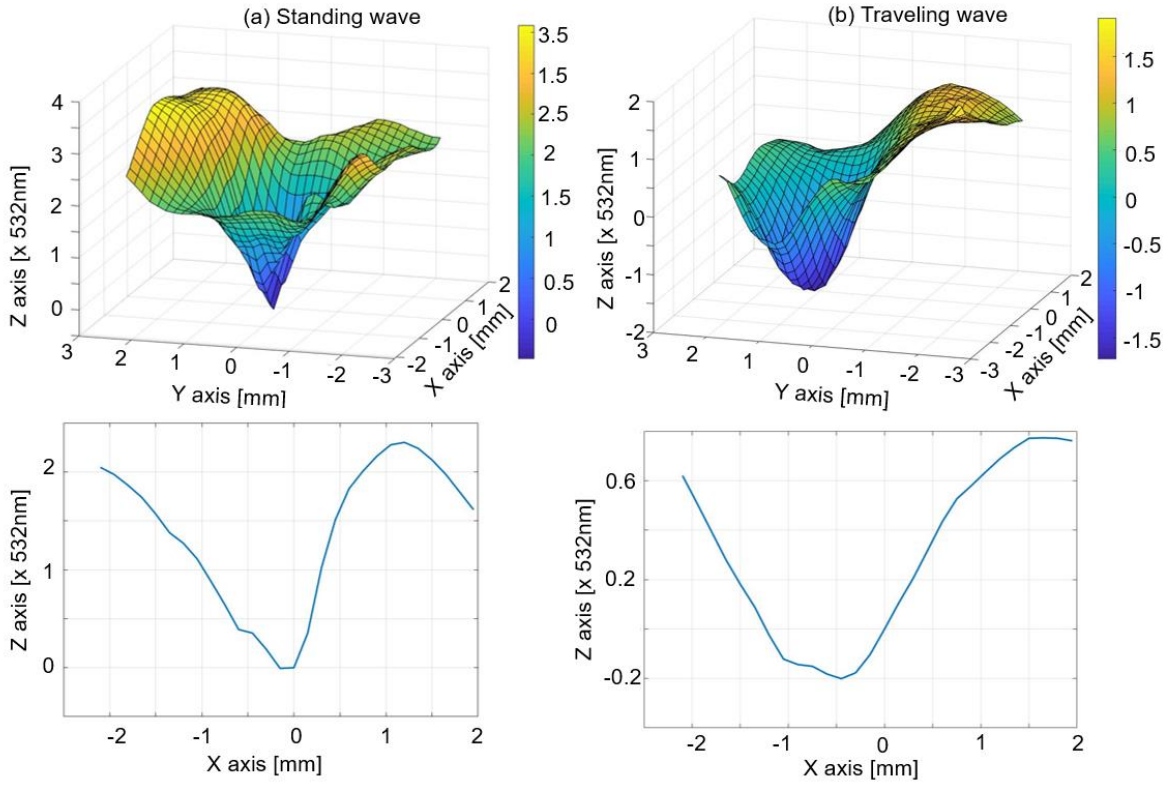

Fig. 5.7 Plots generated using the wavefront sensor showing the shape of a plane wave after it has passed through the lens under ultrasound excitation using (a) an SW and (b) a TW

Table 5.1 High-order Zernike Coefficients of SW and TW Modes

Zernike Coefficients (C_n^m)	Standing Wave	Traveling Wave
Spherical aberration (C_4^0)	-0.059 µm	-0.004 µm
Coma (C_3^1, C_3^{-1})	-0.053 µm, -0.05 µm	-0.030 µm, -0.066 µm
Astigmatism (C_2^2, C_2^{-2})	0.013 µm, -0.012 µm	-0.034 µm, -0.084 µm

Given that the distance equivalent to the LC layer thickness that light will travel in a specified time (Δt) is represented by $\Delta d = c' \times \Delta t$, the time taken to pass through the lens

center is determined using the ratio of 200 μm to the speed of light in the LC layer ($c' = c/n$), where c is the speed of light (3.0×10^8 m/s), and n is the refractive index of LC. According to the LC manufacturer, the refractive index for ordinary light n_o=1.53 (5CB, TCI). By considering the wavefront profile and taking the center of the lens at the valley of the curve to be a reference point (where the LC molecule is vertically oriented), the delay time t_l corresponds to the time difference between the times taken by the light ray to pass through the lens center and the other surface parts based on the Δz distance (vertical axis). In other words, the refractive index (n) for light traveling in the LC medium is given by Δz. The calculations were performed for the LC material 5CB and by analyzing the data acquired from the wavefront sensor represented in the previous figure. The curves in Fig. 5.8 represent the variations in the refractive index in the LC layer for the SW and TW modes. For calculation purposes, we assumed the liquid crystal molecules have the same angle of inclination vertically orientated.

Comparison of the two curves in Fig. 5.8 shows that the TW has a small change in refractive index and a longer focal length when compared with the SW mode. Although the node and antinode positions of the vibration are different for the SW (where the center corresponds to the antinode) and the TW (where the center corresponds to the node) modes, the wavelengths are almost the same. However, the TW aperture is surprisingly larger. These results confirm the relationship between the refractive index and the vibration distribution.

The aperture size difference between the results obtained using the SW and TW modes is attributed to the natures of the two waves and to the vibration mode of the PZT and the sound pressure distribution in the LC layer, which differ in both cases. In the SW mode, the acoustic radiation force acts exclusively more strongly around the center (vibration and acoustic pressure antinode) of the lens and affects the top-glass-substrate boundaries minimally. In the TW mode case, in contrast, the acoustic radiation force acts more strongly at the boundaries of the glass plates (because the TW acting in the PZT element transmits energy while the TW moves in the circumferential direction); around the center of the lens, the action is minimal, but is sufficient to cause incident light to encounter different refractive indices due to the inclination of the LC molecular orientation toward the center of the lens.

This means that the aperture is larger because the acoustic radiation force should move particles away from this point. In other words, the elasticity of the LC causes the refractive index to change smoothly toward the lens center in accordance with the lens vibration mode. Furthermore, the LC lens aperture showed strong relation with the frequency operation, since the larger aperture was obtained under low frequency when compared to the previous lens work [5.1], indicating that the aperture is limited by the lower-resonance frequency. The LC refractive index measurements are fundamentally required to validate the physical models and the LC device design. By considering a single LC molecule, it is possible to estimate the rotational angle ϑ of the single molecule under ultrasound excitation using the following equation [5.8]:

$$\sin^2 \vartheta = \frac{\frac{n_o^2 \times n_e^2}{n_{eff}^2} - n_e^2}{(n_o^2 - n_e^2)} \tag{5.2}$$

Here, n_{eff} is the refractive index of LC (uniaxial material), which variation is represented by the vertical axis in Fig. 5.8 between the ordinary (n_o =1.53) and extraordinary (n_e =1.716) refractive indices. The maximum rotational angles calculated for the SW and TW modes was 2.48^o at x = 1.1 mm and 1.18^o at x = 1.7 mm, respectively, indicating the SW mode promoted a larger change in the refractive index, as already confirmed in the graph of Fig. 5.8. Because the optical characteristics of the LC lens are correlated with the vibrational mode, the rotation angle is also dependent on the vibrational amplitude.

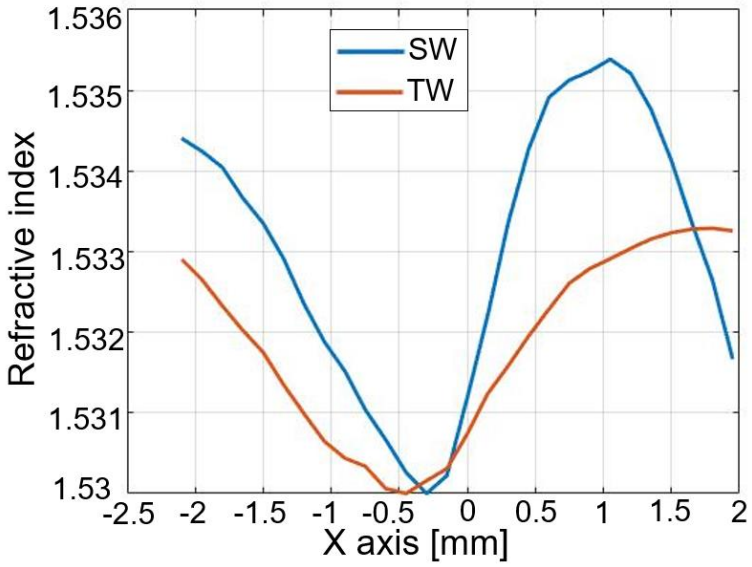

Fig. 5.8 Variation in the refractive index for SW and TW modes

`

5.1.3. FOCAL LENGTH AND VIBRATIONAL AMPLITUDE

The optical observation explained in the Section 4.4.3 with the ultrasound liquid crystal lens by SW using a transmission optical microscope (VW-9000, Keyence) with an objective lens (200×) and a single Nicol element was performed using the new lens based on the TW generation. A test target (1951 USAF) placed between the light source and the polarizer was moved vertically to evaluate the optical characteristics of the lens without and under ultrasound (US) excitation. The focal length was measured by moving the test target vertically between the polarizer and the optical source. It could be confirmed that the focal point changed along the optical axis of the lens under ultrasound excitation using one Nicol element, and the lens thus acted as a variable-focus lens. Figure 5.9 shows the relationship between the vibrational amplitude of the glass substrates and the focal length of the LC lens observed using the microscope, i.e., comparing the TW mode with the SW mode. The focal length without applied ultrasound excitation was considered to be 0 mm. As the vibrational amplitude of the glass substrates increased, the focal length increased as well, indicating the

focal point of the lens could be controlled by the displacement amplitude of the TW. Interestingly, in the case of the LC lens using SW, the focal length did not increase significantly proportionally to the vibrational amplitude. This focal length observed by microscope is different from that one calculated using the wavefront measured by Shack–Hartmann wavefront sensor. Since in the case of the microscope, the focal length observation includes the objective lens of the microscope.

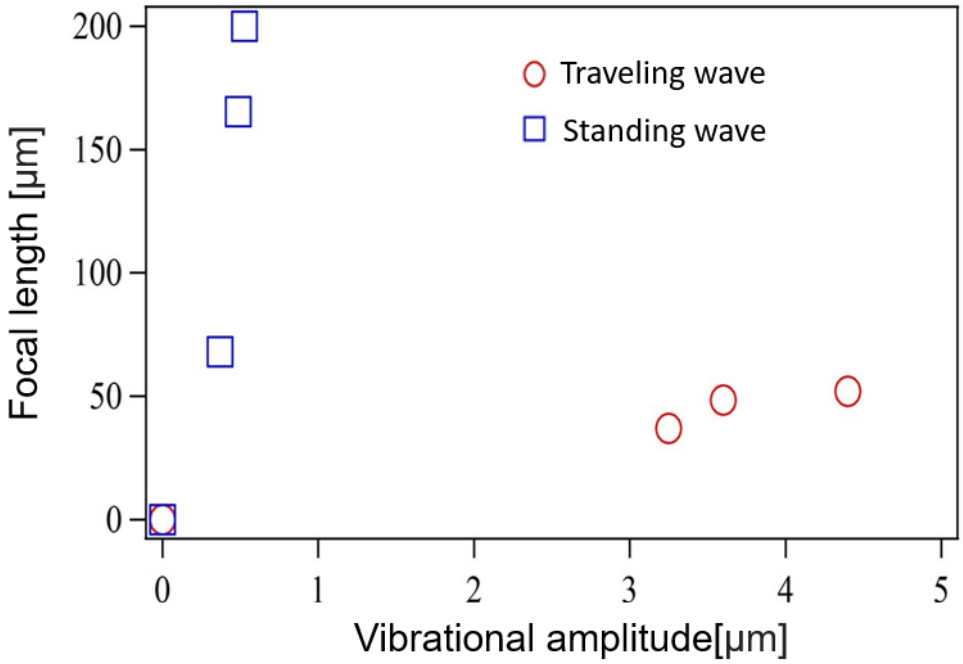

Fig.5.9 Relationship between the vibrational amplitude of the glass substrates and the focal length of the lens using the SW versus the lens using the TW.

5.1.4. ESTIMATION OF THE LENS APERTURE BY OBSERVING THE TRASMITTED LIGHT

The transmitted light distributions for both the TW mode and the SW mode were observed using an inverted polarization microscope (IX83, Olympus) under crossed Nicols conditions [Fig. 5.10]. Under the conditions without ultrasound excitation, the transmitted light was filtered under crossed Nicols conditions because the LC molecules are initially

oriented vertically. When the voltage is applied to the LC lens, the flexural vibration generated in the lens enables the change in the molecular orientation and the periodic pattern consequently appears in the transmitted light distribution (Fig. 5.10 (b), (c)). Both modes showed the same optical pattern, in which a cross-shaped shadow appeared, meaning that the vertical alignment of the LC molecules was maintained at the center. However, when compared with the variable-focus LC lens using the SW, the LC lens using the TW presents an aperture that is approximately two times larger (0.83 and 0.42 mm in the TW and SW modes, respectively). This aperture size could be estimated by measuring the distance between the two brightness peaks in the transmitted light pattern at the center of the lens. These optical patterns indicate where the molecular orientation changes. Although these aperture values are different from 4.4 mm and 2.5 mm calculated from the wavefront sensor data, they present almost the same enlargement ratio (1.76 by wavefront and 1.95 by polarization microscope). This difference of values is attributed to the influence of the microscope lenses.

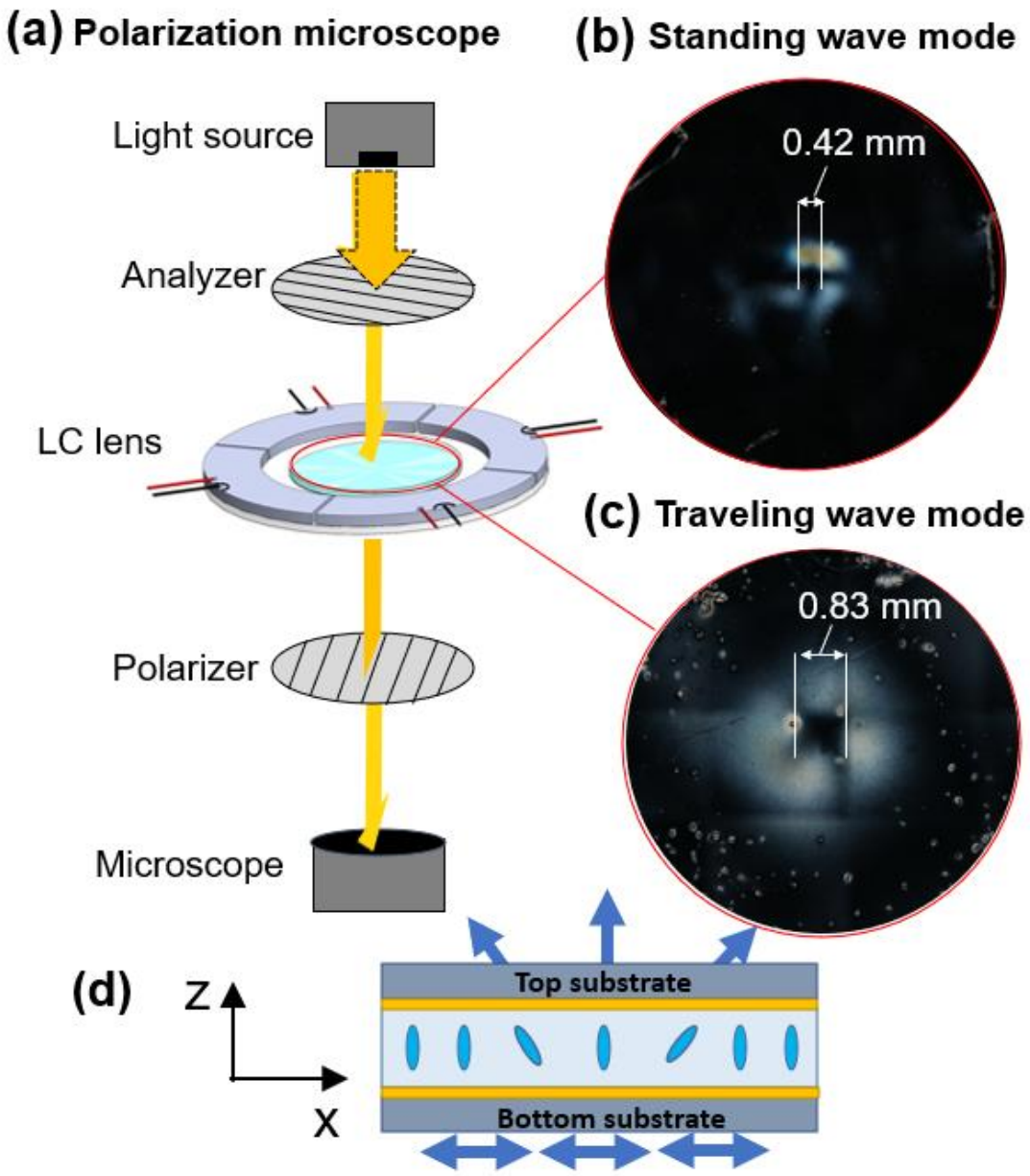

Fig. 5.10 (a) Polarization microscope setup; transmitted intensity light distributions for (b) the SW mode and (c) the TW mode; and (d) molecular orientation in the concave LC lens.

REFERENCES

[5.1] Y. Shimizu, D. Koyama, M. Fukui, A. Emoto, K. Nakamura and M. Matsukawa, "Ultrasound liquid crystal lens," *Applied Physics Letters*, vol. 112, no. 16, p. 161104, 2018.

[5.2] Y. H. Lin, Y. J. Wang and V. Reshetnyak, "Liquid crystal lenses with tunable focal length," *Liquid Crystals Reviews*, vol. 5, no. 2, pp.111-143, 2017.

[5.3] P. Hagedorn and J. Wallaschek, "Travelling wave ultrasonic motors, Part I: Working principle and mathematical modelling of the stator," *Journal of Sound and Vibration*, vol. 155, no. 1, pp.31-46, 1992.

[5.4] T. Martinez, G. Pillonnet, V. Loyau, D. Vasic and F. Costa, "A transverse traveling wave piezoelectric transformer". *Smart Materials and Structures*, vol. 28, no. 7, p. 075012, 2019.

[5.5] J. Onaka, T. Iwase, M. Fukui, D. Koyama and M. Matsukawa, "Ultrasound liquid crystal lens with enlarged aperture using traveling waves". *Optics Letters*, vol. 46, no. 5, pp.1169-1172, 2021.

[5.6] B.C. Platt and R. Shack, "History and principles of Shack-Hartmann wavefront sensing," *Journal of Refractive Surgery*, vol. 17, no. 5, pp. S573-S577, 2001.

[5.7] E. Hecht, "Optics", 4th edition. *Addison-Wesley, San Francisco*, vol. *2*, p.3, 2002.

[5.8] P.P. Chao, Y.Y. Kao and C.J Hsu "A new negative liquid crystal lens with multiple ring electrodes in unequal widths". *IEEE photonics Journal*, vol. 4, no. 1, pp.250-266, 2012.

CHAPTER 6: RADIAL FOCUS CONTROL FOR IMAGE STABILIZATION

6.1. LENS VIBRATION CONTROL

Although an ultrasonically controlled liquid crystal lens using traveling waves was used to obtain a large aperture and by changing the liquid crystal molecular orientation statically via acoustic radiation forces, it was possible to have a variable focus in the lens thickness direction, a shift in the variable-focus position was not performed. Compensation for optical aberrations and control of the focal point can be achieved by using divided electrodes and controlled input voltages [6.1]. In addition, camera modules should enable variable focus in the axial direction to focus on the subject and also enable optical image stabilization (OIS) to avoid blurred images. The traditional OIS system relies on a complete module of sensing, control, multiple lenses, and compensation to correct for undesired camera movement. These movements can be characterized, for instance, in an *x/y* plane detected by sensors. An ultrasonically controlled liquid crystal lens with no mechanical moving parts may replace this module of sensing and control and plays an important role in the miniaturization of optical systems, showing the advantages of robustness and simplification of electronic modules for OIS, since instead of using sensors and actuators to detect the *x/y* location of the OIS lens (to correct the unwanted camera movements for image stabilization), the use of a single lens controlled by ultrasound, presented in this thesis work, is able to perform the variable focus in axial and radial directions (*x/y* plane) and shows the possibility of controlling the focal point freely for the application of image stabilization. Furthermore, the demand for autofocusing and OIS in cameras and smartphones increases every year. These cameras and phones need larger optical apertures for image quality. However, there is a trade-off between these characteristics, and it is necessary to find alternative lens architectures, materials, and processing.

Although according to the literature, if we shift the center of the refractive index gradient generated by the liquid crystal, it would be possible to have OIS [6.2-6.4]. These studies rely on the use of ITO electrodes. In this chapter, the functionalities of a multichannel

PZT transducer were further explored present an ultrasound liquid crystal lens with variable focusing in the radial direction for motion-free autofocusing and OIS. It does not affect the focusing in the axial direction already reported [6.5], with a simple structure by simply varying the sound pressure acting on the liquid crystal layer through the lens's vibration control, inducing an axisymmetric and a nonaxisymmetric deformation of the lens. The optical character altered by changing the vibrational modes as well as its relationship with the liquid crystal molecular orientation will be elucidated.

The configurations of the lens, its material properties, geometrical deformations, and boundary conditions were defined with finite-element analysis (FEA) via ANSYS in Fig. 6.1, whereas all the mechanical properties of the components for the simulation can be found in Table 4.1 (Chapter 4). It determined the resonant flexural vibrational modes on the glass substrates. The modeling revealed that a combination of lens geometry, electrode scheme, and appropriate driving voltages enabled shifts in the focal point in the radial direction. By driving the transducer with a continuous sinusoidal electric signal, several flexural vibration modes were generated in the liquid crystal layer through the two glass substrates at the resonance frequencies of the liquid crystal lens above 20 kHz. The vibration distribution on the upper glass plate was varied with the drive channels. The modeling indicated that, by using three channels, it was possible to change the focal point radially at 26 kHz. The fabricated lens has the same configuration of the lens presented in the Chapter 5 (Fig. 5.1) with 200 μm of liquid crystal layer thickness (5CB material).

The operational characteristics of the simulated lens were tested experimentally to validate the analytical model and the predicted driving conditions (Fig. 6.2). When all four channels were driven in phase using the same voltages and the 31.2-kHz resonance frequency for a flexural standing wave, an axisymmetric flexural vibrational mode was generated in the lens, as reported previously [6.5, 6.6]. The liquid crystal layer was statically deformed by the acoustic radiation forces. Differences between the experimental and simulated resonance frequencies were attributed to differing elastic moduli for the glass plates. Because acoustic radiation is a static force generated by differences in acoustic energy densities in different

media [6.7, 6.8], a considerable part of the acoustic energy generated by the piezoceramic element is reflected at the boundary between the piezoelectric material and the propagation medium. Therefore, when the ultrasound propagated from the standing wave flexural vibration was radiated into the device, it was partially reflected at the boundaries of the liquid crystal layer, the glass substrates, and the surrounding air. This allows the acoustic radiation force to change the liquid crystal molecular orientation and enable the variable-focus lens.

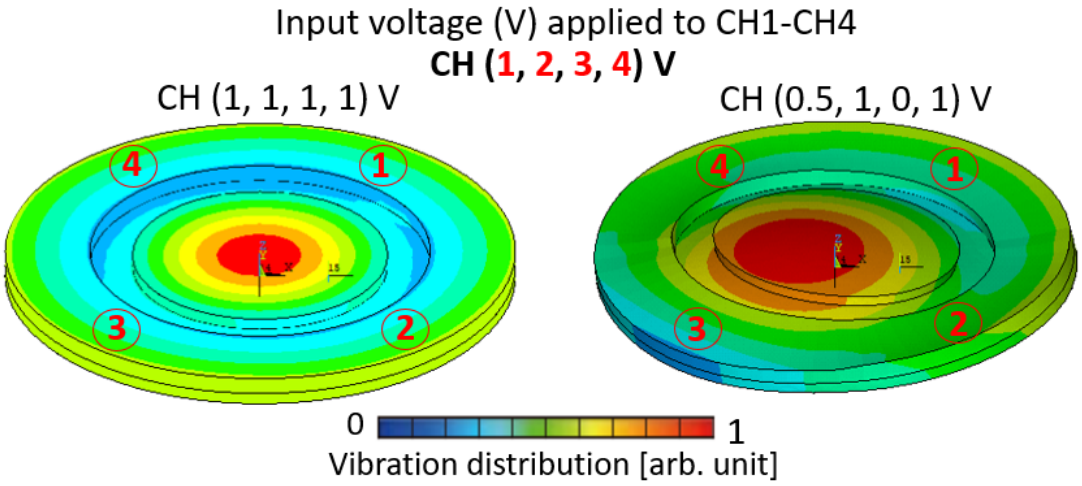

Fig. 6.1 FEA using ANSYS: shifting the focal point in the radial direction at 26 kHz.

The measurement area using LDV was 10x10 mm^2 at the center of the upper glass plate. The distributions of the vibrational displacement amplitude were expressed using a color scale and it was normalized with respect to the maximum value (maximum displacement amplitude was 0.45 µm in the case where the input voltage was 5 V_{pp} for each channel). The plots at the bottom of Fig. 6.2 show profiles along the line A-A' when the input voltages were applied. The curves indicate the distributions of the vibrational displacement amplitude of the glass substrates at the ultrasound frequencies in the simulation and measured by LDV, respectively. The channels positions (CH1, CH2, CH3,

CH4) during the simulations and experiments were specified into the Fig. 6.2. Two cases were highlighted: when the loop is in the center and when the loop has the largest displacement of 2 mm for both simulation and experimental case. Although the driving frequencies used in simulation (26 kHz) and experiments (31.2 kHz) were distinct, the curves have a similar shape, validating the simulated model for variable-focus in radial direction. The vibration distribution of the glass substrate that was measured with the laser Doppler vibrometer was compared with the simulations to observe the loop shape (Fig. 6.3). The vibration distribution on the upper glass plate was varied by controlling the driving channels condition. As the voltage applied to CH1 increased (from 0 V_{pp} to 2 V_{pp}) in Fig. 6.3, the center loop moved in the radial direction proportionally to its input voltage. This means that by using the driving channels control, it was possible to control the lens vibration distribution. Consequently, the shape of the center vibration could be also controlled.

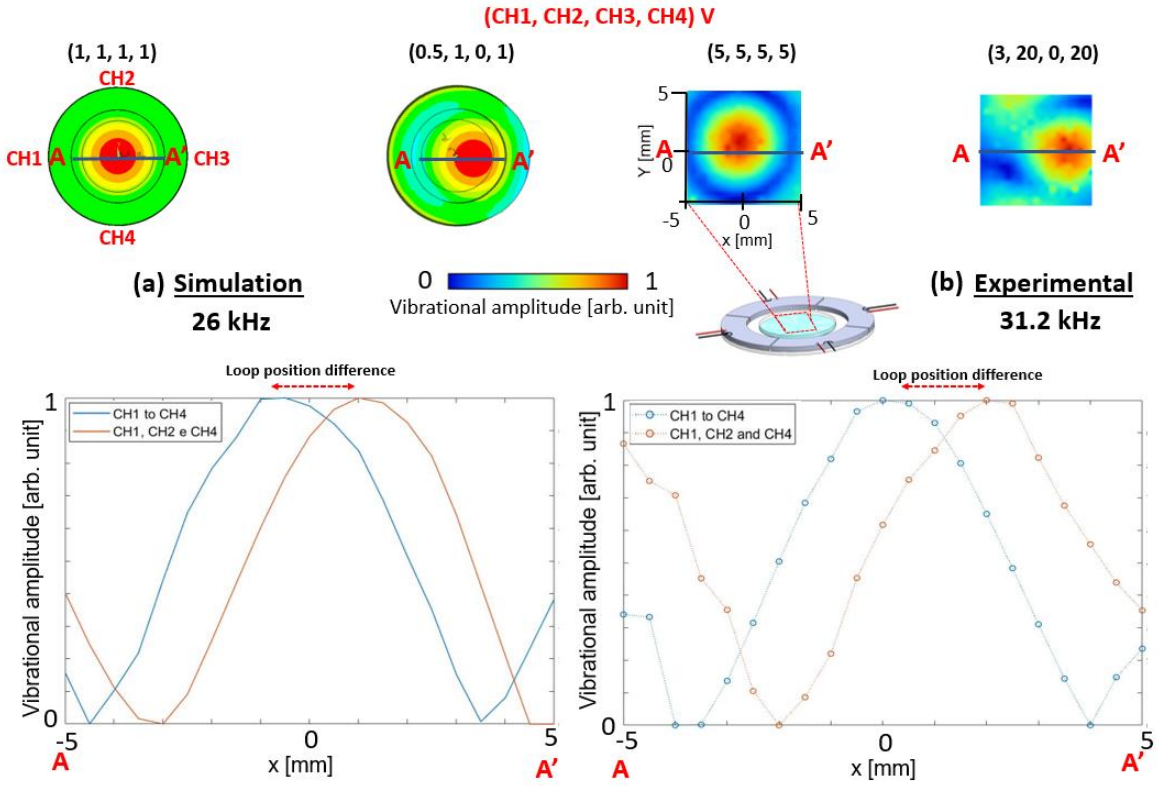

Fig. 6.2 Vibration mode profile: (a) Simulation (26 kHz) and (b) Experimental (31.2 kHz)

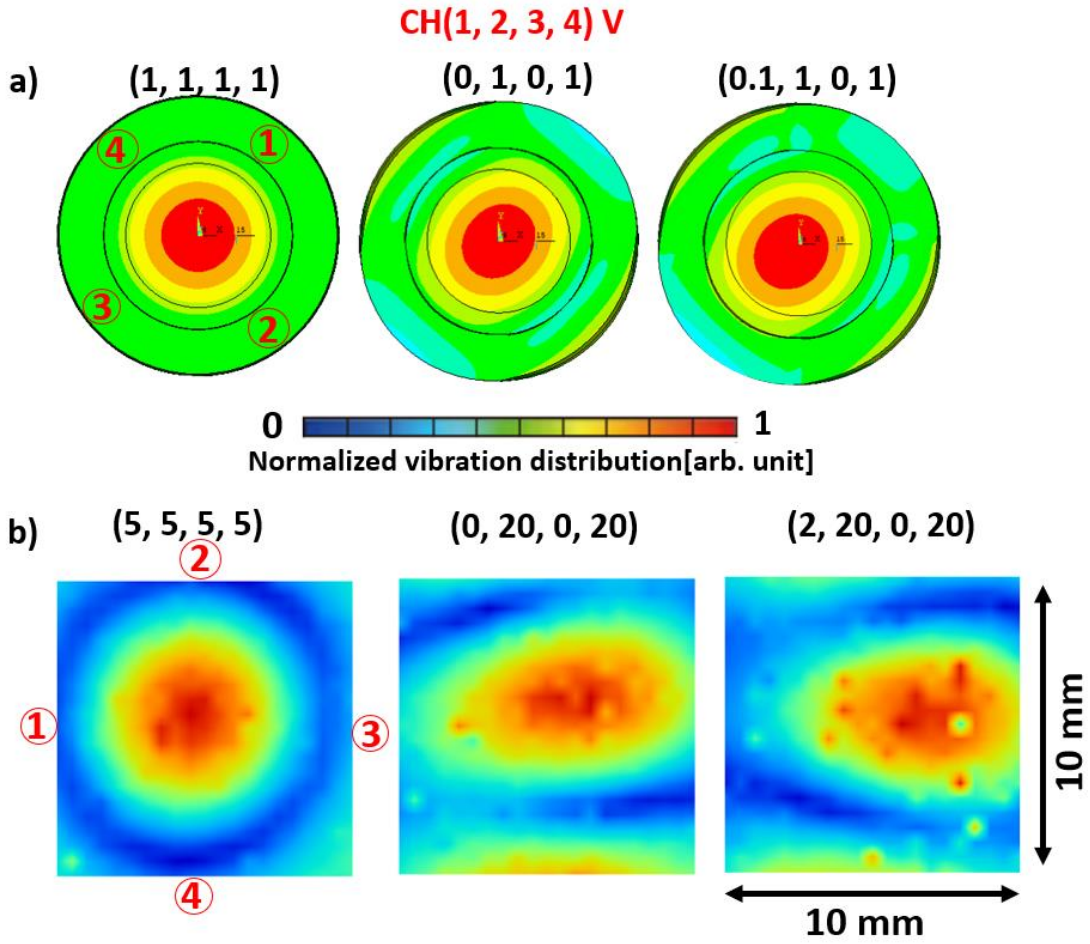

Fig. 6.3 Vibration mode profile: (a) Simulation (26 kHz) by Ansys and (b) Experimental (31.2 kHz) by LDV

6.2. LENS CONTROLABILITY AND OPTICAL CHARACTER

The liquid crystal lens was positioned in parallel between a polarizer and an analyzer arranged orthogonally each other (crossed Nicol conditions). Section 4.4.3 (Chapter 4) shows the experimental system using the photodetector (PD, 2051-FS, Newport, CA). A linear polarized laser beam (He-Ne laser; λ= 632.8 nm; beam diameter: 2 mm) was converted to a circular polarized laser beam through a 1⁄4 wavelength plate. The transmitted

light through the polarizer, the liquid crystal lens, and the analyzer was measured by the photodetector. In order to evaluate the molecular orientation of the liquid crystal, the transmitted light distribution through the lens was measured by rotating two polarizing plates in the in-plane direction (the incident polarization direction θ) while maintaining the crossed Nicol conditions. The driving condition was changed in order to promote the variable focus in radial direction.

Firstly, the experiment was performed by simultaneously driving the four channels [CH (1,2,3,4)] with V_{pp} for an in-phase test of lens controllability. A linear polarized laser beam (He–Ne laser; λ = 632.8nm; beam diameter, 2 mm) was converted to a circular polarized laser beam through a quarter-wavelength plate. The transmitted light through the polarizer, the liquid crystal lens, and the analyzer was measured by the photodetector. Figure 6.4 shows the transmitted light distributions measured by the photodetector through the liquid crystal lens, without and with ultrasound excitation via 5-V inputs at all channels, when the polarization direction of the incident light θ was changed from 0^o to 165^o. The incident light was scanned in the same 10-mm×10-mm measurement area, and the transmitted light intensities were normalized by each maximum value. Without ultrasound excitation, the transmitted light intensity in the measurement area was close to zero because the initial liquid crystal molecular orientation was in the vertical direction and the linear polarized light did not pass through the analyzer under the crossed Nicol conditions. The patterns of the transmitted light were rotated with the incident polarization direction, repeating every 90^o, indicating no polarization dependence under a crossed-Nicols configuration. They were identical every 90^o, using simultaneously and in-phase all the channels, indicating symmetric controllability. However, the transmitted light distributions were not perfectly axisymmetric, and the intensity at one peak (left side) was lower than the other three peaks due to the precision of the lens' fabrication process since the liquid crystal was injected into the gap between the two circular glass substrates via the capillary effect at atmospheric pressure and not under vacuum.

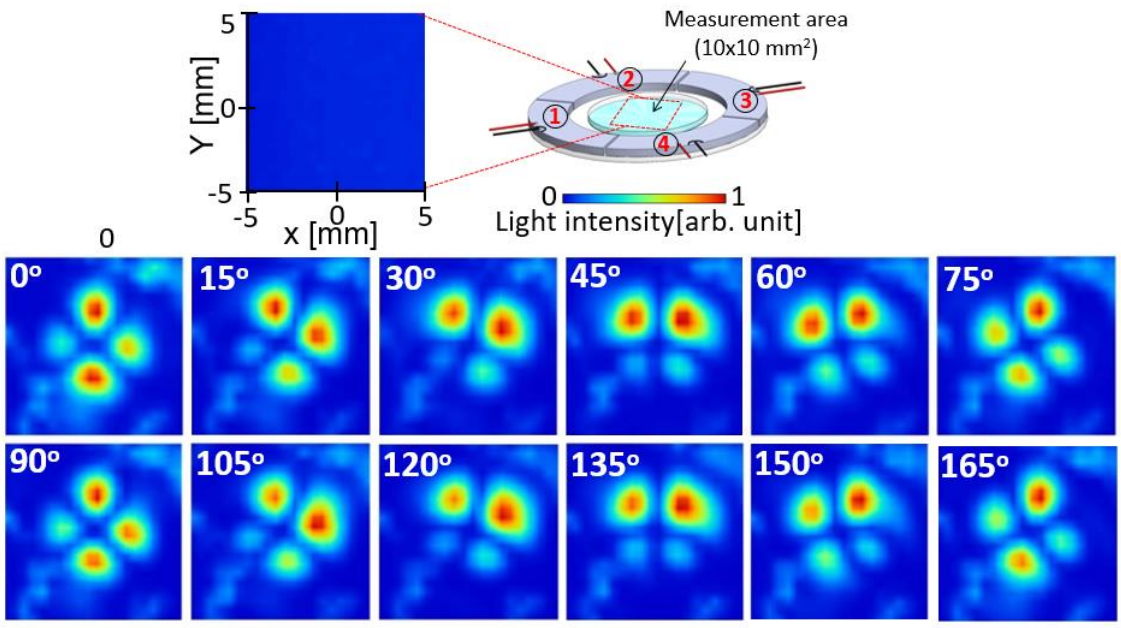

Fig. 6.4 Transmitted light intensity distributions through the liquid crystal lens without (US off) and with 31.2-kHz ultrasound excitation.

Figures 6.5 (a) and 6.5 (b) shows the vibrational and transmitted light distributions, respectively, when the channels were excited at the 31.2-kHz resonance frequency. From transmitted light distributions acquired by changing the incident polarization direction θ (Fig. 6.4), it is possible to estimate the in-plane distribution of liquid crystal molecular orientations [6.5]. The vectors on Fig. 6.5 (a) represent the in-plane distribution of the liquid crystal molecular orientation in the lens. The out-of- plane vibrational distribution on the surface of the glass plate and the orientation direction of the liquid crystal molecules were visualized using a color scale and bars, respectively. The orientation distributions of the liquid crystal were determined to be θ_{max}+45° by measuring the incident polarization direction θ_{max}, which resulted in the maximum light intensity of the transmitted light at each measurement point [in Figs. 6.4 and 6.5 (b)]. The length of the bars represented the relative inclination of the liquid crystal molecules from the vertical direction. This was calculated from the ratio of the maximum-to-minimum transmitted light intensity at each measurement point when rotating

the incident polarization direction (see Fig. 6.4). The concentration of vectors shows the position of the focal point, indicating that it can be controlled by the driving conditions.

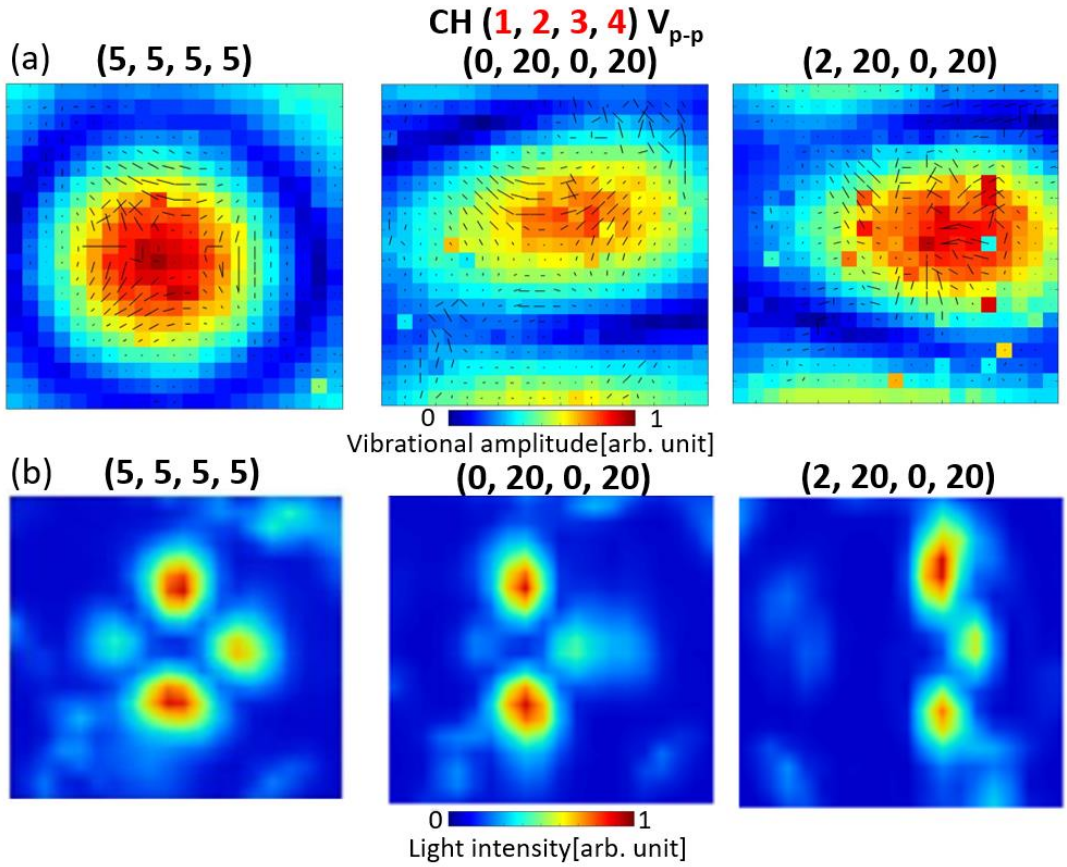

Fig. 6.5 (a)Distributions of vibrational displacement amplitudes (color map) and orientation directions (bar); (b) transmitted light intensity distributions through the liquid crystal lens at 31.2 kHz.

When channels *CH1–CH4* were excited with the same voltage, the axisymmetric flexural vibration mode was generated in the lens [left in Figs. 6.3 and 6.5(a), 6.5(b)]. The liquid crystal layer was statically deformed by the acoustic radiation force acting on the boundaries. When the input voltage for *CH2* and *CH4* was fixed, and that for *CH1* varied from 0 V (middle) to 2 V_{pp} (right) in Figs. 6.3 and 6.5(a), 6.5(b), a nonaxisymmetric flexural

vibration mode was generated. The antinodal position moved according to the input to CH1 (2 mm at $2V_{pp}$). The optical characteristics changed according to the vibrational mode, and the acoustic radiation force changed the liquid crystal molecular orientation in the radial direction. It was expected that the center loop of the vibrational shape [Fig. 6.5(a), top left] could be shifted to the right side while maintaining a circular shape, as in the simulated results in Fig. 6.1; however the vibration mode was not perfectly axisymmetric, which was confirmed in the experimental results, as the loop shape looked slightly distorted into a horizontally long circle [vide Fig. 6.5(a), top right]. For this reason, the optical pattern in Fig. 6.5(b), at the bottom right, presented some distortions.

Since the liquid crystal layer can be considered as a GRIN lens, the focal length will depend on the layer thickness, radius, and refractive index difference from the center to the edge of the gradient layer [6.9]. Through the acoustic stimulation promoted under ultrasound excitation of 31.2 kHz, the liquid crystal molecules are modulated by the acoustic field acting in the glass substrates and liquid-crystal layer. The effective refractive index (n_{eff}) of the liquid crystal molecules changed according to the ultrasound vibration controlling the rotational angle (ϑ), which refers to the angle between its director and the substrate [6.9]. Strictly, the liquid crystal molecule directors were then estimated through the vectors represented in Fig. 6.5(a), according to axisymmetric (focus in the center) and nonaxisymmetric vibration (focus-shifted).

From Fig. 6.5(a), Fig. 6.6(a) was generated with two circular lines obtained from all the transmitted light distributions (0–165^{o}) for the four-channel and three-channel (focus-shifted) cases. In the vector graphs of Fig. 6.5(a), there was a displacement of the region where the vector modules were more significant. Then, a mask was generated to highlight the region of significant vectors and was plotted in a level curve for the four-channel and three channel cases. For a 5.5-mm radius from the center of Fig. 6.5(a) (wide bars), all adjacent variations above 5% were plotted in Fig. 6.6(a) to highlight the region where the molecular orientation was changed significantly. This indicated the focal position. Because the lengths of the bars represented relative inclinations of the liquid crystal molecules, the

center of the graph, located in the internal circular line, represented the portion where the liquid crystal molecules were still vertically oriented (i.e., no transmitted light).

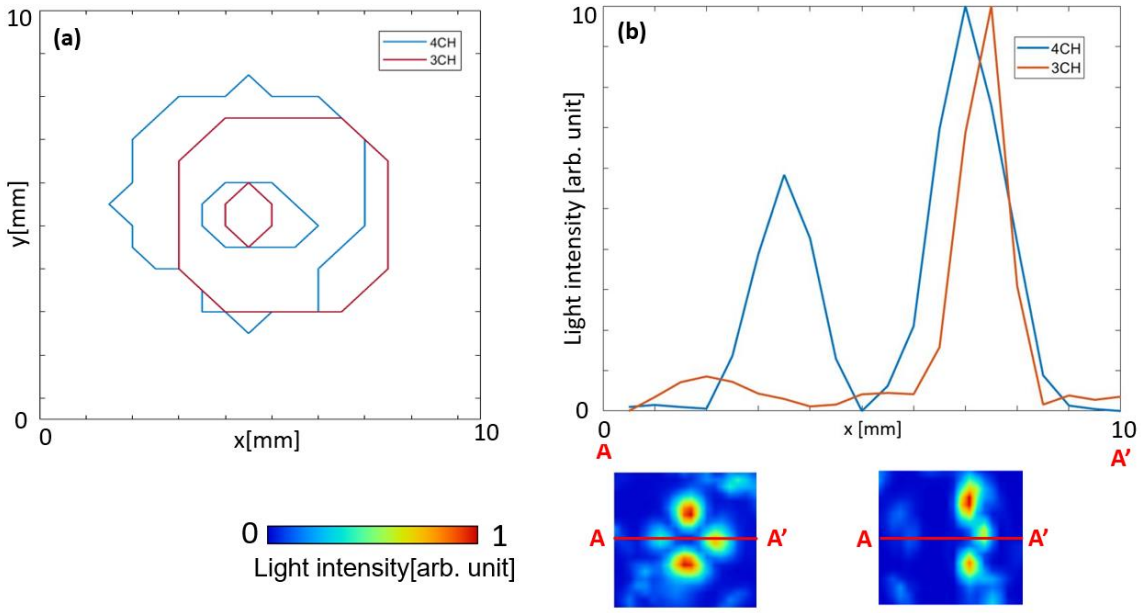

Fig. 6.6 (a) Significative vector plots for each polarization direction (θ=0–165º) from Fig. 6.5; (b) distributions of transmitted light intensity along the line A-A' for four driven channels (4CH) and three driven channels (3CH, focus-shifted) at 31.2 kHz.

In Fig. 6.6(b), distributions of the transmitted light intensity along line A-A' were plotted to evaluate the distribution resulting from channels driven at 31.2-kHz. Regions in the Figs. 6.6(a) and 6.6(b) plots where the molecular orientation changed significantly [delimited by the curves in Fig. 6.6(a)] had the same displacement, as shown by the transmitted light distribution profile [Fig. 6.6(b)]. In both cases, the displacement was approximately 0.5 mm.

6.3. TWO-DIMENSIONAL FAST FOURIER TRANSFORM TO FIND THE FOCAL POINT POSITION

Observations with a transmission optical microscope, (VW9000, Keyence) equipped with a 200× objective lens and a single Nicol element, were performed with the liquid crystal lens to verify the changing focal point in the radial direction. A static test target (1951, United States Air Force) placed between the light source and the polarizer was used to evaluate the optical characteristics of the lens under ultrasound excitation and variable driving conditions, as described in the Chapter 4 (Section 4.4.3); however, to evaluate the focal point position according to the channels driving conditions, the optics characteristics were observed maintaining the target static while changing the lens' driving conditions.

To identify the focused regions of three images (defocused, that focused by four driving channels, and focal changes in the radial direction), a method based on the fast Fourier-transform (FFT) power spectrum was used [6.10]. Because the FFT processing was performed on sub-regions of each full image, we divided it into small regions, as shown in Fig. 6.7. The resolution of the small area was 48×48 pixels, and the 1920×1440-pixel dimensions of the entire image were converted into 30×40-pixel areas. The frequency component for each 30×40-pixel area in the three microscope images was calculated using two-dimensional FFT (2D FFT) to obtain a power-spectrum density (PSD) histogram. Then, a straight line obtained by least squares was used to judge whether the image was focused or not from the slope of the line.

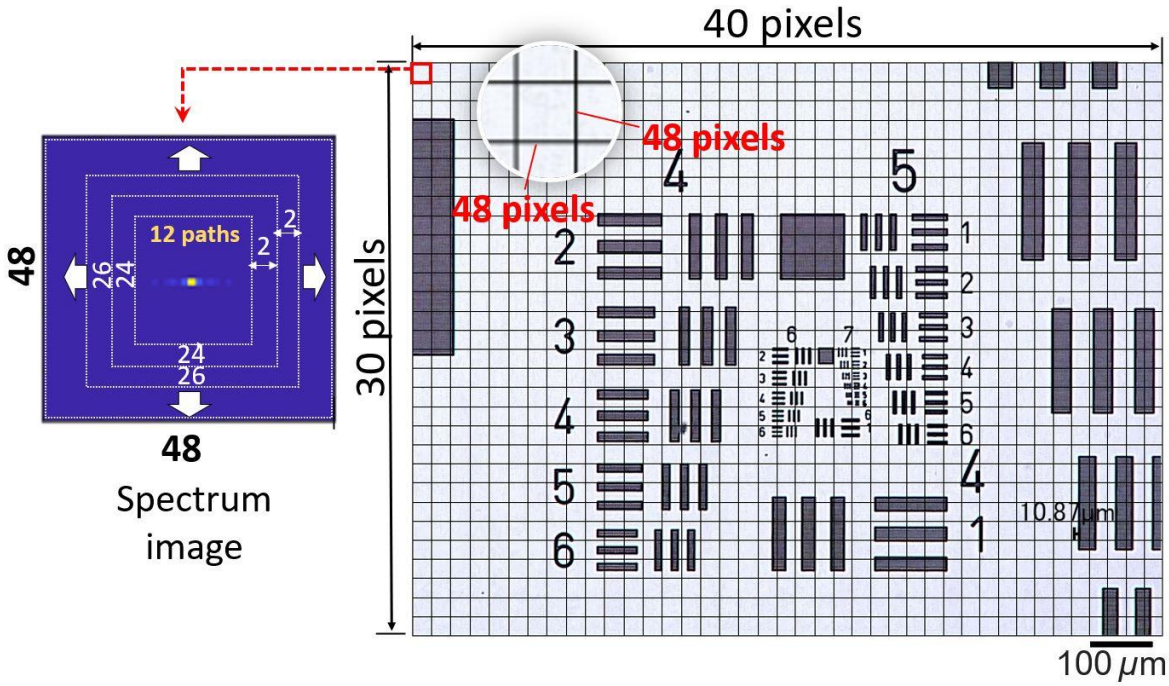

Fig. 6.7 Segmentation of the image into 48x48-pixel areas for two-dimensional fast Fourier transforms.

Before the FFT image processing, the entire image was converted to three gray-scale images via a weighted method from National Television Standards Committee - NTSC [weights of red (R), green (G), and blue (B)] [6.11], according to their wavelengths. The brightness value I after the gray-scale conversion is given by:

$$I = 0.298912 \times R + 0.58661 \times G + 0.114478 \times B \tag{6.1}$$

Figure 6.8 was generated from the three gray-scale microscope images after performing 2D-FFT over 48×48-pixel areas and defining the PSD histogram with Eq. 6.2. The latter was used to determine the focused and defocused areas by analyzing the slope (m) steepness of the line. A slope close to zero indicated focused, while a negative slope indicated defocused. The steeper negative slope was of the order of 10^7. We assumed $m > -1000$ equals 1; i.e., focus and defocus were binarized to yellow (focus) and blue (defocus).

$$PSD(\omega) = \frac{1}{\| \text{Path}(\omega) \|} \sum_{(u,v)}^{\text{Path}(\omega)} |S(u,v)|^2 \, dudv \tag{6.2}$$

The square |S(u, v)|2 of the spectrum S (u, v) is the power spectrum. Because a digital image is a discrete value, 2D-FFT was performed to analyze the frequency spectrum of the 2D matrix data (Fig. 6.7). Path (ω) was the integral-squared path [Fig. 6.7, left] used for each 48×48-pixel region to obtain the PSD (ω) and the slope. It was defined by twelve squared path integrations, starting in the center and expanding by two (i.e., 24×24 pixels, 26×26 pixels).

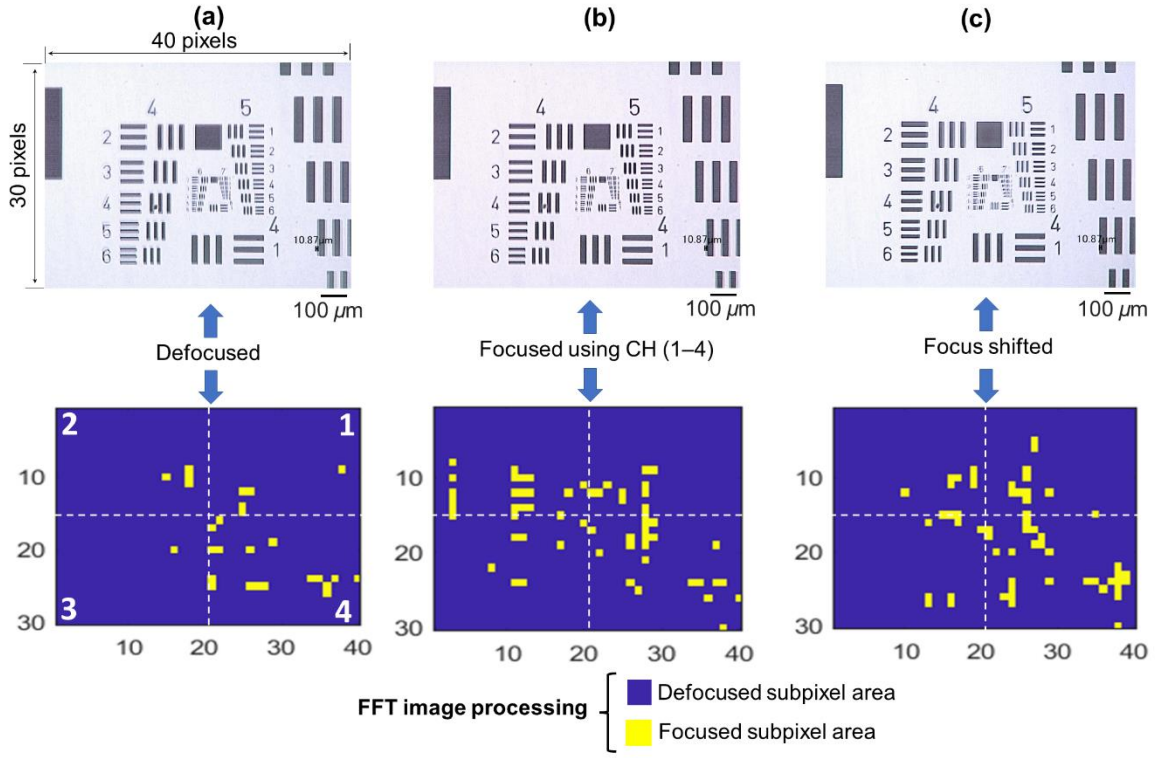

Fig. 6.8 (a) Defocused image, (b) focused image using CH (1–4), (c) focus shifted in the radial direction.

In Fig. 6.8 (a), the focused area represented by yellow pixels was random and spread out in the defocused image, as expected. By comparing Fig. 6.8 (b,c) the density of the focused area was shifted in the right side of the image. This indicated that the focal point was displaced when using three channels, relative to the focal point using four channels. Relative

to quadrants 1 and 4 in Fig. 6.8(b), the yellow pixels in Fig. 6.8 (c) increased by 35%. It can be noticed that the concentration of pixels is moving slightly toward the lower right side. The cause is that the lens was fabricated manually and under atmospheric pressure, which implies that the liquid crystal layer might present a nonuniformity.

Additionally, since the focal point is defined by the density of yellow pixels displayed in Fig. 6.8, by calculating the center of mass of a system of particles [6.12], it was possible to estimate how much the focal point effectively shifted,

$$X_{CM} = \frac{x_1 m_1 + x_2 m_2 + \ldots + x_N m_N}{m_1 + m_2 + \ldots + m_N} \tag{6.3}$$

Given that X_{CM} is the center of mass in the x component of the center of the mass vector to estimate the displacement in the radial direction, where m is the number of pixels per position x and the denominator of the fraction is the total number of yellow pixels on the image, the calculated X_{CM} for the case of Fig. 6.8(b) and 6.8(c) was 19.68 pixels and 24.31 pixels, respectively; thus the difference between the center of mass of both figures is equal to 4.63 pixels. This result corresponds to 0.2 mm, which represents the effective focal displacement of the focal point radially.

In summary, the results suggested the possibility of controlling the vibrational mode and the center loop of the vibrational shape via the lens channels. The optical characteristics of the lens depended directly on the vibrational amplitude distribution, allowing the focal point to change in the radial direction. By 2D-FFT processing of the digital images, it was possible to confirm focal-point displacements.

REFERENCES

[6.1] D. Koyama, M. Hatanaka, K. Nakamura, and M. Matsukawa, “Ultrasonic optical lens array with variable focal length and pitch,” *Optics Letters*, vol. 37, no. 24, pp. 5256–5258, 2012.

[6.2] M. Ye and S. Sato, “Liquid crystal lens with focus movable along and off axis,” *Optics Communications*, vol. 225, no. 4-6, pp. 277–280, 2003.

[6.3] M. Ye, B. Wang, and S. Sato, “Liquid crystal lens with focus movable in focal plane,” *Optics Communications*, vol. 259, no. 2, pp. 710–722, 2006.

[6.4] N. Fraval and F. Berier, “Liquid crystal lens auto-focus extended to optical image stabilization for wafer level camera,” *Proceedings of SPIE*, vol. 7930, p. 793009, 2011.

[6.5] Y. Shimizu, D. Koyama, M. Fukui, A. Emoto, K. Nakamura and M. Matsukawa, “Ultrasound liquid crystal lens,” *Applied Physics Letters*, vol. 112, no. 16, p. 161104, 2018.

[6.6] J. Onaka, T. Iwase, M. Fukui, D. Koyama and M. Matsukawa, “Ultrasound liquid crystal lens with enlarged aperture using traveling waves,” *Optics Letters*, vol. 46, no. 5, pp.1169-1172, 2021.

[6.7] D. Koyama, R. Isago, and K. Nakamura, “Ultrasonic variable-focus optical lens using viscoelastic material,” *Applied Physics Letters*, vol. 100, no. 9, p. 091102, 2012.

[6.8] B. T. Chu and R. E. Apfel, “Acoustic radiation pressure produced by a beam of sound,” *Journal of the Acoustical Society of America*, vol. 72, no. 6, pp. 1673-1687, 1982.

[6.9] K. Chen, Y. Hou, S. Chen, D. Yuan, H. Ye, and G. Zhou, “Design, fabrication, and applications of liquid crystal microlenses,” *Advanced Optical Materials*, vol. 9, no. 20, p. 2100370, 2021.

[6.10] P. D. Welch, “A direct digital method of power spectrum estimation,” *IBM Journal of Research and Development*, vol. 5, no. 2, pp. 141–156, 1961.

[6.11] Y. Faroudja, “NTSC and beyond (TV),” *IEEE Transactions on Consumer Electronics*, vol. 34, no. 1, pp. 166–178, 1988.

[6.12] S. Alrasheed, “System of Particles”, *Springer*, Cham, pp. 87−102, 2019.

CHAPTER 7:DOUBLE-LAYERED BASED LENS

7.1. LENS MODEL

Nematic liquid crystal lenses based on double-layered nematic liquid crystals have been proposed previously in the literature [7.1–7.3]. These lenses consisted of two liquid crystal layers that were attached orthogonally and showed improvements in terms of optical power; however, all these lenses relied on the use of ITO electrodes.

Ultrasound liquid crystal lenses with different layer thicknesses, including 50 μm [7.4], 100 μm, 200 μm, and 300 μm [7.5 – 7.7] have been investigated. Among these lenses with their different thicknesses, the lens with the 200-μm-thick LC layer presented the best optical performance because a large change in the focal length was observed at a smaller driving voltage, thus indicating that this 200 μm layer thickness was most appropriate for use in a variable-focus lens controlled via ultrasound [7.6]. Furthermore, ultrasound liquid crystal lenses with the same layer thickness (200 μm) [7.5, 7.7] were able to produce a large aperture using traveling waves [7.5] and variable focusing behavior in the radial direction that is suitable for image stabilization [7.7], as already discussed in Chapter 5 and Chapter 6.

Although a thicker liquid crystal layer can lead to the lens having a larger focal length range and a larger aperture, the thicker liquid crystal cell gap might affect the optical properties of the lens because the liquid crystal's molecular orientation is dependent on the interactions among the acoustic radiation force, the liquid crystal material, and the anchoring force based on the alignment film orientation. When the distance from the alignment film increases, the effect of the alignment film then weakens, illustrating that there is a trade-off between the liquid crystal lens thickness and the lens' optical performance. As a result, understanding of the physical properties of the liquid crystal and consideration of an appropriate design approach to minimize the elastic distortion [7.8] of the liquid crystal material becomes an important issue, because the alignment allows the director n to be dictated within the bulk of the device. Additionally, the anchoring behavior is also related to the liquid crystal's bulk properties, and depends on the relationship between the liquid crystal material and the surface, which means that it is not a surface property alone. This suggests

that by tailoring the liquid crystal material parameters, e.g., the birefringence and the dielectric anisotropy, in combination with other parameters (liquid crystal type, layer thickness, glasses), it would be possible to control both the anchoring strength and the lens birefringence, which could improve the optical properties of the ultrasonically controlled liquid crystal lens.

In this Chapter, a pair of 100-μm-thick LC layers that share a common piezoelectric transducer and represent a total liquid crystal layer thickness of 200 μm, which allowed two ultrasonically controlled lenses using different liquid crystal materials (5CB and RDP-85475) but the same configuration to be fabricated and compared. In addition, the effects of the different material properties of the liquid crystals (including the birefringence, elastic constants, and dielectric anisotropy) on the optical characteristics of the two ultrasound-controlled double-layered fabricated lenses were investigated and compared with the common sandwich-type lens with a single layer.

Figure 7.1 shows the double-layered ultrasound liquid crystal lens structure. The first lens used two layers of the nematic liquid crystal RDP-85475 (DIC, Japan ; refractive index n_o=1.525; n_e=1.823 at 589 nm; transition temperature of smectic-to-nematic (SN) transition point: 10°C; nematic-to-isotropic (NI) transition point: 123.7°C; rotational viscosity γ: 93.7 mPa·s); the second lens used two layers of the nematic liquid crystal material *4-cyano-4'-pentylbiphenyl* (5CB; TCI, Japan; refractive index n_o=1.533; n_e=1.716 at 589 nm and 24°C; rotational viscosity γ at 25°C: 28 mPa·s). The birefringence (optical anisotropy) Δn of the liquid crystals represents the difference between the extraordinary and ordinary refractive indices (i.e., $\Delta n = n_e - n_o$). Our group have used both liquid crystal materials (RDP-85475[5.1] and 5CB [5.5, 5.19, 5.20]) formerly, and in this thesis work, the optical performances of these two materials in a double-layered ultrasound liquid crystal lens will be analyzed.

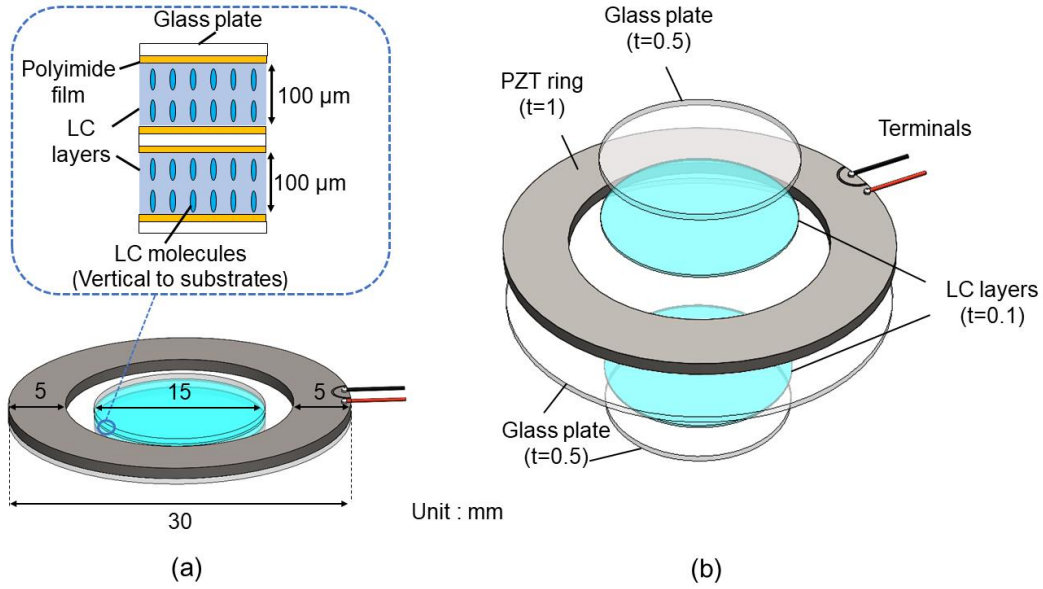

Fig. 7.1 Double-layered ultrasound liquid crystal lens: (a) lens configuration; (b) exploded diagram.

On the interior surfaces of these glasses, polyimide films (vertical alignment type, SE-5811, Nissan Chemical, Japan) cover the surfaces and define the initial molecular orientation of the liquid crystal molecules without rubbing; the intermolecular interaction between the oriented film and the liquid crystal promotes homeotropic alignment – the same initial alignment of the previous fabricated lenses. An annular piezoelectric lead zirconate titanate (PZT) ultrasound transducer (C-213, Fuji Ceramics; thickness: 1 mm; inner diameter: 20 mm; outer diameter: 30 mm) was bonded to the 30-mm-diameter glass substrate using epoxy.

7.2. LENS VIBRATION, BIREFRINGENCE AND OPTICAL ANALYSIS

The liquid crystal lens configurations were determined by FEA using Ansys software by applying the material properties (for the transducer and the glass substrates) and appropriate boundary conditions to determine the resonant flexural vibration modes on the glass substrates. By excitation of the piezoelectric transducer using a continuous sinusoidal

electric signal, several resonant vibration modes were generated on the liquid crystal layer through the glasses at resonance frequencies within the 20–100 kHz range over the entire liquid crystal lens for each liquid crystal lens. During this time, the axisymmetric flexural vibration modes in the thickness direction at f = 53.5 kHz (RDP-85475) and f = 51.5 kHz (5CB) within the relatively low ultrasound frequency range were used; the liquid crystal layers are so thin that the resonance frequencies of the two lenses were almost identical. The entire lens body vibrated, and the liquid crystal molecules were vibrated by acoustic waves that were generated by the inverse piezoelectric effect on the PZT transducer. In other words, the acoustic field acting in both the glass substrates and the liquid crystal layers induced an acoustic energy difference between these media. The acoustic radiation force that resulted from this energy difference then acted on the boundaries between the liquid crystal layer, the glass substrates, and the surrounding air, allowing the collective liquid crystal orientation to be changed and thus producing the variable-focus lens [7.4]. Furthermore, because the liquid crystal molecules have uniaxial optical anisotropy and exhibit birefringence, the material refractive index is dependent on the propagation direction and the light polarization, which means that the light beam that propagates into the liquid crystal will be refracted in accordance with the refractive index variations caused via ultrasound excitation.

The liquid crystal lens' performance is strongly dependent on the birefringence of the liquid crystal material because the ultrasound liquid crystal lens is categorized as a GRIN lens. Additionally, the liquid crystal material and its interactions with the substrate surfaces with which it is in contact (i.e., the oriented film, glasses) are of paramount importance to the performance of the liquid crystal lens. Furthermore, optically isotropic materials such as glass can be given a preferred direction for the light by application of stress or bending, and thus become birefringent; therefore, the influence of ultrasound vibration on the entire liquid crystal lens should be investigated. In this thesis, it was used a birefringence profiler system [7.9], shown in Fig. 7.2, to measure the two-dimensional effective birefringence distribution for the double-layered fabricated liquid crystal lenses. This birefringence profiler measures the optical effective birefringence distribution without use of crossed polarizers, as described in Chapter 4, Section 4.4.4.

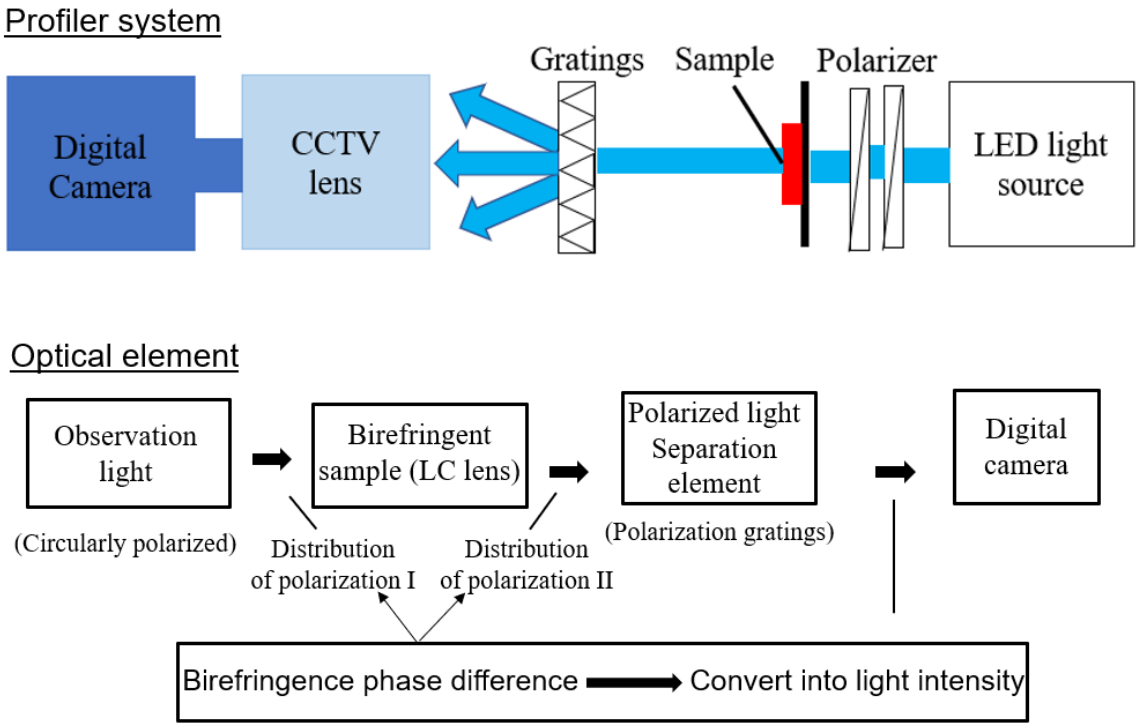

Fig. 7.2 Optical system of two-dimensional birefringence profiler

Figure 7.3 shows a comparison between the simulated and experimental results for the out-of-plane vibrational distributions generated on the surfaces of the glass substrates for the proposed lens model. The former was determined by Ansys simulation (Fig. 7.3(a)), in which the vibration distribution on the back part of the simulated lens is the same as that on the front part, and the latter vibration was measured (Fig. 7.3(b)) using the LDV. The measurement area was the 10×10 mm^2 area measured at the center of both liquid crystal lenses by the LDV. The concentric flexural vibration mode was generated at the second resonance at approximately 50 kHz for both the simulated and experimental results. The experimental results were satisfactory and showed excellent agreement with the double-layered model that was tested (Fig. 7.3(c)).

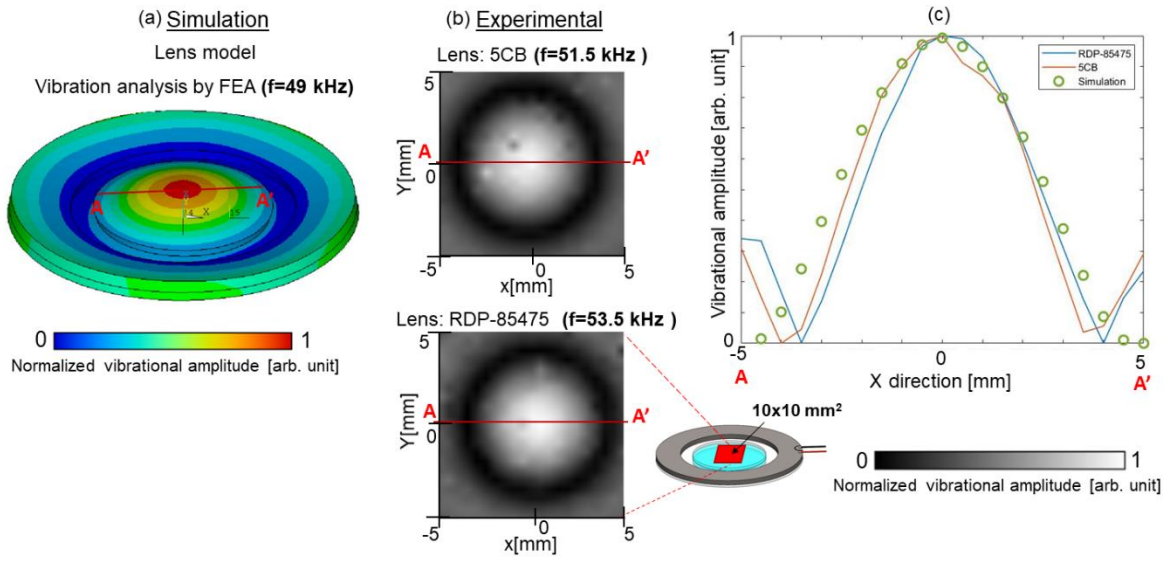

Fig. 7.3 Vibrational amplitude distributions of the glass substrates as simulated using Ansys software (a) and experimentally determined via a laser Doppler vibrometer (LDV) (b) for the fabricated lenses composed of 5CB and RDP-85475. The plots (c) show the vibrational displacement profiles along the line A-A'.

Figure 7.4(a) and (b) show the birefringence distributions of the double-layered ultrasonic liquid crystal lens, and Fig. 7.4(c) shows the single-layer birefringence distribution. In each case, the center of the lens was observed over an area of 30×30 pixels (total measurement lens area: 160×160 pixels). For all these lenses, which are composed of 5CB (a), (c) and RDP-85475 (b), the effective birefringence distribution is low over the entire lens when the ultrasonic waves are not driven (0 V) because the liquid crystal molecules are vertically oriented (homeotropic alignment). In contrast, under ultrasound excitation, the liquid crystal molecular orientation was changed by the acoustic radiation force, and the birefringence distribution appeared at the centers of both lenses in accordance with the voltage applied; this molecular reorientation can be understood by considering the Freedericksz transition [7.10]. The birefringence distributions in Fig. 7.4 showed doughnut-

shaped patterns at their centers for both the double-layered lens and the single layer lens, which was also observed in Chapter 6 (see Section 5.1.4), where the optical pattern of a single-layer lens was verified using an inverted polarization microscope. However, despite observation of the doughnut-shaped pattern, a crossed pattern could be observed over the doughnut-shape because the lens was under the crossed-Nicols condition. In this birefringence observation through use of the birefringence profiler, the crossed pattern is not observed over the doughnut shape because crossed polarizers were not used to perform these measurements, and also because of the effects of the distance between the profiler's camera system and the liquid crystal lens. Most importantly, and independent of the shape observed, the areas in which the liquid crystal refractive index changed significantly, i.e., at the center region of the lens, as a result of the applied acoustic radiation force agree well with the previous studies [7.11], since the remarkable changes occur in the same areas, i.e., in the middle of the lenses.

Figure 7.3 (b) shows the vibrational modes of the glass substrates as measured using the LDV under ultrasound excitation generated by the flexural standing wave, where the antinode of the vibration represents the maximum displacement, and where the vibrational amplitude was normalized with respect to the maximum value. The vibrational amplitude is related directly to the ultrasound liquid crystal lens optical characteristics at the resonance frequencies, and there is a strong relationship between the refractive index and the vibration distribution. Figure 7.4 shows that the birefringence distribution (representing the refractive index variation) within the liquid crystal layer under excitation by ultrasound vibration increases with increasing input voltage, and consequently is proportional to the vibrational amplitude (which increases steadily with increases in the voltage applied to the piezoelectric transducer).

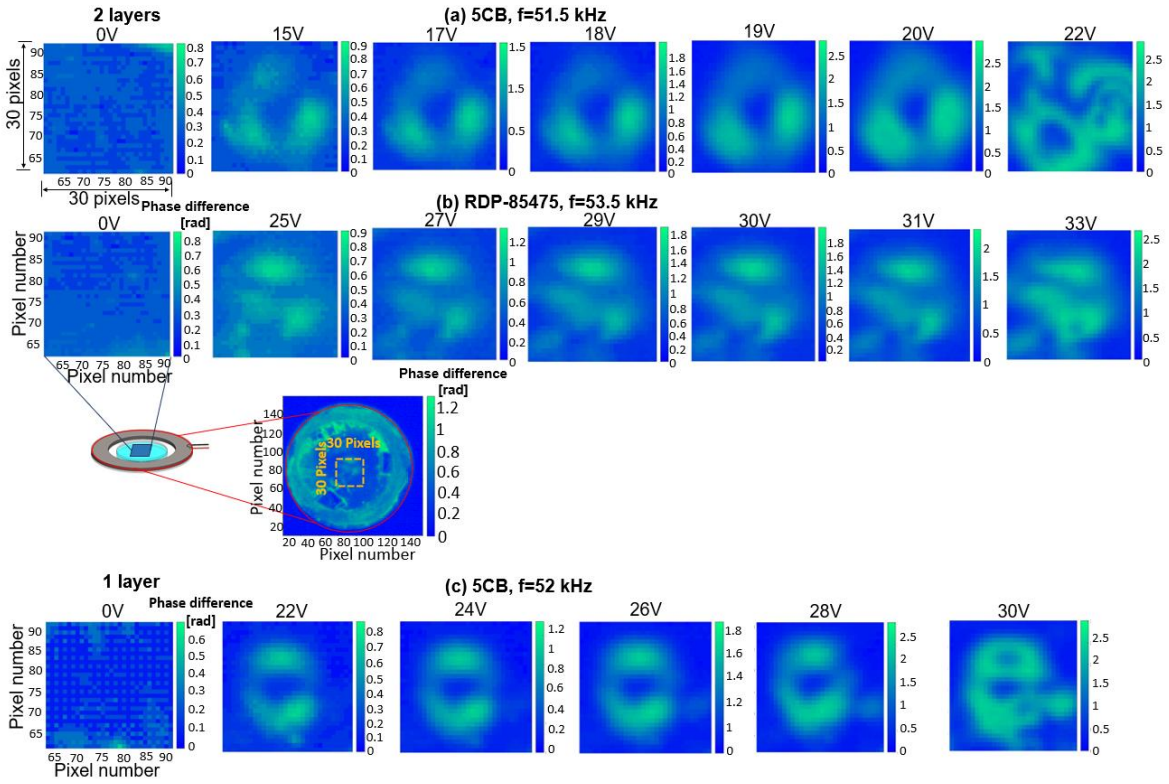

Fig. 7.4 Effective birefringence distributions of the liquid crystal lenses without and with ultrasound excitation at the resonance frequency. Double-layered lenses: (a) 51.5 kHz (5CB), and (b) 53.5 kHz (RDP-85475); single layer lens: (c) 52 kHz

For the 5CB lens case, the minimum operating voltages were 15 V (double-layered lens) and 22 V (single lens), and the threshold voltages for dynamic light scattering [7.12] were over 20 V (double-layered lens) and over 28 V (single lens). The RDP-85475 lens, in contrast, presented a minimum operating voltage of 25 V and a threshold voltage for dynamic light scattering of more than 30 V, although this was expected because 5CB has smaller elastic constant values, as noted in Chapter 4, Table 4.2. In addition, because the refractive index is varied spatially by application of different input voltages, the light that passes through different lens areas will have different propagation speeds. As a result, with application of the appropriate input voltage, the molecules will bend sufficiently to make the light bend after it passes through the liquid crystal lens. In addition, the light can be refracted

more strongly as the curvature of the refractive index profile increases in the layer. Therefore, with the appropriate voltage profile, the optical path difference (OPD) will have a parabolic shape, and the light can then be focused after it exits the lens, enabling characterization of the focal length. However, when the applied voltage exceeded the threshold for all lenses (5CB at 22 V (double-layered) and at 30 V (single layer), and RDP-85475 at 33 V, as shown in Fig. 7.4), the effective birefringence distribution increased dramatically, and the layer became cloudy, indicating dynamic scattering. In addition, the orientations of the liquid crystal molecules that receive torque become unstable under the application of a voltage, causing light scattering that is characterized by time-varying localized changes in the optical refractive index. Moreover, a larger acoustic radiation force will affect the optical properties directly with a large input voltage, because the acoustic radiation force is a quadratic function of the voltage that is applied across the transducer [7.13]. It was noticeable that both lenses that contained the liquid crystal material 5CB with the same 200 μm thickness but different configurations (i.e., double layer and single layer) showed different operating voltage ranges and different birefringence distributions, thus confirming the influence of the interactions of the liquid crystal with additional surfaces.

Because of the strong anchoring that occurs at the surfaces, the molecular reorientation of the liquid crystal is not entirely uniformly distributed throughout the layer. The molecular orientation is initially oriented around the center of the lens and then gradually expands as the applied voltage increases, as shown in Fig. 7.4. However, in the absence of any external stimulation (i.e., without ultrasound), the orientation of the liquid crystal molecules in the layer is determined by the anchoring condition of the alignment layer (which has vertical alignment as its initial condition). Easy reorientation of the liquid crystal molecules under ultrasound excitation is highly desirable for high ultrasound liquid crystal lens performance. Usually, nematic liquid crystal devices are mostly dependent on voltage-induced reorientation of the liquid crystal within the liquid crystal layer, and the region near the surface is strongly anchored [7.14]; therefore, an alternative to weak anchoring to enable lower power operation is used that involves setting the two layers in combination with the liquid crystal material properties to improve the overall lens performance.

Figure 7.5 was generated from Fig. 7.4 by selecting the maximum value of the effective birefringence in the 30×30-pixel area located at the center of the liquid crystal lenses (left vertical axis). The liquid crystal lens based on 5CB showed more variation in its effective birefringence distribution (as measured by the birefringence profiler) when compared with the lens using RDP-85475 for both the double-layered and single layer lenses. It was also confirmed by the results on the right axis, in which the affected area of the effective birefringence increased with increasing applied voltage, thus confirming that the liquid crystal molecular orientation change from the center of the lens was not entirely uniformly distributed throughout the layer, and this area gradually expands with increases in the input voltage (the affected areas were obtained by selecting the regions with more than 0.5 rad of effective birefringence per measurement as the threshold value).

Figure 7.6 was also generated from Fig. 7.4, and using the formulation presented in Chapter 4 (Section 4.4.4) to calculate the angular variation (i.e., the deviation angle $\Delta\theta$ [deg]) for both the double-layered liquid crystal lenses and the single layer lens. The liquid crystal lenses using 5CB promoted greater molecular rotation under ultrasound excitation than the lens that used RDP-85475. The line A-A' was a transverse line selected for all measurements taken below the threshold voltage for dynamic light scattering for both lenses. This line was selected to observe the angular variation profile of the liquid crystal molecules based on the voltage applied. Regardless of the layer thickness, the physical properties of the liquid crystal materials affected the lens' molecular inclination and the operating voltage. A lower threshold voltage could be obtained using 5CB, which has lower dielectric anisotropy and a smaller elastic constant than the RDP-85475 material.

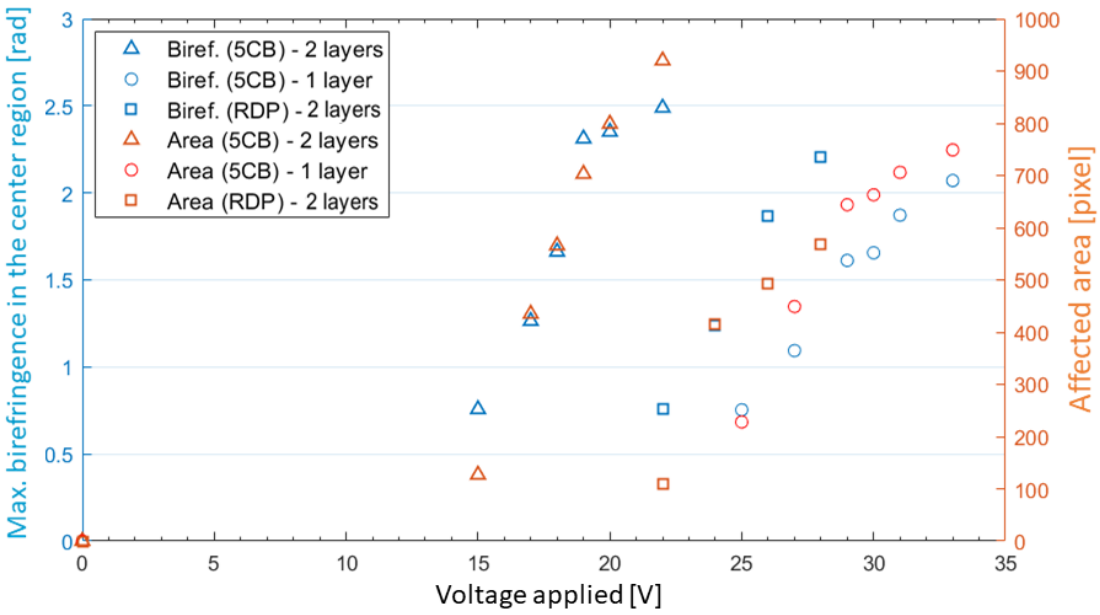

Fig. 7.5 Maximum effective birefringence (Biref.) value in the center region per unit voltage applied (left vertical axis, blue); affected effective birefringence area versus the input voltage (right vertical axis, red) for the double-layered lenses and the single layer lens. The data were plotted according to their respective vertical axis colors.

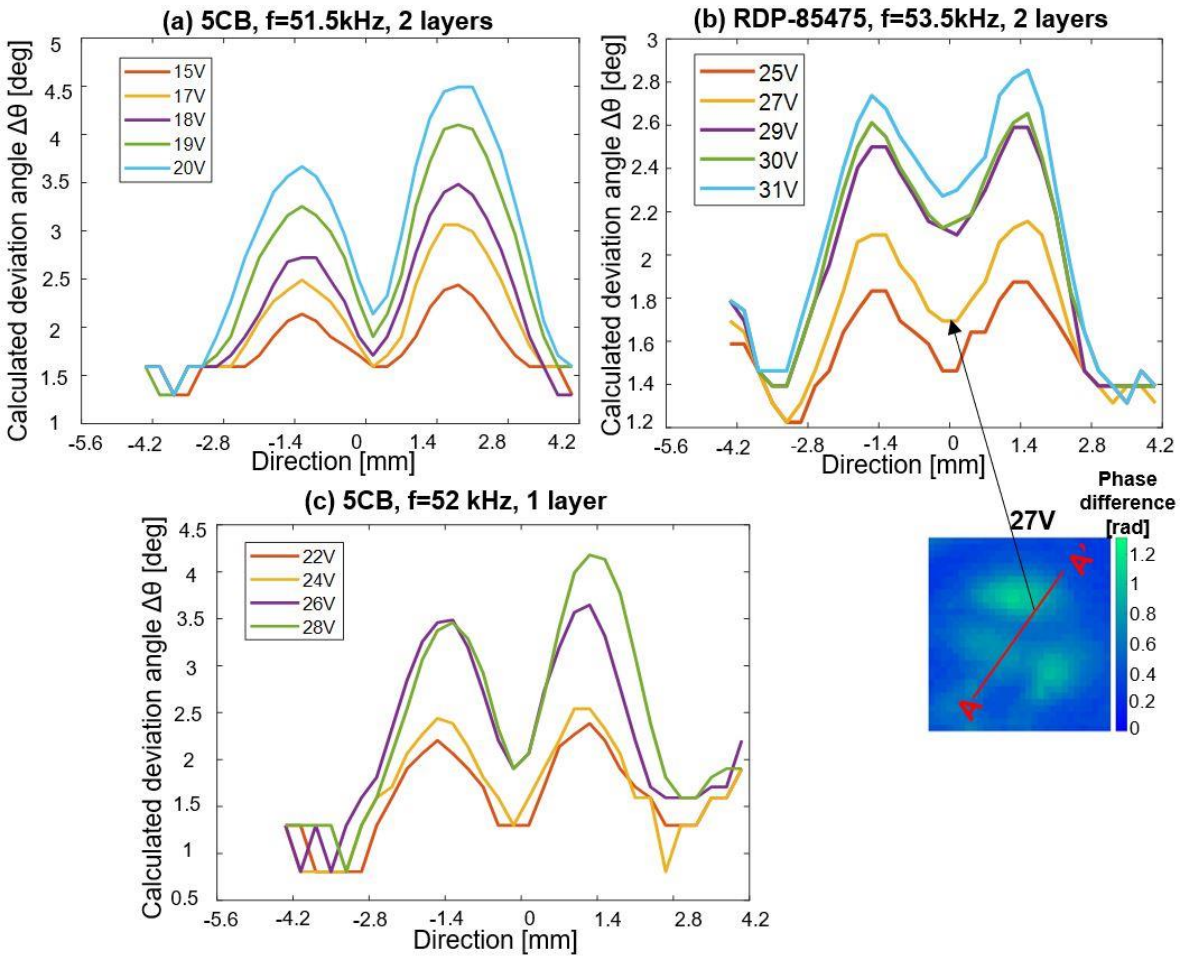

Fig. 7.6 Calculated deviation angle $\Delta\theta$ with respect to the input voltage for lenses with (a) 5CB and (b) RDP-85475 (double-layered lens) and (c) 5CB (single-layer lens); the region of the plotted line in the graphs is indicated by A–A'.

Optical observation of the ultrasound double-layered liquid crystal lenses using a transmission optical microscope (VW-9000, Keyence) with an objective lens (200×) and a single Nicol element was performed using the two lenses. A test target (1951 USAF) was placed between the light source and the polarizer and was moved vertically to evaluate the optical characteristics of the two lenses without and with ultrasound excitation. It was confirmed that the focal point varied along the optical axis of the lenses under ultrasound excitation using one Nicol element, and both lenses thus acted as a convex variable-focus lens. Their focal lengths were measured by moving the test target vertically between the polarizer and the optical source. Figure 7.7 shows the relationship between the input voltage (V) and the focal length (μm) of the double-layered ultrasound liquid crystal lens using 5CB when compared with the corresponding properties of the lens using RDP-85475. The focal length without applied ultrasound excitation was considered to be zero. When the input voltage under ultrasound excitation increased, the focal length increased in tandem. Figure 7.7 indicates that the birefringence variation with the applied voltage may contribute to the variable focus function of the lens. It also suggests that the model based on the double-layered lens makes it easier to vary the orientation of the liquid crystal molecules, and this orientation changes significantly even in the lower input voltage range, thus producing a variable-focus lens within a lower operating voltage range. Larger changes in the refractive index due to the applied voltage under ultrasound vibration excitation in the liquid crystal layer means that the focal length variation is also larger (5CB case). In other words, if there is a large optical birefringence distribution, the optical path lengths can then be controlled over a wide range via the application of a voltage.

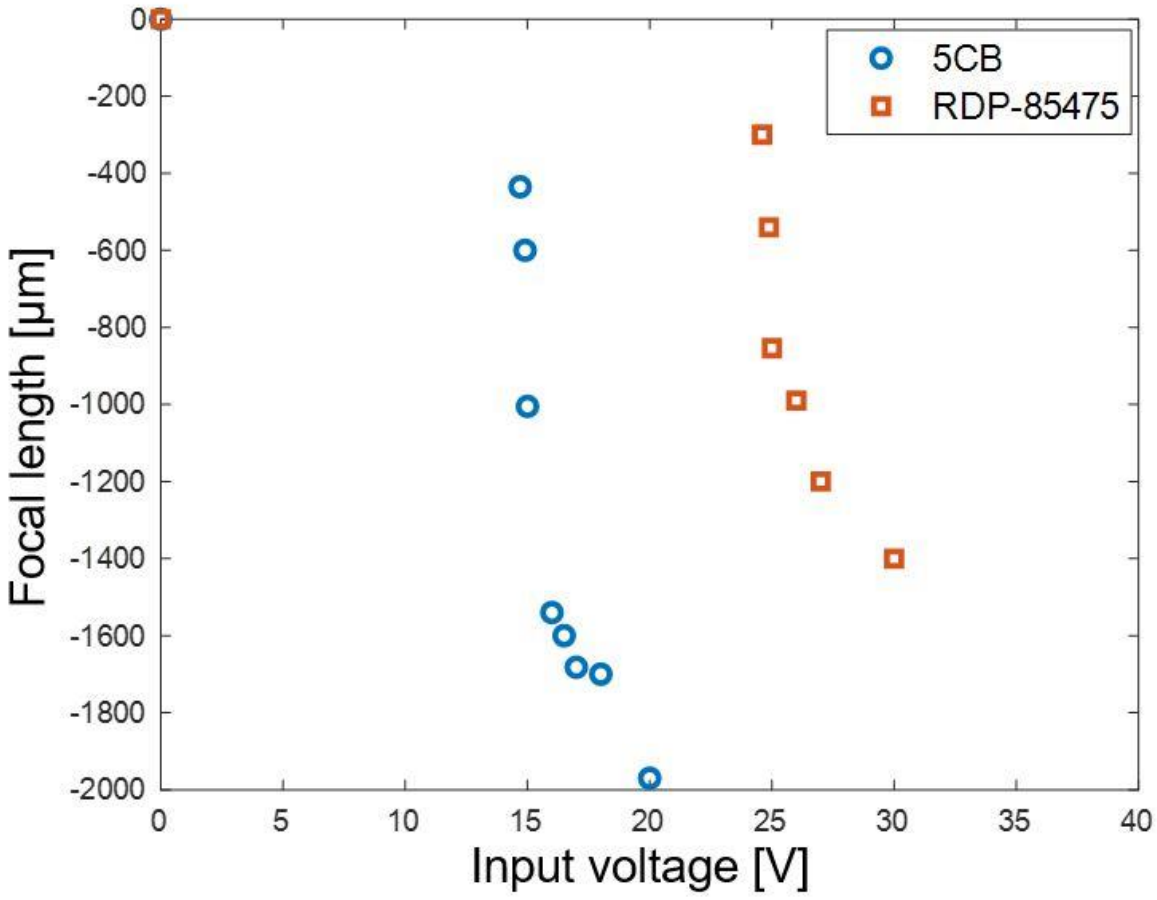

Fig. 7.7 Relationship between the input voltage and changes in the focal length of the double-layered ultrasound liquid crystal lenses.

REFERENCES

[7.1] M. Ye and S. Sato, "Liquid crystal lens of two liquid crystal layers," *Molecular Crystals and Liquid Crystals*, vol. 422, no. 1, pp.197-207, 2004.

[7.2] H.S. Chen, Y.J. Wang, C.M. Chang, and Y.H. Lin, "A polarizer–free liquid crystal lens exploiting an embedded–multilayered structure," *IEEE Photonics Technology Letters*, vol. 27, no. 8, pp. 899–902, 2015.

[7.3] M. Ye, B. Wang, M. Kawamura and S. Sato, "Image formation using liquid crystal lens," *Japanese Journal of Applied Physics*, vol. 46, no. 10R, p.6776, 2007.

[7.4] Y. Shimizu, D. Koyama, M. Fukui, A. Emoto, K. Nakamura and M. Matsukawa, "Ultrasound liquid crystal lens," *Applied Physics Letters*, vol. 112, no. 16, p. 161104, 2018.

[7.5] J. Onaka, T. Iwase, M. Fukui, D. Koyama and M. Matsukawa, "Ultrasound liquid crystal lens with enlarged aperture using traveling waves," *Optics Letters*, vol. 46, no. 5, pp.1169-1172, 2021.

[7.6] T. Iwase, J. Onaka, A. Emoto, D. Koyama, M. Matsukawa, "Relationship between liquid crystal layer thickness and variable-focusing characteristics of an ultrasound liquid crystal lens," *Japanese Journal of Applied Physics*, vol. 61, no. SG, p. SG1013, 2022.

[7.7] J. Onaka, T. Iwase, A. Emoto, D. Koyama, M. Matsukawa, "Ultrasound liquid crystal lens with a variable focus in the radial direction for image stabilization," *Applied Optics*, vol. 60, no. 33, pp. 10365-10371, 2021.

[7.8] Z. Zhang and W. Ye, "The elastic distortion and stability of biaxial nematic liquid crystal on the surface grooves," *Liquid Crystals*, vol. 36, no. 8, pp.885-888, 2009.

[7.9] A. Emoto, N. Otani, and T. Fukuda, "Birefringence measurement device and birefringence measurement method," (U.S. patent 10,119,904 2018).

[7.10] H. Zhou, E.P. Choate and H. Wang, "Optical Fredericks transition in a nematic liquid crystal layer," In *Liquid Crystalline Polymers,* Springer, Cham, pp. 265-295, 2015.

[7.11] J. Onaka, T. Iwase, M. Fukui, D. Koyama, and M. Matsukawa, "Supplementary document for Ultrasound liquid crystal lens with enlarged aperture using traveling waves - 5071177.pdf," *Optics Letters* (published online 2021).

[7.12] S. T. Wu and D. K. Yang, "Fundamentals of Liquid Crystal Devices", *John Wiley & Sons*, Hoboken, NJ, 2006.

[7.13] S. Nagai, A. Peters and S. Candau, "Acousto-optical effects in a nematic liquid crystal," *Revue de Physique Appliquée*, vol. 12, no. 1, pp.21-30, 1977.

[7.14] J. Jones, "Liquid crystal displays," in *The Handbook of Optoelectronics*, CRC Press, pp. 137–224, 2017.

CHAPTER 8: CONCLUSIONS

This doctoral thesis covered the study, development, and analysis of an ultrasonically controlled liquid crystal lens with a simple structure that uses acoustic actuation rather than transparent electrodes. The conducted simulations and experiments considering the driving scheme were determinative parameters for expanding the lens aperture by using traveling waves, as well as, to perform the variable-focus in radial direction function for image stabilization using standing waves. Both above mentioned approaches used a piezoelectric ceramic divided into four quadrants that are independently driven with sinusoidal voltages at the resonant frequency of the lenses. Furthermore, optical, physical, and fabrication characteristics of a new double-layered ultrasound liquid crystal lens were analyzed. Results obtained in this research, conclusions and future prospects are summarized in this final chapter.

Evaluation of the vibration distribution is an important parameter in the design of ultrasonically controlled liquid crystal devices, since the molecular orientation of liquid crystal material is correlated to the device vibrational mode. Furthermore, the optical characteristics is also vibration mode related. Firstly, the configurations of the transducer and the glass substrates were predicted via finite element analysis (FEA) using the software ANSYS to determine the resonance flexural vibration modes on the glass substrates for generating a standing wave and a traveling wave using a multichannel transducer. Then, the ultrasound liquid crystal lens was fabricated, and experiments were performed to validate the simulation model of the lens by comparison with the laser Doppler vibrometer (LDV) measurements. LDV results indicate the vibration mode changed due to the number of driving transducers and excitation scheme.

Additionally, optical characteristics were evaluated experimentally. Standing wave and traveling wave actuation mechanisms were applied to the liquid crystal lens by using the multichannel transducer model, and further reported about its optical characteristics using a Shack-Hartmann wavefront sensor to better understand the ultrasonically controlled liquid

crystal lens properties. Moreover, it was possible to perform optical characterization of the liquid crystal lens by the wavefront analysis and it may also be used to optimize the lens fabrication method. The surface data obtained from the sensor was analyzed and the optical aberrations were measured. Traveling wave mode actuation showed small optical aberrations and larger aperture when compared to the standing wave mode, indicating a higher image quality. Additionally, various combinations of the four-channel ultrasound transducer can be used to define the focal point of the liquid crystal lens. Clear optical images could be obtained with the lens. By using two-dimensional fast Fourier transforms, the focal point position was defined and shifted in the radial direction.

Optical characteristics changed according to the vibration mode control through the driving channels. Strictly speaking, optical characteristics of the lens depends directly on the vibrational distribution amplitude allowing the focal point to change in radial direction for a standing wave excitation; whereas for traveling wave excitation, a traveling motion propagating identically alongside the circumference of the transducer can make possible a lens with a larger aperture (i.e. two times larger when compared to a lens using standing wave mode). The reason was that the traveling wave carries energy across a distance in the medium (i.e., piezoelectric transducer) and this energy can be used as a propulsion mechanism to enable lens functionality with larger aperture sizes. Moreover, since the molecular orientation is correlated to the lens vibrational distribution, when the standing wave mode is used, the lens aperture tends to be smaller, since the center of the lens corresponds to the antinode of vibration in this case, in which the acoustic radiation force does not act.

The lens performance may be affected by the thickness and configuration of the liquid crystal layer. Further optical improvements can be made by changing the lens thickness. Meanwhile, it has to be large in order to obtain a large dynamic focus range and thin to obtain a low response time, which consists in a trade-off in performance. Besides that, for practical use of ultrasound liquid crystal lens, it is necessary to evaluate other parameters such as the liquid crystal material and alignment film conditions to make possible not only a wide focusing range, but also light weight and low operating voltage lens. The double-layered

model showed that by combining two liquid crystal layers while maintaining the same 200 µm thickness as the single lens, improvements in the ultrasound liquid crystal lens (single layer) were realized in terms of lower operating voltages, longer focal lengths, and easier reorientation of the liquid crystal molecules. The birefringence profiler results indicated that the variation of the birefringence distribution upon ultrasound excitation led to a steeper refractive index profile within a lower operating voltage range for the double-layered lens when compared with the previous lens model that relied on a single-layer structure. Although the anchoring force of the liquid crystal molecules to the alignment films decreases when the liquid crystal layer thickness increases, and the optimum liquid crystal layer thickness for the ultrasound liquid crystal lens was defined to be 200µm, the results presented here showed that use of two layers in combination with the appropriate liquid crystal physical parameters, i.e., birefringence, dielectric anisotropy, and elastic constants, provided a solution to produce weak anchoring of the liquid crystal, thus improving the lens performance and contributing to the lower operating voltage range for longer focal lengths.

Although the ultrasound liquid crystal lenses show potential to reduce the size, weight, materials and assembly costs of optical systems with less mechanics, the limitation of these technologies are related to the materials' properties and trade-off between focal length, thickness and response time. It is necessary to find alternative lens architectures, materials, and processing for further improvements.

The lens model based in a multichannel showed the possibility of controlling the focal point freely for image stabilization, as well as, to increase the lens aperture. The double-layered lens model tailored based on the liquid crystal's physical properties, e.g., its dielectric anisotropy and elastic constants, is an alternative method to improve the lens's optical performance while forming weak anchoring surfaces for nematic liquid crystals, thus promoting easier reorientation of the liquid crystal molecules.

The ultrasonically controlled liquid crystal lenses presented in this doctoral thesis have a potential to be used in microdevices and miniature cameras. It might be possible to develop in the future a lens that has both convex and concave functions with possible control

of these features, with desired application for auto-focusing and optical zoom systems through new lens design and approaches.